

ROBUST L_2 NONLINEAR CONTROL OF EDFA WITH AMPLIFIED
SPONTANEOUS EMISSION

by

Nemanja Stefanovic

A thesis submitted in conformity with the requirements
for the degree of Master of Applied Science
Graduate Department of Electrical and Computer Engineering
University of Toronto

Copyright © 2005 by Nemanja Stefanovic

Abstract

Robust L_2 Nonlinear Control of EDFA with Amplified Spontaneous Emission

Nemanja Stefanovic

Master of Applied Science

Graduate Department of Electrical and Computer Engineering

University of Toronto

2005

Erbium Doped Fiber Amplifiers (EDFAs) must be controlled in optical networks such that the output channel powers do not vary significantly from input power variation. Common control schemes for EDFAs currently involve using linear approximation methods around equilibrium points. Heuristic methods are usually employed to switch between the various operating points. Amplified Spontaneous Emission (ASE) is usually ignored in EDFA models.

In this thesis, an EDFA model with ASE is derived. A nonlinear L_2 control methodology is outlined to exploit the nonlinear nature of the EDFA system. This eliminates the need for heuristics since the system is free to operate over the state space with only one controller. Furthermore, robust control techniques are utilized to allow for parameter and signal variation due to uncertainty.

Dedication

I dedicate this work to my family, Gradimir, Mersija, and Filip, who are still a significant part of my life. I would also like to dedicate this work to Kristina, who has made the last six years some of my best.

Acknowledgements

I would like to thank my supervisor, Dr. Lacia Pavel, for the incredible guidance she has given me throughout the course of my work. A lot of her previous work has been the foundation of the results herein. More importantly, however, she taught me how to systematically approach research projects, and organize my work coherently.

I would also like to thank Dr. Manfredi Maggiore, from which his lectures in both undergraduate and graduate courses inspired me to pursue Control Theory.

Contents

1	Introduction	1
1.1	The Application and Science of EDFAs	1
1.2	Motivation	2
1.3	Literature Review	5
1.4	Thesis Statement and Objectives	7
1.5	Thesis Organization	8
2	EDFA System Models and Specifications	10
2.1	EDFA Model without ASE	10
2.2	Derivation of EDFA Model with ASE	11
2.2.1	EDFA System Variables	12
2.2.2	Simplifying Assumptions	12
2.2.3	Model Derivation	13
2.2.4	Model Discussion	15
2.3	Simulation of EDFA Model Terms with ASE	15
2.4	Open Loop Dynamic Simulation of EDFA with ASE	18
3	Background	21
3.1	Mathematical Definitions	21
3.2	L_2 Nonlinear Control	24
3.3	Robust Control	28

4	L_2 Nonlinear Control of EDFA	33
4.1	FI Problem Construction	33
4.2	Linear FI Problem Solution	34
4.3	Nonlinear FI Problem Solution	36
4.4	Simulation Results	41
5	Gain Scheduling and L_2 Control Comparison	49
5.1	Gain Scheduling Overview	49
5.2	Gain Scheduling Design	50
5.2.1	Design Objectives	51
5.2.2	Linear Control Design	51
5.2.3	Gain Scheduling Extension	54
5.3	L_2 Control Design	56
5.3.1	Design Objectives	56
5.3.2	L_2 Controller Design with Parameters Constrained to Physical Limitations	57
5.4	Gain Scheduling and L_2 Control Simulation Comparison	58
5.4.1	Simulation Results Analysis	58
5.4.2	Extreme Case for Gain Scheduled PID Control	62
5.4.3	Extreme Case for L_2 Control	63
6	Robustness Design	67
6.1	State Uncertainty Derivation	68
6.2	State Uncertainty for Parametric Representation	70
6.3	Robust Modeling of EDFA with ASE	73
6.4	Robustness Simulation Results	77
6.4.1	Controller Derivation	78
6.4.2	Simulation of Uncertainty Cases	81

6.4.3	Simulation of Uncertainty with Channel Drops	94
7	Conclusion	107
7.1	Significant Results	107
7.2	Limitations to Work	109
7.3	Future Work	110
A	Polynomial Solution To Hamilton-Jacobi Equation	112
B	EDFA System Parameters and Input Values	116
C	List of MATLAB Simulation Files	119
	Bibliography	122

List of Tables

4.1	Nonlinear EDFA System Terms	35
5.1	Linearized EDFA Model Parameters[10]	52
5.2	The PID controller's parameters	54
6.1	Enumerated EDFA System Terms	70
6.2	Subdivision of Term 2	71
6.3	X_u Scaling Values for Robustness Test Cases	79
B.1	EDFA Input Values	116
B.2	EDFA parameters	117
B.3	EDFA Signal and Pump Bands	118
C.1	Files in directory 'MastersThesisASEmodel'	120
C.2	Files in directory 'MastersThesisHJEsolver \ FIsolver' and 'MastersThesisRobustness \ robustsolver'	121

List of Figures

2.1	ASE model State Equation Terms in Steady State for 32 Channels	16
2.2	ASE model State Equation Terms in Steady State for 2 Channels	17
2.3	Dynamic ASE model response with 50% channel drop	18
2.4	Dynamic ASE model response with 97% channel drop	19
2.5	Dynamic ASE model response with 100% channel failure	19
3.1	Block Diagram of Applied L_2 Controller on System	23
3.2	Block Diagram of Feedback Uncertainty	30
3.3	Input Multiplicative Uncertainty	32
4.1	An Example of $V(x) > 0$ and $V(x) = 0$ in a neighborhood around $x_0 = 0$	37
4.2	An Example of $V_x(x) < 0$ for $x < 0$ and $V_x(x) > 0$ for $x > 0$ in a neighborhood around $x_0 = 0$	38
4.3	$f(x)$ Has a Stable Vector Field	39
4.4	$f(x) + \frac{1}{2}Q_{FI}(x)V_x(x)$ Showing a Stable Vector Field to Satisfy Theorem	
	3.2.1 Condition 2	40
4.5	$V_{FI}(x)$ versus Average Inversion	42
4.6	$\frac{\partial V_{FI}}{\partial x}(x)$ versus Average Inversion	43
4.7	$Q_{FI}(x)$ versus Average Inversion	44
4.8	$f(x) + \frac{1}{2}Q_{FI}(x)V_x(x)$ Showing a Stable Vector Field to Satisfy Theorem	
	3.2.1 Condition 2	45

4.9	Closed Loop System Response of x for 97% channel drop.	46
4.10	Closed Loop System Output Response for 97% channel drop.	47
4.11	$f(x)$ vs. Taylor Approximation to $f(x)$	48
5.1	Conceptual diagram of the linear model of the EDFA with an controller [10]	53
5.2	System response with one channel dropped from two channels	59
5.3	System response with 16 channel dropped from 32 channels	60
5.4	System response with 31 channels dropped from 32 channels	61
5.5	System response with one channel dropped from two channels with 20mW pump power and 100% estimation error	64
5.6	Extreme 32 Channel Case with High L_2 Gain and 50 percent channel drop.	65
5.7	Extreme 32 Channel Case with High L_2 Gain and 97 percent channel drop.	66
6.1	Input Multiplicative Test Case for 2 Channels with 5% and 10% Input Uncertainty	82
6.2	Input Multiplicative Test Case for 32 Channels with 5% and 10% Input Uncertainty	83
6.3	State Uncertainty Test Case for 2 Channels with 0.01 and 0.001 State Uncertainty	85
6.4	State Uncertainty Test Case for 2 Channels with 0.01 and 0.001 State Uncertainty	86
6.5	State Uncertainty Test Case for 32 Channels with 0.01 and 0.001 State Uncertainty	87
6.6	State Uncertainty Test Case for 32 Channels with 0.01 and 0.001 State Uncertainty	88
6.7	State Uncertainty and Multiplicative Uncertainty Test Case for 2 Channels with 0.01 and 0.001 State Uncertainty and 5% and 10% Input Uncertainty	90

6.8	State Uncertainty and Multiplicative Uncertainty Test Case for 2 Channels with 0.01 and 0.001 State Uncertainty and 5% and 10% Input Uncertainty	91
6.9	State Uncertainty and Multiplicative Uncertainty Test Case for 32 Channels with 0.01 and 0.001 State Uncertainty and 5% and 10% Input Uncertainty	92
6.10	State Uncertainty and Multiplicative Uncertainty Test Case for 32 Channels with 0.01 and 0.001 State Uncertainty and 5% and 10% Input Uncertainty	93
6.11	Input Multiplicative Case for 2 Channels with 5% Input Uncertainty and Channel Drops	96
6.12	Input Multiplicative Case for 32 Channels with 5% Input Uncertainty and Channel Drops	97
6.13	State Uncertainty Case for 2 Channels with 0.001 State Uncertainty and Channel Drops	98
6.14	State Uncertainty Case for 2 Channels with 0.001 State Uncertainty and Channel Drops	99
6.15	State Uncertainty Case for 32 Channels with 0.001 State Uncertainty and Channel Drops	100
6.16	State Uncertainty Case for 32 Channels with 0.001 State Uncertainty and Channel Drops	101
6.17	State Uncertainty and Multiplicative Uncertainty Case for 2 Channels with 0.001 State Uncertainty and 5% Input Uncertainty with Channel Drops	102
6.18	State Uncertainty and Multiplicative Uncertainty Case for 2 Channels with 0.001 State Uncertainty and 5% Input Uncertainty with Channel Drops	103
6.19	State Uncertainty and Multiplicative Uncertainty Case for 32 Channels with 0.001 State Uncertainty and 5% Input Uncertainty with Channel Drops	104

6.20 State Uncertainty and Multiplicative Uncertainty Case for 32 Channels with 0.001 State Uncertainty and 5% Input Uncertainty with Channel Drops	105
---	-----

Chapter 1

Introduction

A short description about the operation and physics of the EDFA is first presented. The motivation for control work on the EDFA is then given. Next, a brief literature review is provided followed by the the thesis statement and objectives of the work. A brief description of the remaining chapters of the thesis are provided in the final section.

1.1 The Application and Science of EDFAs

Erbium Doped Fiber Amplifiers (EDFAs) are cost effective devices used to amplify the optical power in light signals in optical fiber cables. Signal amplification is necessary every 80 to 100 kilometers for long-haul fiber optic connections [1][2][3]. Examples of some of these long-haul fiber optic connections include the networking of two cities separated by thousands of kilometers across a continent or transoceanic links. EDFAs are usually daisy chained together in these long distance communication links. On a much larger level, EDFAs make up component elements of vast interconnected fiber optic communication networks. As such, their peak performance properties and their ability to dynamically handle changing signal powers have received close scrutiny in the past few years.

An EDFA is an optical fiber that is usually a few meters in length that has been doped with Erbium ions (Er^{3+})[6]. The Erbium ions absorb certain wavelengths of light

energy to excite the atoms into higher energy states. The proportion of the Erbium atoms that are excited into the higher energy states is called the inversion level of the Erbium doped fiber. An atom that is not excited is at ground state. Incident signal photons will interact with the excited Er^{3+} ions to release their stored energy as photons in the 1550nm band [3]. The resultant released photon propagates with the same phase, polarity and direction as the incident photon, hence, signal amplification is realized.

Wavelength division multiplexing (WDM) is utilized to combine input signals into one beam of light. Each input channel is designated its own wavelength in the light. This light signal passes through the Erbium doped fiber to emerge amplified at the output. The various wavelengths of light within the beam are amplified by different amounts according to the absorption and emission spectrums of the EDFA. The source of amplification energy for the EDFA comes from a pump, which is a laser light at the input operating at 980nm or 1480nm wavelengths[3]. Erbium ions are easily excited at these particular wavelengths of light, so the purpose of the pump is to provide energy to these atoms for signal amplification.

Amplified Spontaneous Emission (ASE) is a specific EDFA effect [2]. The excited Erbium atoms can release their energy spontaneously without the catalyst of an incident photon. This results in photons with a random phase, polarization and direction. These random photons also become amplified by the same process that amplifies the input signal. Since ASE does not carry signal information, it contributes to noise. The effect becomes more pronounced in long connections of EDFAs because ASE can propagate and amplify along these chains[4][5].

1.2 Motivation

Modern day applications of EDFAs extend into optical networks responsible for dynamically routing information between multiple locations. As such, data channels are

expected to be added and dropped at designated points in the network such that minimal power transients occur at the output. Furthermore, communication channels in the optical networks must allow for rerouting around broken connection links or congested traffic routes. For the most part, modern day optical networks still employ static point to point configurations [1] which are subject to predefined designs that are not adaptable to variations in real time. It is expensive and time consuming to dispatch technicians reconfigure EDFAs if their operating conditions change. It is therefore desirable to have extremely robust and dynamic EDFA devices that could operate over a wide range of operating conditions.

The primary focus of using control theory on the EDFA device is to regulate either the total system gain or the output channel powers. In the event of changes to the input power, the output power and system gain change. In each case, a transient will manifest itself on the signal output of the EDFA. These transients can cause data error in the signals. Furthermore, the problem is compounded by the fact that daisy chained EDFAs actually cause power transients to increase in speed as they propagate through the devices [4][5]. This makes it clear that applying controls to each individual EDFA is necessary.

Previous work on control applications to EDFA devices has ignored ASE [1][6][7][8]. However, it has been shown in [9] that ASE can have a significant effect on the output power in the EDFA. Large channel drops are one example where the ASE increases significantly on the remaining channels. It is necessary to have a more inclusive EDFA model that takes amplified spontaneous emission into account.

Typical control schemes for EDFA devices are based on a simple system model with linear control methods as in [1][7][10]. This results in a number of defined equilibrium points where a controller is scheduled based on the measured input and output values of the system in real-time. The operating region over which a linear controller works can be very small. Having a linear controller in place for a nonlinear system can only

give an approximate behaviour. [10] derives a more systematic approach using linear controllers in combination with gain scheduling. [10] provides an excellent baseline to test any nonlinear control law that is developed.

The output powers of each channel are directly affected by the average inversion level. If channel powers change, the average inversion level will change. If the average inversion is kept constant, the output channel powers will remain constant [1][8]. We can minimize the variation of the average inversion through L_2 nonlinear control [11]-[16]. L_2 nonlinear control, like its linear counterpart [17]-[19], will ensure a direct attenuation between a disturbance input on the channel powers to the average inversion level. The necessity of EDFA device controllers that attenuate the changes in average inversion are further justified in [4] and [5] that show cascaded transients speed up with chains of EDFAs.

Finally, any control law implementation must be made to take uncertainties into account. Physical implementations of controllers on devices are never perfect since parameter data and signal measurements may not be ideal. System models may also neglect important information about the system. As such, a robustness structure must be imposed on the system to limit unwanted effects on the nonlinear system. Unstructured uncertainty in the signal powers [15][12] and uncertainty in the average inversion from parameter values can be minimized using L_2 nonlinear control.

This thesis is not only a further development of EDFA control, but it is a good example of a practical application of nonlinear theory [11] to a challenging model. The following will tackle a highly nonlinear and stiff [20] system, and provide it with a practical control solution. Taylor approximations will be utilized to achieve the final control results [21][12].

1.3 Literature Review

The following works comprise the literature sources for this thesis. Each reference is briefly addressed and its contribution to the thesis is noted. We begin by outlining the basic optical network and EDFA device reference material. Next, the literature dealing with EDFA system models is presented. The sources relating to ASE and its impact on the EDFA are then discussed. General H_∞ control and L_2 nonlinear control theory references are provided. We then present the main body of work from which this thesis extends. Finally, a few sources about computational techniques are provided.

In [1], a transient power control scheme that uses a PID controller along with system linearization is outlined, simulated and experimentally verified. The work in [1] serves as the basis from which this thesis extends its results. The work also provides an excellent overview for this topic. A great textbook for a basic introduction to optical networks and their operation is provided in [3]. Another good tutorial valued book that explains the history and operation of optical networks from a more practical perspective is given in [2].

A detailed explanation about the physics and modeling of the Erbium Doped Fiber Amplifier is provided in [22]. It is renowned as a significant source for EDFA information. The raw EDFA rate and propagation equations in PDE form are presented in [6]. This work is the foundation for the EDFA model in many papers. [6] provides an in depth discussion into the physics of the EDFA.

A common EDFA system model is derived in [7]. The model forms the basis for many control schemes in literature. Many of the assumptions made in [7] are incorporated in the ASE model that is derived in this thesis. An example of a linear control application to EDFAs is presented in [23]. The work depicts common test parameters and is useful as a general comparison of results. Examples of both pump compensation and light compensation for EDFA control are presented in [24]. Insight into both compensation types as well as the practical implementation of the control is given.

Another control example for the EDFA is presented in [8]. This source includes ASE information in the model which was valuable as guide to the newly derived ASE model presented in this thesis. A paper submission from [25] parallels the EDFA model with ASE presented herein without dynamic analysis of the system. An example of how ASE can be significant during EDFA operation is found in [9]. Increasing transient speed of output response in cascaded EDFA systems is the primary topic in [4] and [5]. The results from these works help to justify the necessity of control for the EDFA.

Extremely important H_∞ control and L_2 nonlinear control theorems are presented in [13] and [14]. In particular, the theorems of H_∞ control connect the linear problem into the L_2 nonlinear control framework. Furthermore, the work is presented in state-space form in accordance with the work in this thesis. The theoretical basis for L_2 nonlinear control is given in [11]. The definitions involving L_2 control theory are presented therein with examples. The work serves as a tutorial introduction to the theory. Further reading about H_∞ control is provided in [17] that is referenced throughout literature. In [19] a tutorial approach is presented to introduce the H_∞ control problem. The work gives a historical perspective and outlines useful system structures such as the Full Information problem. A good reference book for the basics of H_∞ control theory is presented in [18]. Ancillary material relating to dissipative systems that is used in certain assumptions for the robust control theory is presented in [26].

This thesis primarily extends the work presented in [12] and [15]. These papers present L_2 nonlinear control for general systems of extended state space form. The work outlines the framework for using L_2 nonlinear control to compensate for unstructured uncertainty. [12] is particularly detailed in the analysis, and it includes a computational approach to solving the Hamilton Jacobi Equation using Taylor approximation. [16] is the source for the extension of [12] and [15] as well as an excellent reference to the framework of L_2 nonlinear control. The work presented in this thesis regarding the L_2 nonlinear control methodology is rooted in [27] and expanded upon.

A gain scheduling approach involving linearization techniques for the EDFA system is presented in [10]. The work derived therein serves as the basis of comparison for the results derived in the paper. Furthermore, the comparison plots and simulation data is originated from [28]. The framework for gain scheduling is explained in [29]. The work explains the results depicted in [10] that are represented subsequently in this thesis. Also, a good example of the application of gain scheduling is found in [30].

A brief explanation of ODE integration algorithms and the nature of stiff equations is presented in [20]. A good reference book for any control related query is provided in [31]. The computational approach outlined for the solution of the Hamilton Jacobi Equation is first stated in [21]. The notation from [12] is adopted and reiterated for clarity in Appendix A. The work of [21] serves as the essential basis for solving the L_2 control problem presented herein. Currently, there is no other means to solve the Hamilton Jacobi Equation either publicly or commercially. Hence, the work in [21] was utilized in a script program written in MATLAB for this thesis.

1.4 Thesis Statement and Objectives

A common EDFA control paradigm consists of using incomplete models that do not include amplified spontaneous emission (ASE), linear approximate control laws and a heuristic scheduling system to switch between controllers. An EDFA model that includes ASE is necessary for significant accuracy in cases of large average inversion. Furthermore, an L_2 nonlinear control scheme would eliminate the need for heuristics and replace the multiple linear approximate controllers with one nonlinear controller that would be more accurate and also improve performance. Including robustness makes the nominal control design less sensitive to uncertainty.

The objectives of the work within this thesis are:

- Derive a new EDFA state space model that includes amplified spontaneous emission

(ASE)

- Apply L_2 nonlinear control to the EDFA model with ASE to limit output power variation with respect to input power changes.
- Compare L_2 nonlinear control of EDFA with ASE to an appropriate baseline reference and compare the performances of the two control schemes. Here, a PID controlled system with gain scheduling on an EDFA model without ASE is chosen as the baseline comparison case.
- Apply robust control techniques to the EDFA system with ASE to reject uncertainties that may arise in a practical implementation. Important uncertainties to address are input multiplicative uncertainty and state parametric uncertainty.

1.5 Thesis Organization

The remaining chapters of the thesis are organized as follows:

- **Chapter 2:** A description of the common EDFA system model without ASE is presented along with all of the parameters and their meanings. A description of the raw rate and propagation equations for the EDFA are presented in PDE form. These equations are then simplified and reformulated into state space form that includes amplified spontaneous emission(ASE). An extensive analysis of the steady-state and dynamic response of the open loop EDFA model is performed to understand its behaviour.
- **Chapter 3:** Background is introduced that is relevant to L_2 nonlinear control and robustness. The fundamental theory of H_∞ linear control and L_2 nonlinear control are introduced that will be later applied to the EDFA with ASE. Many fundamental definitions and assumptions are introduced as well. Finally, robustness theory is

addressed focusing on unstructured uncertainty. The robust theory is related to L_2 nonlinear control theory.

- **Chapter 4:** The application of L_2 nonlinear control onto the EDFA with ASE is presented here. The EDFA system equations are structured into the Full Information (FI) problem and solved using the linear H_∞ control theory. The linear solution is then used as a starting point for the expansion of the theory to solve the nonlinear FI problem of the EDFA model. An example result is shown with a global solution to the nonlinear FI problem for a specified EDFA performance.
- **Chapter 5:** The results of using L_2 nonlinear control on an EDFA model with ASE are compared to the results of using PID control with gain scheduling. Both the PID control law and the L_2 control law are designed with comparable real-world constraints. An extensive set of comparison tests are presented to compare and contrast the two methods of control.
- **Chapter 6:** The EDFA model with ASE is augmented to include input uncertainty and state uncertainty terms. A new output performance equation is developed, and along with the use of L_2 nonlinear control, the uncertainties are handled by more robust controllers. A final set of graphs are presented that show the performance of the robust controller for all uncertainties individually, together, and in combination with input channel drops.
- **Chapter 7:** Summary of Results. The significant results from the thesis are reiterated. Limitations of the work are outlined in the subsequent section. The work is concluded with suggestions about future endeavors based on the results obtained herein.

Chapter 2

EDFA System Models and Specifications

A common EDFA model is presented that does not incorporate amplified spontaneous emission (ASE). A new EDFA model with ASE is then derived and represented in state space form such that control techniques can be applied to the system. Simulations for both the steady-state and dynamical behaviour of the EDFA system with ASE are presented using specified data.

2.1 EDFA Model without ASE

The basic mechanisms in an EDFA are stimulated emission, which amplifies the signal, and spontaneous emission, which causes noise. The pump signal is responsible for exciting the Erbium atoms, while channel signals interact with the atoms to release that energy in the form of coherent light. Amplified Spontaneous Emission (ASE) results from excited atoms that release this energy without stimulus from the input channel powers. This results in a random phase, polarity and direction for this new light, which causes noise[2]. The effects of ASE also compound as they propagate through chained EDFAs.

The system model developed in [7] describing the EDFA does not include any terms

for ASE. The rate equation and output equations in state space form are

$$\begin{aligned}\dot{x} &= -\frac{x}{\tau} - \frac{1}{\rho SL} \sum_k [e^{[(g_k + \alpha_k)x - \alpha_k]L} - 1] Q_k^{in}(t) \\ Q_k^{out}(t) &= e^{[(g_k + \alpha_k)x - \alpha_k]L} Q_k^{in}(t)\end{aligned}\quad (2.1)$$

where $x = \int_0^L N_2(z, t) dz$ and $N_1(z, t) + N_2(z, t) = 1$. L is the length of the Erbium Doped fiber. x is the average inversion level of the EDFA and $N_1(z, t)$ and $N_2(z, t)$ are the ground state and excited Erbium ion concentrations compared to the total concentrations. τ is the spontaneous lifetime of the excited energy level. ρ represents the number density of active Erbium atoms. S is the fiber core cross section. Also, Q_k^{in} and Q_k^{out} represent the normalized input and output powers of the k^{th} EDFA channels respectively. They are called photon flux [6][7], and defined as $Q_k = \frac{P_k}{h\nu_k}$, where P_k denotes the power of the k^{th} light channel in Watts. The pump signal, which is the control input to this system, is one of the Q_k^{in} signals at the 980nm wavelength. The pump signal does not have an output equation since it is absorbed by the EDFA.

In [6], the raw equations for EDFAs with ASE in PDE form are outlined. The equations by themselves can not be used for control. We will make certain key assumptions to simplify the general equations and a state space model with ASE will be developed. In [8], an EDFA model is derived that includes an ASE term, but it was not placed in a state space form, nor was the ASE term utilized. [25] derives a representation of the EDFA model with ASE in parallel with the model derived herein, but does not include the dynamic transient behaviour of the system for changes in state or input power.

2.2 Derivation of EDFA Model with ASE

The derivation of the EDFA model with ASE will progress as follows in the next subsections. The EDFA system variables and their corresponding physical equations are initially presented. Simplifying assumptions for the EDFA physics are then provided.

Next, a step by step mathematical derivation of the new EDFA system model with ASE is provided. The final section is a discussion about the new model.

2.2.1 EDFA System Variables

We begin by defining some common variables within the EDFA model along with a more rigorous mathematical description of the absorption and emission coefficients. These variables and equations will be used to convert raw integral EDFA equations in PDE form into an explicit state space representation in subsequent subsections. Necessary notations are presented here that will be used throughout.

Let $n_i(r, \phi, z)$ for $i = 1, 2, t$ represent the ground state, excited state and total erbium ion populations, respectively. Here r is the radius, ϕ is the azimuth angle, and z is the distance along the EDFA fiber [6]. $P_k(z)$ will denote the power of the k th beam of light in Watts, or the channel power, as a function of distance along the EDFA fiber. The frequency of the light beam is indicated by ν_k , and centered at $\lambda_k = \frac{c}{\nu_k}$.

Among the important characteristic values that define the EDFA system, two of the more important are the absorption and gain spectra, α_k and g_k , respectively [6].

$$\alpha_k = \sigma_{ak} \int_0^{2\pi} \int_0^\infty i_k(r, \phi) n_t(r, \phi, z) r dr d\phi \quad (2.2)$$

$$g_k = \sigma_{ek} \int_0^{2\pi} \int_0^\infty i_k(r, \phi) n_t(r, \phi, z) r dr d\phi \quad (2.3)$$

$i_k = \frac{I_k(r, \phi, z)}{P_k(z)}$ is the normalized optical intensity, and $I_k(r, \phi, z)$ is the light intensity distribution. σ_{ak} and σ_{ek} are the absorption and emission cross sections, respectively.

2.2.2 Simplifying Assumptions

From [6], we can state some of the underlying standard assumptions used to simplify the EDFA model. First,

Assumption 1. $E r^{3+}$ is assumed to be radially symmetric and decreasing monotonically from $r = 0$.

Definition 1. Define b_{eff} as

$$b_{eff} = \left[\frac{1}{2} \int_0^{2\pi} \int_0^\infty \frac{n_t(r)}{n_t(0)} r dr d\phi \right]^{\frac{1}{2}} \quad (2.4)$$

so we get the average density of Erbium ion population as:

$$\bar{n}_i(z) = \frac{\int_0^{2\pi} \int_0^\infty n_i(r, \phi, z) r dr d\phi}{\pi b_{eff}^2} \text{ for } i = 1, 2, t \quad (2.5)$$

with this, the erbium population is now only a function of the distance along the fiber.

The above assumption can be taken one step further, such that from [6]:

Assumption 2. Erbium populations are distributed uniformly in a disk of radius b .

Also, to further simplify, we assume:

Assumption 3. The erbium populations are uniformly distributed along the length of the EDFA fiber.

We are only interested in the average Erbium concentration as a whole. Thus, now n_i represents the average Erbium concentration along the radius, ϕ angle, and length of the entire EDFA fiber.

2.2.3 Model Derivation

The EDFA rate and propagation equations with ASE [6] are written as

$$\frac{dn_2}{dt} = \sum_k \frac{P_k i_k \sigma_{ak}}{h\nu_k} n_1(r, \phi, z) - \sum_k \frac{P_k i_k \sigma_{ek}}{h\nu_k} n_2(r, \phi, z) - \frac{n_2(r, \phi, z)}{\tau_o} \quad (2.6)$$

$$\begin{aligned} \frac{\partial P_k}{\partial z} = & u_k \sigma_{ek} \int_0^{2\pi} \int_0^\infty i_k(r, \phi) n_2(r, \phi, z) r dr d\phi (P_k(z) + mh\nu_k \Delta\nu_k) \\ & - u_k \sigma_{ak} \int_0^{2\pi} \int_0^\infty i_k(r, \phi) \cdot n_1(r, \phi, z) r dr d\phi (P_k(z)) \end{aligned} \quad (2.7)$$

Here, u_k represents either the forward or reverse direction of propagation through the EDFA with either +1 or -1, respectively. m represents the number of modes in the fiber, and is usually set to 2. $\Delta\nu_k$ represents the effective noise bandwidth, and is set to 100GHz here.

We take the average inversion level across the EDFA length. Based on the foregoing assumptions, and changing the propagation equation to use α_k , (2.2), and g_k , (2.3), we obtain

$$\left(\frac{\partial}{\partial t} + \frac{1}{\tau_o} - \frac{1}{\zeta\tau_o} \sum_k g_k m \Delta\nu_k\right) \frac{n_2}{n_t} = \frac{-1}{\zeta\tau_o} \sum_k u_k \frac{1}{h\nu_k} \frac{\partial P}{\partial z} \quad (2.8)$$

$$\frac{\partial P_k}{\partial z} = u_k P_k(z) \left\{ (\alpha_k + g_k) \frac{n_2}{n_t} - (\alpha_k + \ell_k) \right\} + u_k g_k \frac{n_2}{n_t} m h \nu_k \Delta\nu_k \quad (2.9)$$

where $\zeta = \frac{\rho S}{\tau}$ is the saturation parameter and ℓ_k is an additional loss term in a channel. We assume $\ell_k = 0$ in the forthcoming simulations.

We apply classical solution techniques to solve the differential equation for P_k explicitly from (2.9). Since the inversion population, n_2 , does not depend on the length z , we can define

$$Q(z) = -u_k \left\{ (\alpha_k + g_k) \frac{n_2}{n_t} - (\alpha_k + \ell_k) \right\} \quad (2.10)$$

$$R(z) = u_k g_k \frac{n_2}{n_t} m h \nu_k \Delta\nu_k \quad (2.11)$$

Then, from the propagation equation (2.9) we derive the solution for $P_k(L)$, the power at the end of the fiber

$$P_k(L) = e^{-H(L)} \left\{ \int_0^L e^{H(z)} R(z) dz + P_k(0) \right\} \quad (2.12)$$

where $H(z) = \int_0^z Q(p) dp$. If we substitute $z = L$ into $H(z)$, we obtain $H(L) = Q(z)L$.

We can now express $P_k(L)$ explicitly as

$$P_k(L) = \frac{-g_k \frac{n_2}{n_t} m \nu_k \Delta\nu_k}{(\alpha_k + g_k) \frac{n_2}{n_t} - (\alpha_k + \ell_k)} \left[1 - e^{u_k \{ (\alpha_k + g_k) \frac{n_2}{n_t} - (\alpha_k + \ell_k) \} L} \right] + e^{u_k \{ (\alpha_k + g_k) \frac{n_2}{n_t} - (\alpha_k + \ell_k) \} L} P_k(0) \quad (2.13)$$

Finally, we explicitly integrate the rate equation (2.8) along the length of the fiber and divide by L . Also, we take the state variable to be $x = \frac{n_2}{n_t}$, and we normalize the power into photon flux, denoted by Q_k . We can now state the final, state-space representation

of the EDFA model with ASE included.

$$\begin{aligned}
\dot{x} &= -\frac{x}{\tau} - \frac{1}{\zeta\tau L} \sum_k (-g_k m \Delta\nu_k L x \\
&+ u_k \left[\frac{-g_k m \Delta\nu_k x}{(\alpha_k + g_k)x - (\alpha_k + \ell_k)} (1 - e^{u_k\{(\alpha_k + g_k)x - (\alpha_k + \ell_k)\}L}) \right. \\
&+ \left. (e^{u_k\{(\alpha_k + g_k)x - (\alpha_k + \ell_k)\}L} - 1) Q_k^{in} \right] \\
Q_k^{out} &= \frac{-g_k m \Delta\nu_k x}{(\alpha_k + g_k)x - (\alpha_k + \ell_k)} [1 - e^{u_k\{(\alpha_k + g_k)x - (\alpha_k + \ell_k)\}L}] \\
&+ e^{u_k\{(\alpha_k + g_k)x - (\alpha_k + \ell_k)\}L} Q_k^{in}
\end{aligned} \tag{2.14}$$

2.2.4 Model Discussion

There are some interesting differences between (2.1) and (2.14). We see two new terms in the state equation, and one new term in the output equation in (2.14). These terms are due to ASE contribution. As we can see, given a dropped channel, there will still be an ASE contribution as depicted by the output equation. Also note that in the state equation we have one linear ASE term and one nonlinear ASE term.

The derived model (2.14) possesses terms that are highly nonlinear in nature. Due to the enormous changes in the magnitude of the terms that constitute the vector field for \dot{x} , the equations are stiff [20]. There are a large number of design variables that have to be assigned that couple with each other. These observations add to the technical challenge.

2.3 Simulation of EDFA Model Terms with ASE

The analysis will plot the four major terms of the state equation (2.14) versus average inversion. We can plot all of the terms logarithmically to view their individual contributions to state changes over the average inversion level. Figure 2.1 shows the terms graphically for the 32 channel input case.

The channel numbers and their input powers are shown in Table B.1. The parameter data for the EDFA is listed in Table B.2. The signal and pump wavelengths with ab-

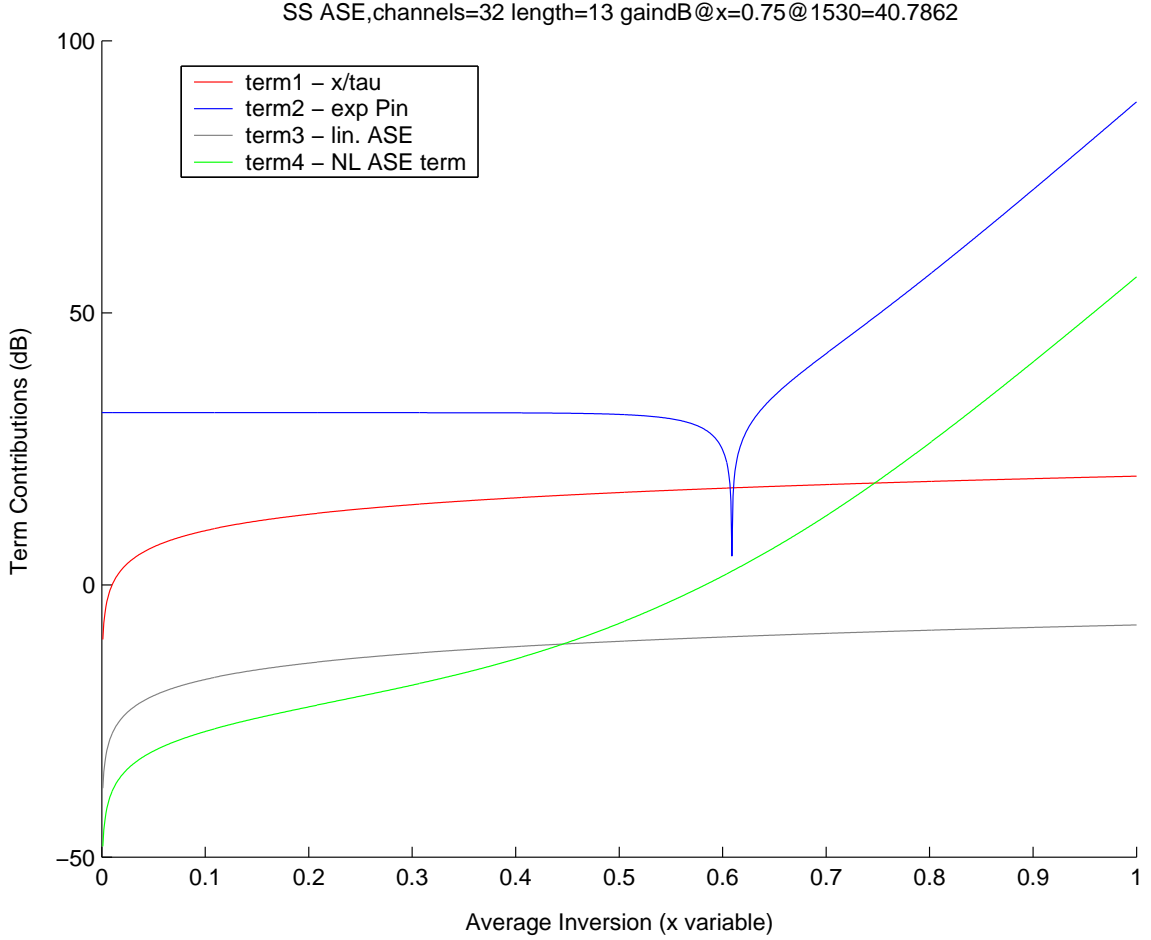


Figure 2.1: ASE model State Equation Terms in Steady State for 32 Channels

sorption and emission ranges are provided in Table B.3. Note that the channels that are utilized begin from the lower wavelengths, increasing by a 0.75nm spacing.

From Figure 2.1, the linear terms are represented by the two parallel looking plots, where the higher offset plot is the linear portion from (2.1), and the lower offset plot is the ASE. The linear ASE term is almost three orders of magnitude smaller than the $\frac{x}{\tau}$ linear term and will have a small effect on the state.

The term with the singularity in the middle is the input power term. The singularity is simply the result of the logarithmic function onto the value 0. The plot shows the individual channel and pump terms as one consolidated sum. If the input powers increase,

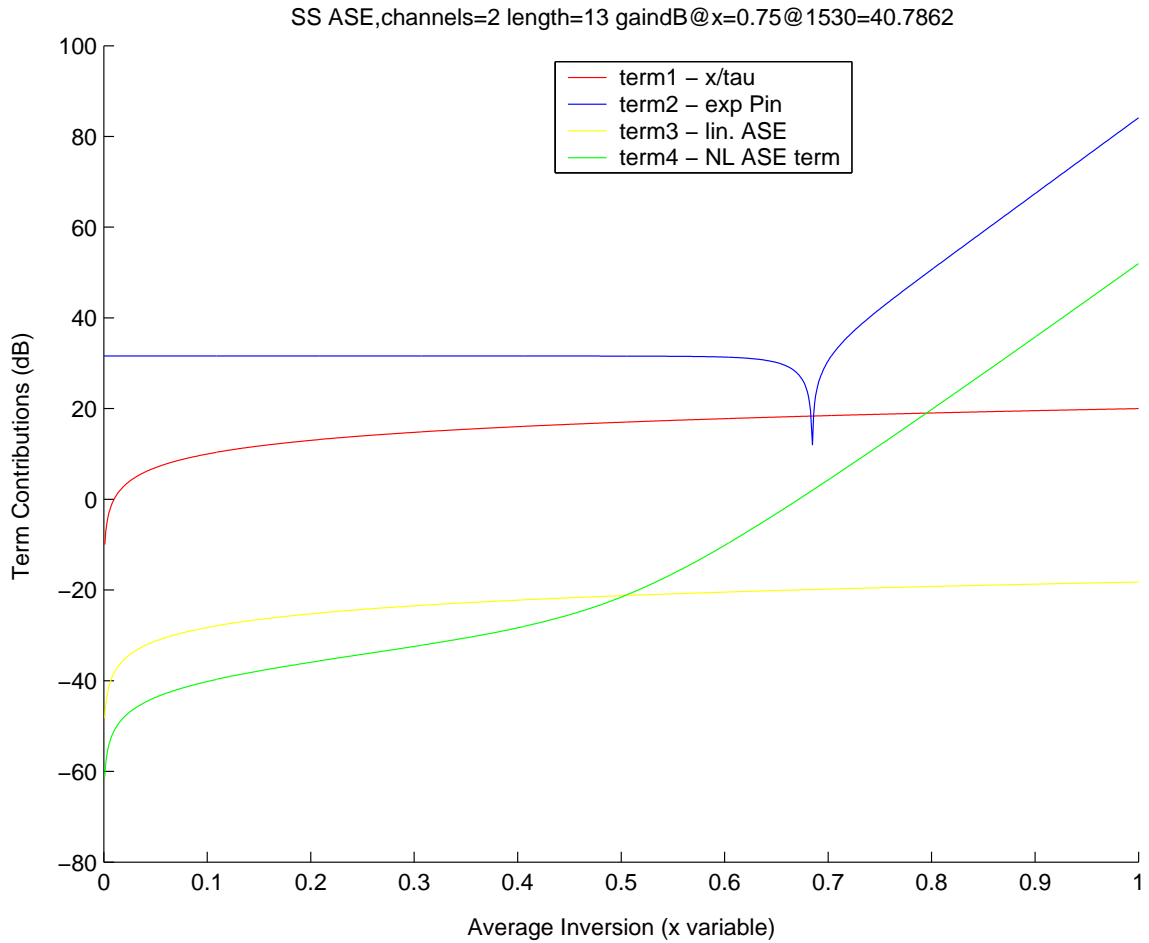


Figure 2.2: ASE model State Equation Terms in Steady State for 2 Channels

we should see these terms increase proportionally. This term is most dominant for high average inversions.

The most interesting plot is given by the nonlinear ASE term. It starts as the smallest term and then grows to be the second largest, next to the input term. Since the input term is very dependent on the input powers, we see that the nonlinear ASE term may have a significant effect on the state equation for relatively low input powers at high inversion levels. This confirms ASE experiments [9].

The 2 channel steady state plot is included in figure 2.2. We see that the terms are all similar to the 32 channel case. Thus, these steady state figures are useful for providing

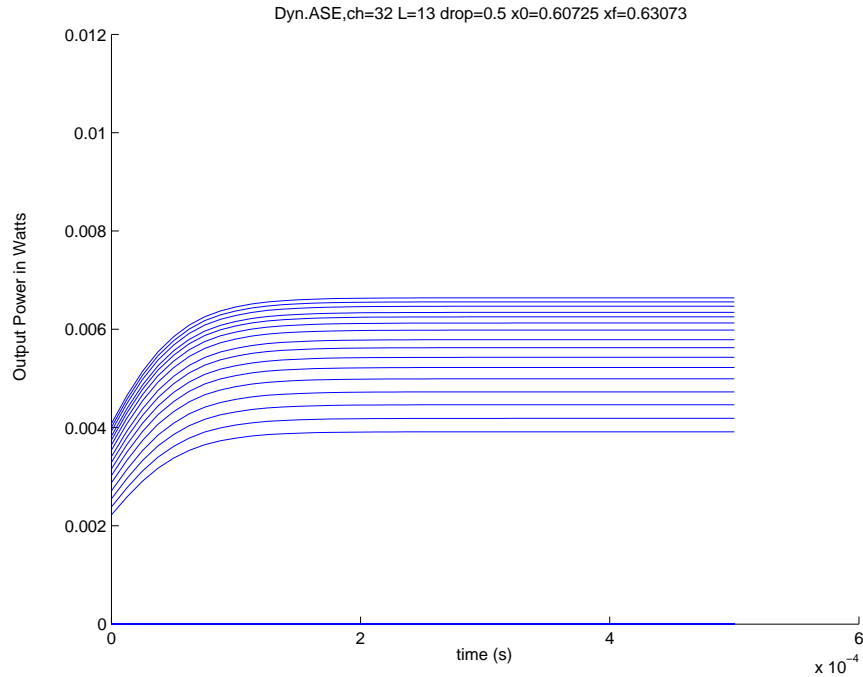


Figure 2.3: Dynamic ASE model response with 50% channel drop

a general intuition for the behaviour of the EDFA system with ASE.

2.4 Open Loop Dynamic Simulation of EDFA with ASE

We take the number of channels to be 32 to explore multiple channel dropping cases. The same input powers are taken as in the steady state analysis shown in Table B.1. We also adhere to the same parameters as defined in Tables B.2 and B.3. We show two main channel drop situations, a 50% channel drop, or 16 channels, starting from the lower wavelengths, and a 97% channel drop, or 31 channels, are reduced to zero. Also, the full channel failure case is considered where 100%, or 32 channels, are dropped and the transient response is analyzed.

First of all, we can note the different impact that ASE has in Figures 2.3, 2.4 and

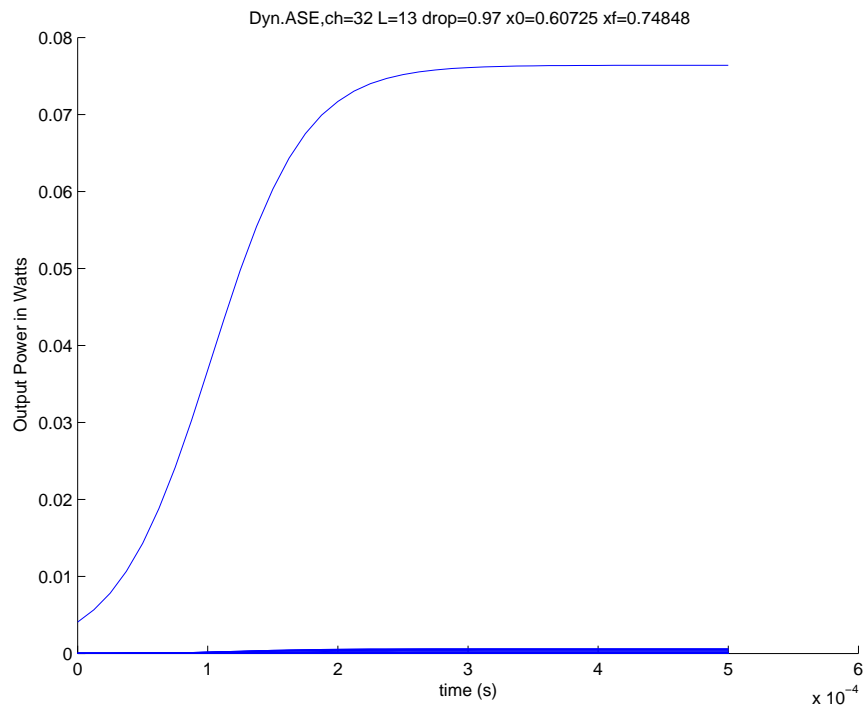


Figure 2.4: Dynamic ASE model response with 97% channel drop

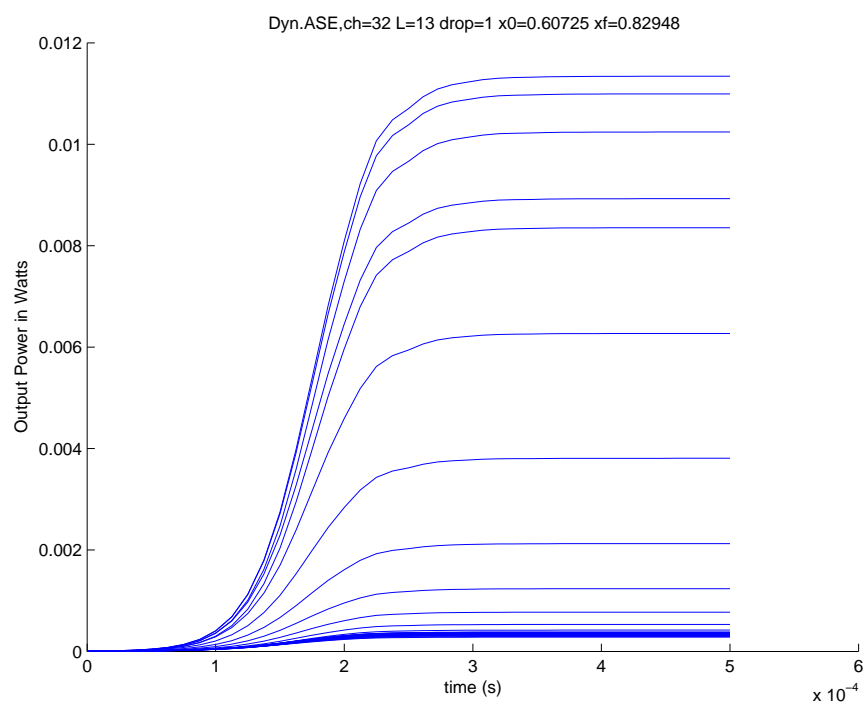


Figure 2.5: Dynamic ASE model response with 100% channel failure

2.5. The effect of ASE for a 50% drop is very small. The component due to ASE grows larger for the 97% drop case. The largest ASE magnitude manifests itself for the 100% drop case, which is much larger than either of the other cases. The reason for this can be seen from the changes in the average inversion levels, x , in each case. The larger channel drops results in a much larger increase for x , approximately $\Delta x = 0.14123$ for 97% drop and $\Delta x = 0.22223$ for 100% drop cases. This in turn results in the ASE term being much larger. In fact, the magnitude of the ASE plot in the 100% drop case surpasses that of the channel output powers for the 50% drop case. If we can control the variation in the state, we can restrict variation in ASE.

The 100% channel drop case is a special example that represents a total channel failure. It depicts the extreme increase of ASE noticeable from Figure 2.1. Moreover, since EDFAs are interconnected in optical networks, such a channel failure could result in a disturbance to other EDFAs in the network. If uncontrolled, the transient could propagate down an EDFA chain and increase its transient speed through the fiber length as demonstrated in [4] and [5].

We can see in Figure 2.3, that the power increases on the remaining channels by approximately 3 dB. Figure 2.4 shows an even greater power increase of approximately 12dB. This is due to the increasing of the average inversion variable, x .

Chapter 3

Background

Some fundamental mathematical definitions are first presented. The problem formulation and control theory for L_2 nonlinear control are then described. The remaining section introduces robust control in the context of L_2 theory.

3.1 Mathematical Definitions

We define the concept of a norm for a signal u , $\|u\|$, according to [11] as having to satisfy three properties:

- The norm of a signal is zero iff the signal is identically zero and is strictly positive otherwise.
- $\|au\| = a\|u\|$ for any positive constant a and every signal u .
- The norm satisfies the triangle inequality $\|u_1 + u_2\| \leq \|u_1\| + \|u_2\|$ for any u_1 and u_2

For the space of piecewise continuous square integrable functions, we define the norm as [11]

$$\|u\|_{L_2} = \sqrt{\int_0^\infty u^T(t)u(t)dt} < \infty$$

We refer to this representation as the L_2 norm. This norm defines the space of the signal which is denoted as L_2 . To deal with unbounded signals, we extend the space, L_2 , to become [11]

$$L_{2e} = \{u | u_T \in L_2, \forall T \in [0, \infty)\}$$

and u_T is defined by

$$u_T(t) = \begin{cases} u(t), & 0 \leq t \leq T \\ 0, & t > T \end{cases}$$

Note that the notation of [15] is also adopted which refers to the extended space as $L_2[0, T]$.

Definition 2. [11] A mapping $H : L_{2e} \rightarrow L_{2e}$ is said to be finite-gain L stable if there exist nonnegative constants γ and β such that

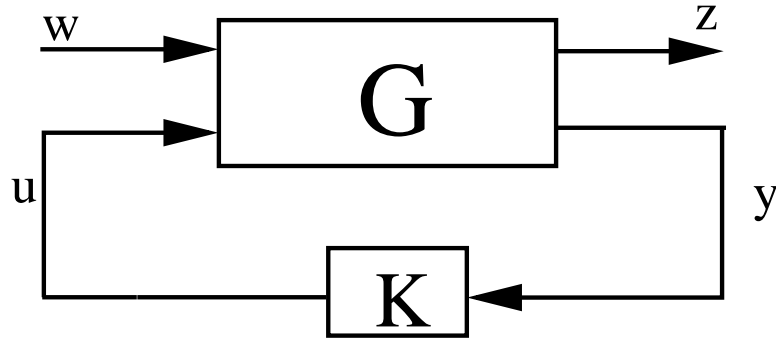
$$\|(Hu)_T\|_{L_{2e}} \leq \gamma \|u_T\|_{L_{2e}} + \beta$$

for all $u \in L_{2e}$ and $T \in [0, \infty)$.

The generalized nonlinear plant, which will be referred to as G , is represented below in its extended state-space form:

$$G : \begin{cases} \dot{x} = f(x) + g_1(x)w + g_2(x)u \\ z = h_1(x) + k_{11}(x)w + k_{12}(x)u \\ y = h_2(x) + k_{21}(x)w + k_{22}(x)u \end{cases} \quad (3.1)$$

Here, w represents the disturbance input while u represents the system input. z represents the performance output that the designer would specify. The purpose of the z equation will be to choose which variables to attenuate in the model. The application of L_2 control methods to our EDFA model (2.14) will necessitate rewriting (2.14) in the form of (3.1).

Figure 3.1: Block Diagram of Applied L_2 Controller on System

Assume we have a system in the extended state space form in (3.1) and a controller, K , applied to the system from u to y as in figure 3.1. We define a lower fractional transform [15] as the following relationship between w and z

$$z = F_\ell(G, K)w \quad (3.2)$$

where,

$$\begin{bmatrix} z \\ y \end{bmatrix} = G \begin{bmatrix} w \\ u \end{bmatrix}, \quad u = Ky \quad (3.3)$$

Definition 3. The system, G , is reachable (or $[f(x), g(x)]$ is reachable) from 0 if for all $x \in \mathfrak{R}^n$ there exists a time, T , and an input $u \in L_2[0, T]$ such that the state is driven from $x(0) = 0$ to $x(T) = x$.

The last two definitions, 4 and 5, are ancillary to the work presented in this thesis. They play a role in the assumptions presented in the robust control theory. Although they are only mentioned in passing, they are outlined for clarity and completeness.

Definition 4. [26] Let w_a be a real-valued function defined as $w_a(u(p), y(p))$ called the supply rate. $u \in \mathfrak{R}^m$ is the system input and $y \in \mathfrak{R}^q$ is the system output. Here, $p \in \mathfrak{R}$. $u \in \mathfrak{R}^m$ is a member of the set of piecewise continuous functions defined on \mathfrak{R} . Also, w_p

satisfies

$$\int_0^t |w_a(p)| dp < \infty \quad \forall t \geq 0 \quad (3.4)$$

Definition 5. [26] The Available Storage Function, denoted as V_a , of a system with supply rate w_a is the function defined by

$$V_a(x) = \sup_{x^0, u \in \Omega, t \geq 0} \left\{ - \int_0^t w_a(p) dp \right\} \quad (3.5)$$

where Ω is the set of inputs that consist of piecewise continuous functions defined on \mathfrak{R} . x^0 is any value in the state space. t denotes time.

3.2 L_2 Nonlinear Control

We can now state the fundamental control problem for the nonlinear system G , (3.1), using a controller K as given in (3.3).

L_2 Control Objective[15]: *To find a controller K applied to G such that*

1. $F_\ell(G, K)$ is asymptotically stable for $w = 0$
2. $F_\ell(G, K)$ has L_2 gain from w to z less than or equal to a specified number γ .

L_2 nonlinear control will serve to attenuate input disturbance effects on the state and input variable. A system model is defined by a state equation that outlines the dynamics of the state variable, and an output equation. We include an additional performance output equation along with the measured output equation to apply L_2 control theory [15][12]. This general form is given in (3.1).

We define a simplified subproblem that is relevant to the development of our nonlinear controller. This subproblem is relevant to the system because of the potential availability of the state variable in practice. The Full Information Problem (FI) [15][16][19] is defined as:

Definition 6. Full Information Problem (FI)

$$\begin{cases} \dot{x} = f(x) + g_1(x)w + g_2(x)u \\ z = h_1(x) + k_{11}(x)w + k_{12}(x)u \\ y = \begin{bmatrix} x \\ 0 \end{bmatrix} + \begin{bmatrix} 0 \\ I \end{bmatrix} w \end{cases} \quad (3.6)$$

where the control objective is identical to the L_2 Control Objective.

Here, w represents the disturbance input while u represents the system input. z represents the performance output that the designer would specify. The state is directly available for measurement.

For a nonlinear system (3.6) we say that the system has an L_2 gain, γ , if the following holds:

$$\int_0^T \|z(t)\|^2 dt \leq \gamma^2 \int_0^T \|w(t)\|^2 dt \quad (3.7)$$

where γ represents the amount of attenuation from the disturbance $w(t)$ to the defined variable $z(t)$.

The majority of the work developed herein is an application of the theoretical results developed in [12]-[16]. Theorem 3.1 of [12] (or see [15]) is the most important theorem in the analysis and is restated below as Theorem 3.2.1.

Theorem 3.2.1. *The L_2 control objective is achievable for the FI problem, assuming $k_{12}(x)$ has full column rank, and $S_1(x) < 0 \quad \forall x \in R^n$, where $S_1(x) = k_{11}(x)^T k_{11} - \gamma^2 I$ with feedback $u = F_{2\infty}(x)$ as long as:*

$$1) \exists V(x) \geq 0, V(0) = 0 \text{ solution of } H_{FI}(V, x) \leq 0 \quad (3.8).$$

2) $\dot{x} = f(x) + g(x)F_\infty(x)$ is asymptotically stable, where:

$$\begin{aligned} g(x) &= [g_1(x) \quad g_2(x)] \\ F_\infty(x) &= \begin{bmatrix} F_{1\infty}(x) \\ F_{2\infty}(x) \end{bmatrix} \\ &= -S^{-1}(x) \left[\frac{1}{2} g^T(x) V_x^T(x) + k_1^T(x) h_1(x) \right] \\ S(x) &= k_1^T(x) k_1(x) - \begin{bmatrix} -\gamma^2 I & 0 \\ 0 & 0 \end{bmatrix} \\ k_1(x) &= [k_{11}(x) \quad k_{12}(x)] \end{aligned}$$

where $H_{FI}(V, x) \leq 0$ is expressed in definition 7.

Definition 7. Hamilton-Jacobi Inequality (HJI), $H_{FI}(V, x) \leq 0$ is defined as [15]:

$$H_{FI}(V, x) = V_x(x) f(x) - F_\infty^T(x) S(x) F_\infty(x) + h_1^T(x) h_1(x) \quad (3.8)$$

where $V_x(x)$ is equivalent to $\frac{dV(x)}{dx}$. If (3.8) is represented as an equality, $H_{FI}(V, x) = 0$, it is referred to as the Hamilton-Jacobi Equation (HJE).

The conditions of Theorem 3.2.1 can be difficult to satisfy on their own. To help facilitate this task, two other theorems from [14] are presented. The first Theorem provides the necessary and sufficient conditions to solve the linear H_∞ control problem. The second Theorem links the linear H_∞ control problem to the L_2 nonlinear control problem.

First, the following assumptions are listed:

Assumption 4. We have a nonlinear system with the following structure:

$$\begin{aligned} \dot{x} &= f(x) + g_1(x)w + g_2(x)u \\ y &= h(x) \end{aligned}$$

where $f(x_0) = 0$ and $h(x_0) = 0$. Here, $u \in \mathfrak{R}^m$, $y \in \mathfrak{R}^p$, $d \in \mathfrak{R}^q$ and $x \in \mathfrak{R}^n$.

The linearization of the system is represented as:

$$\begin{aligned}\dot{\bar{x}} &= F\bar{x} + G_1\bar{w} + G_2\bar{u} \\ \bar{y} &= H\bar{x}\end{aligned}\tag{3.9}$$

where \bar{x} is the linearization of x around x_0 . \bar{w} and \bar{u} are the linearizations of w and u around w_0 and u_0 , respectively.

Assumption 5. (F,G) is stabilizable and (H,F) is detectable.

Assumption 4 is the system form that is outlined in [14]. The same form is expressed in the theorems in [14]. Assumption 5 is necessary for the application of the theorems from [14].

Definition 8. For the linearized system (3.9), let T_L be the transfer matrix[14]:

$$T_L : \bar{w} \rightarrow \bar{z} = \begin{pmatrix} \bar{y} \\ \bar{u} \end{pmatrix}\tag{3.10}$$

where $\bar{u} = L\bar{x}$ such that $F + G_2L$ is asymptotically stable. Then we define [14]

$$\|T_L\|_{H_\infty}^2 := \sup_{\bar{w} \neq 0} \frac{\|\bar{y}\|_{L_2}^2 + \|\bar{u}\|_{L_2}^2}{\|\bar{w}\|_{L_2}^2}\tag{3.11}$$

Definition 8 defines the least upper bound over all possible uncertainties, \bar{w} . The above definitions and assumptions are utilized in the following theorems from [14].

Theorem 3.2.2. [14] *Let assumptions 4 and 5 be satisfied. Then, for $\gamma > 0$ and L satisfying definition 8,*

$$\inf_L \|T_L\|_{H_\infty} < \gamma\tag{3.12}$$

iff there exists a symmetric solution $P \geq 0$ of

$$F^T P + P F - P(G_2 G_2^T - \frac{1}{\gamma^2} G_1 G_1^T) P + H^T H = 0\tag{3.13}$$

satisfying

$$\sigma(F - G_2 G_2^T P + \frac{1}{\gamma^2} G_1 G_1^T P) \subset \mathcal{C}^- \quad (3.14)$$

Furthermore, one possible L satisfying definition 8 and $\|T_L\|_{H_\infty} < \gamma$ is given by $L = -G_2^T P$.

Theorem 3.2.3. *Let assumptions 4 and 5 be satisfied. Suppose (3.12) is satisfied for the linearized system.*

Then there exists a neighborhood W of x_0 and a nonlinear feedback $u = l(x)$ such that

$$\dot{x} = f(x) + g_2(x)l(x)$$

is asymptotically stable on W and

$$\|y\|_{L_2}^2 + \|u\|_{L_2}^2 < \gamma^2 \|w\|_{L_2}^2$$

for all disturbances, $w \in L_2$.

Theorems 3.2.2 and 3.2.3 are useful in providing a starting point to satisfy the conditions of Theorem 3.2.1.

3.3 Robust Control

Robust control refers to a system's ability to reject disturbances or uncertainties so that the system behaves as closely to its nominal operation as possible. All system models are not perfect and it is impossible to take every physical factor into account with exact precision. There are always precision issues involved when parameters data is measured. The model itself may not have exact descriptions of the physical laws taking place, and as such, the model may not be accurate enough for real-world purposes. Furthermore, there are always internal and external physical and environmental effects that are manipulating the system in unpredictable ways. All of the above mentioned examples are forms of system uncertainty that cause system models and input and output signals to deviate

from their ideal operation. It is imperative that this uncertainty be taken into account for any real-world application of control theory.

There are two major forms of uncertainty that one could investigate, structured and unstructured uncertainty. Structured uncertainty refers to uncertainty within specific parameters within a system such as α or g in the EDFA model. The same general representation of the model is assumed with the acknowledgements that the parameters and terms within the model may be subject to unknown deviations. Unstructured uncertainty is more general than structured uncertainty in that any signal in a system model can be influenced by some unknown factor.

In [15][12], unstructured uncertainties are handled by using L_2 nonlinear control. The fundamental assumption about the unstructured uncertainty is that the input signal directly multiplies the uncertainty in an input affine form. This allows the use of L_2 control to limit the effects of the uncertainty. Clearly, given a large signal, the uncertainty output will increase. Thus, if an L_2 controller is designed to limit the signal value multiplying the uncertainty, we minimize the uncertainty output. L_2 control is perfect for this task since its main function is to maintain a design specified L_2 gain limit. We represent the input to the uncertainty as a performance output, z , which we then restrict by choosing an appropriate L_2 gain.

Assumption 6. Uncertainties are all input affine in their behaviour, ie., $w = \Delta z$, where the uncertainty, w , is the product of a signal z multiplied by an uncertainty term.

Definition 9. The Upper Fractional Transform on G by Δ relates u to y as

$$y = G_{\Delta}u$$

The plant, G , with feedback uncertainty is depicted in figure 3.2, and denoted as

$$\begin{bmatrix} z \\ y \end{bmatrix} = G \begin{bmatrix} w \\ u \end{bmatrix}, \quad w = \Delta z \quad (3.15)$$

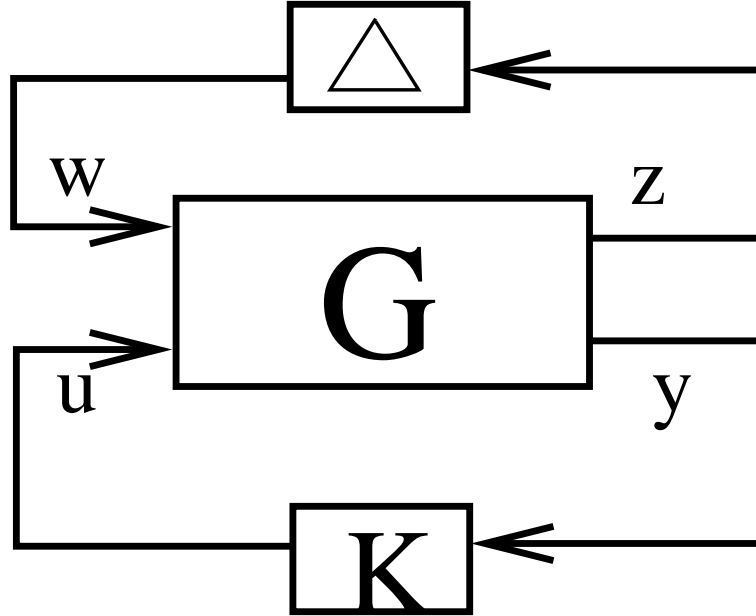


Figure 3.2: Block Diagram of Feedback Uncertainty

with $\Delta \in \Phi(\epsilon)$ where

$$\Phi(\epsilon) := \{\Delta \mid \Delta \text{ is internally asymptotically stable and has } L_2 \text{ gain } \leq \epsilon\}.$$

Definition 10. Let Δ be represented by the following state-space description:

$$\Delta : \begin{cases} \dot{\tilde{x}} = a(\tilde{x}) + b(\tilde{x})z \\ w = c(\tilde{x}) + k(\tilde{x})z \end{cases} \quad (3.16)$$

The following assumptions are necessary to apply the robust theory [15].

Assumption 7. The closed loop system G_Δ is well-posed, ie., $I - k_{11}(x)k(\tilde{x})$ is invertible for all x, \tilde{x} .

Assumption 8. The nominal closed loop system, $F_\ell(G, K)$ is well-posed, reachable from 0, with smooth available storage function.

Assumption 9. The uncertain plant Δ is reachable from 0 with smooth available storage function.

We can now state the formal objective for imposing robust properties on the system, G .

Generic Robust Stabilization Problem[15]: *To find a controller, K , from y to u such that the composite uncertain system, G_Δ is internally asymptotically stabilized by K for every $\Delta \in \Phi(\epsilon)$*

The following theorem from [15] gives sufficient conditions to solve the generic robust stabilization problem

Theorem 3.3.1. *Under assumptions 7 through 9, a controller, K , asymptotically stabilizes G_Δ for all uncertainties $\Delta \in \Phi(\epsilon)$ if the following conditions hold.*

1. K internally stabilizes G
2. the nominal closed loop system $F_\ell(G, K)$ has L_2 gain $\leq \gamma$.
3. $0 < \gamma < 1/\epsilon$

Theorem 3.3.1 tells us that the general robust stabilization problem can be achieved with an L_2 nonlinear controller. Notice that the first two conditions are satisfied given that Theorem 3.2.1 is satisfied and applied to our FI plant. The final condition specifies the extent of the robustness given a chosen γ value with respect to ϵ . However, we still have to provide the framework to be able to apply Theorem 3.3.1 for a meaningful uncertainty case.

There are many forms of unstructured uncertainty that exist, but the main form that we are interested in is input multiplicative uncertainty. Input Multiplicative uncertainty is the uncertainty on the inputs of the system as a function of the input signal. It is depicted in figure 3.3.

The state space description of P is described by

$$P : \begin{cases} \dot{x} &= f_p(x) + g_p(x)u_0 \\ y_0 &= h_p(x) + d_p(x)u_0 \end{cases}$$

Chapter 4

L_2 Nonlinear Control of EDFA

The EDFA system equations with amplified spontaneous emission (ASE) are written in the form of the Full Information (FI) problem. The subsequent section solves the linear FI problem. Next, the linear solution is used as a starting point to solve the nonlinear FI problem. Finally, simulation results are presented in the last section.

4.1 FI Problem Construction

Before the L_2 control design, a few observations about the system, (2.14), can be made. We can directly compute the value of our state x in real-time using measurements of the input and output powers from a designated channel. Theorem 3.2.1 does not require the use of the individual disturbance values in the controller, but only of the state x . The above observations indicate the significance of solving the FI problem on its own.

The developed EDFA model (2.14) can be associated to the FI problem (3.6). In our model, w represents the normalized input channel powers, and u represents the normalized input pump power. A standard nonlinear shift will be used later in the thesis to denote $x = 0$, $w = 0$ and $u = 0$ as the equilibrium point to generate a specific average inversion level, x_0 , with particular input powers. Any deviations from the equilibrium point will result in non-zero values of x , w and u .

Next, we must design the performance output, z , such that $k_{12}(x)$ has full column rank and $S_1(x) < 0$. The performance variable, z , represents the variable to be attenuated. We desire to attenuate the state, x , primarily, but it would also be beneficial to minimize the input, u . Note that any scalar multiples of the state and input, u , could also be used as design parameters.

One possible option is to use:

$$z = \begin{bmatrix} x \\ 0 \end{bmatrix} + \begin{bmatrix} 0 \\ \beta \end{bmatrix} u \quad (4.1)$$

such that the L_2 gain(3.7) is taken from the disturbance inputs of the system directly to the state and pump power input. Here, β is a scalar of arbitrary choosing, and it is set to unity for our system. With (4.1) chosen, we can state $H_{FI}(V, x)$ for the EDFA system with ASE as:

$$H_{FI}(V, x) = A_{FI}(x) \frac{dV(x)}{dx} + \frac{1}{4} \frac{dV(x)}{dx} Q_{FI}(x) \frac{dV(x)}{dx} + R_{FI}(x) \quad (4.2)$$

Where,

$$A_{FI}(x) = f(x) \quad (4.3)$$

$$Q_{FI}(x) = \frac{1}{\gamma^2} g_1(x) g_1^T(x) - g_2(x) g_2^T(x) \quad (4.4)$$

$$R_{FI}(x) = x^2 \quad (4.5)$$

To implement the entire state space model, we use real EDFA data with $f(x)$, $g_1(x)$ and $g_2(x)$ appropriately defined from the right hand side of (2.14) after the nonlinear shift from x_0 (see Table 4.1).

4.2 Linear FI Problem Solution

We can find an explicit mathematical representation for the valid range of γ in the linearized system. It is shown in Theorem 3.2.3, that the linearized γ representation is

Table 4.1: Nonlinear EDFA System Terms

Terms	Expression
$f(x)$	$-\frac{x}{\tau_o} - \frac{1}{\zeta\tau_o L} \sum_k (-g_k m \Delta\nu_k L x + u_k [\frac{-g_k m \Delta\nu_k x}{(\alpha_k + g_k)x - (\alpha_k + \ell_k)} (1 - e^{u_k \{(\alpha_k + g_k)x - (\alpha_k + \ell_k)\}L})])$
$g_1(x)$	$-\frac{1}{\zeta\tau_o L} [u_1 (e^{u_1 \{(\alpha_1 + g_1)x - (\alpha_1 + \ell_1)\}L} - 1) \quad \dots \quad u_N (e^{u_N \{(\alpha_N + g_N)x - (\alpha_N + \ell_N)\}L} - 1)]$
$g_2(x)$	$-\frac{1}{\zeta\tau_o L} u_{pump} (e^{u_{pump} \{(\alpha_{pump} + g_{pump})x - (\alpha_{pump} + \ell_{pump})\}L} - 1)$

valid for some neighborhood in the nonlinear system. Thus, we can take the linearized system, and solve for γ directly, then extend the results to the nonlinear system.

We distinguish the linear representation of any function from its nonlinear representation by using a capital letter and dropping the function of x notation. So, for example, the nonlinear $f(x)$ term would be represented as F . This notation will be used throughout.

Taking only the linear terms of the HJE, $H_{FI}(V, x) = 0$, we obtain the linear Riccati equation

$$A^T P + PA + PQ_{FI}P + R = 0 \quad (4.6)$$

From basic H_∞ theory [18], we restrict $Q_{FI} \leq 0$ and solve for $P > 0$. From this restriction on Q_{FI} , we can explicitly write out a restriction for γ .

$$\gamma \geq \sqrt{\frac{G_1 G_1^T}{G_2 G_2^T}} \quad (4.7)$$

Note that here, G_1 and G_2 represent the linear parts of $g_1(x)$ and $g_2(x)$ and hence are not functions of x , but are explicit constants.

The above relation (4.7) would not be very useful if we were given an unsatisfactory static lower bound for γ . To address this, we scale the pump input and disturbances. We let the scaled channel power disturbances $\Delta w = X_w w$, where X_w is the scaling factor multiplying the channel disturbances, w . We can do the same for the pump power input, $\Delta u = X_u u$, where X_u represents the scaling factor multiplying the pump power input.

We re-write the EDFA system model in FI form below, including the scaling factors.

$$\begin{cases} \dot{x} &= f(x) & + \frac{g_1(x)}{X_w}(\Delta w) & + \frac{g_2(x)}{X_u}(\Delta u) \\ z &= \begin{bmatrix} x \\ 0 \end{bmatrix} & & + \begin{bmatrix} 0 \\ 1 \end{bmatrix}(\Delta u) \\ y &= \begin{bmatrix} x \\ 0 \end{bmatrix} & + \begin{bmatrix} 0 \\ I \end{bmatrix}(\Delta w) \end{cases}$$

We treat the scaling terms X_w and X_u as positive scalar values for simplicity. However, they can be used in matrix form as well. Based on this scaling, we can manipulate the γ variable. Notice that $A_{FI}(x) = f(x)$ and $R_{FI}(x) = x^2$ are not affected by the scaling factors. With scaling, (4.7) becomes

$$\gamma \geq \frac{X_u}{X_w} \sqrt{\frac{G_1 G_1^T}{G_2 G_2^T}} \quad (4.8)$$

The γ that achieves equality in (4.8) represents γ_{min} , the smallest possible γ for a valid solution. We want to satisfy the L_2 expression:

$$\|x\|^2 + \|u\|^2 \leq \gamma^2 \|w\|^2 \quad (4.9)$$

Now, we can substitute γ_{min} from (4.8) into (4.9) to obtain

$$\|x\| \leq \left(\frac{X_u}{X_w} \sqrt{\frac{G_1 G_1^T}{G_2 G_2^T}} + \epsilon \right) \|\Delta w\| \quad (4.10)$$

Here, the ϵ is a non negative value. This completes the design tools necessary to solve the linear problem.

We apply the controller $u = -G_2^T P x$ from Theorem 3.2.2. Notice that the linear controller that we applied here is a linearization of the full nonlinear controller in Theorem 3.2.1.

4.3 Nonlinear FI Problem Solution

With the linear solution framework laid, the nonlinear controller can be developed. As mentioned in Theorem 3.2.3, if the linear theory is satisfied, there exists a neighborhood

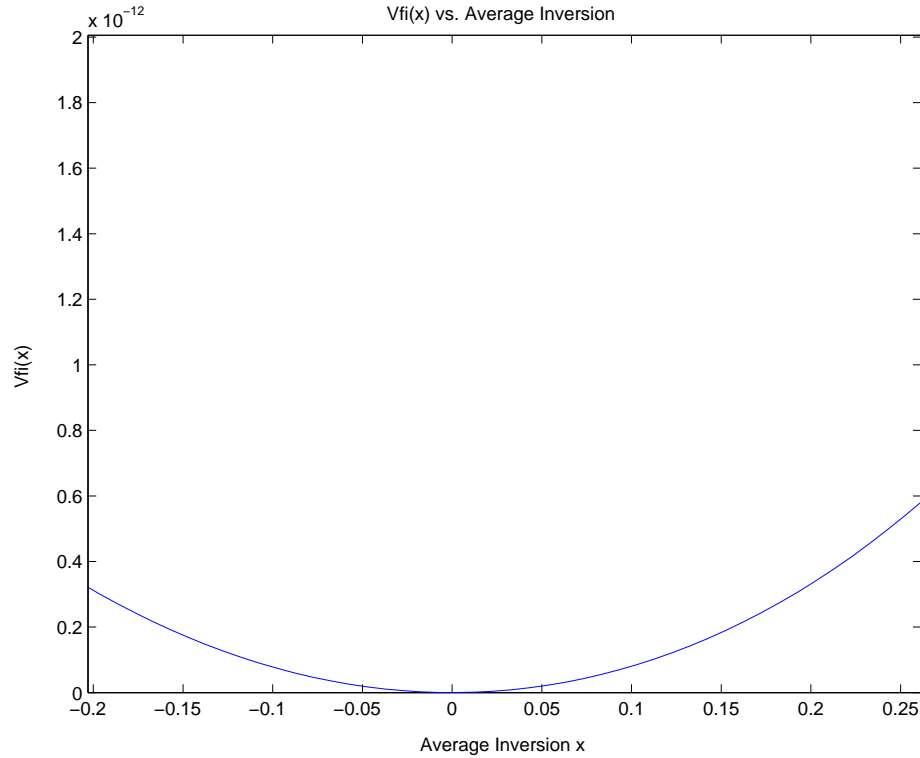


Figure 4.1: An Example of $V(x) > 0$ and $V(x) = 0$ in a neighborhood around $x_0 = 0$

about the operating point such that (4.9) is satisfied for a nonlinear controller.

We add the positive value, $0.2x^2$, to $R_{FI}(x)$ to solve the HJI (4.2) as a specific Hamilton-Jacobi Equality (HJE). To facilitate this task, we extend the work from [21] and [12] which use Taylor approximations of the nonlinear equations. It can be proven inductively that each Taylor term coefficient for $V(x)$ is calculable given the previous coefficients of $V(x)$. See Appendix A for details.

$Q_{FI}(x)$ is manipulated by increasing the γ value from its minimum value, but its multiplicative influence on $V_x(x)$ (see Theorem 3.2.1 conditions) is unclear because $V(x)$ is not known in advance. However, a few inferences can be made. First of all, we do know that since the linear part is valid, $V(x)$ will satisfy $V(x_0) = 0$ and $V(x) > 0$ at least in some region around x_0 . Figure 4.1 shows an example of $V(x) > 0$. The shape is parabolic in this region, so that $V_x(0) = 0$ and $V_x(x) < 0$ for $x < 0$, and $V_x(x) > 0$ for $x > 0$ in a neighborhood of x_0 . Figure 4.2 depicts this visually for $V_x(x)$.

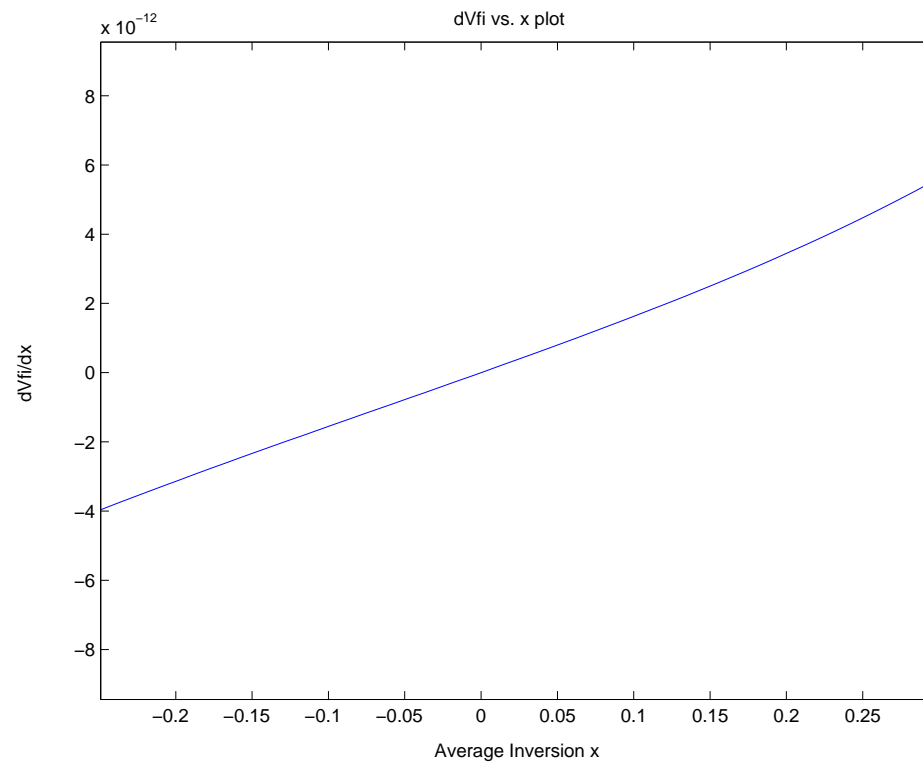
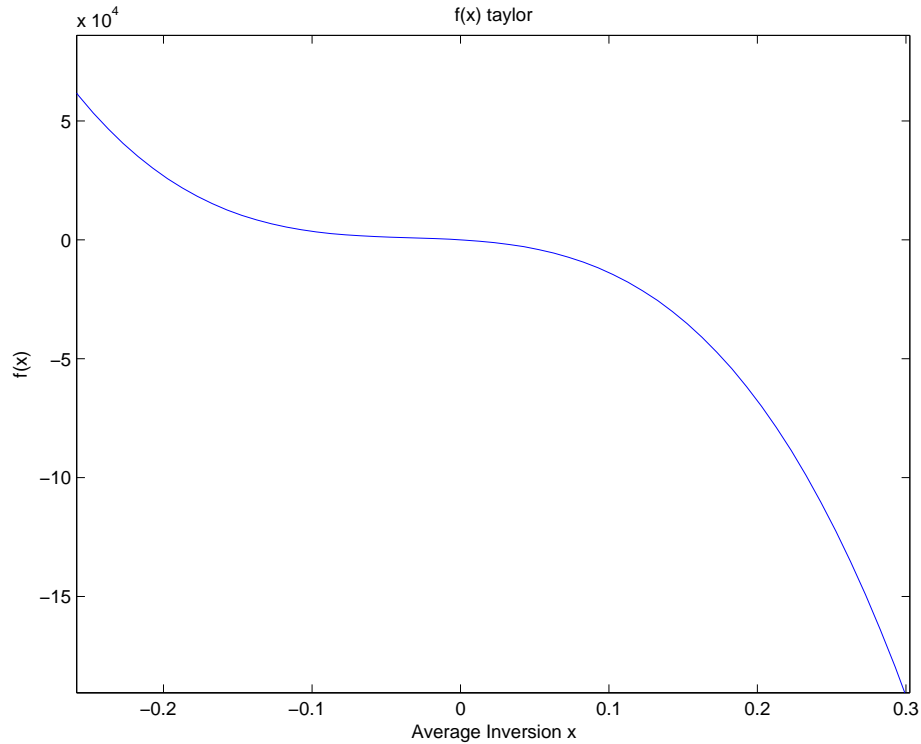


Figure 4.2: An Example of $V_x(x) < 0$ for $x < 0$ and $V_x(x) > 0$ for $x > 0$ in a neighborhood around $x_0 = 0$

Figure 4.3: $f(x)$ Has a Stable Vector Field

We have to satisfy two conditions according to Theorem 3.2.1. If we are able to find the solution of the HJI, $H_{FI}(V, x) \leq 0$, (4.2), the second condition is that

$$\dot{x} = f(x) + \frac{1}{2}Q_{FI}(x)V_x(x) \quad (4.11)$$

is asymptotically stable. The first term in (4.11), $f(x)$ has a stable vector field over the state space. If we can guarantee that the second term in (4.11) has a stable vector field, or an unstable vector field that does not have sufficient magnitude to overcome the first term, then the second condition of Theorem 3.2.1 will be satisfied. We can do this by examining the geometry of the terms over the state space.

If we can obtain a $V(x)$ that looks parabolic, all that would be necessary is to make $Q_{FI} < 0 \quad \forall x$ (assuming $\frac{1}{2}Q_{FI}(x)V_x(x)$ is stable, or of sufficiently small magnitude not to dominate $f(x)$). If we look at the structure of Q_{FI} , we can see that the first term is positive, and the second term is negative. Hence, if the second term dominates the

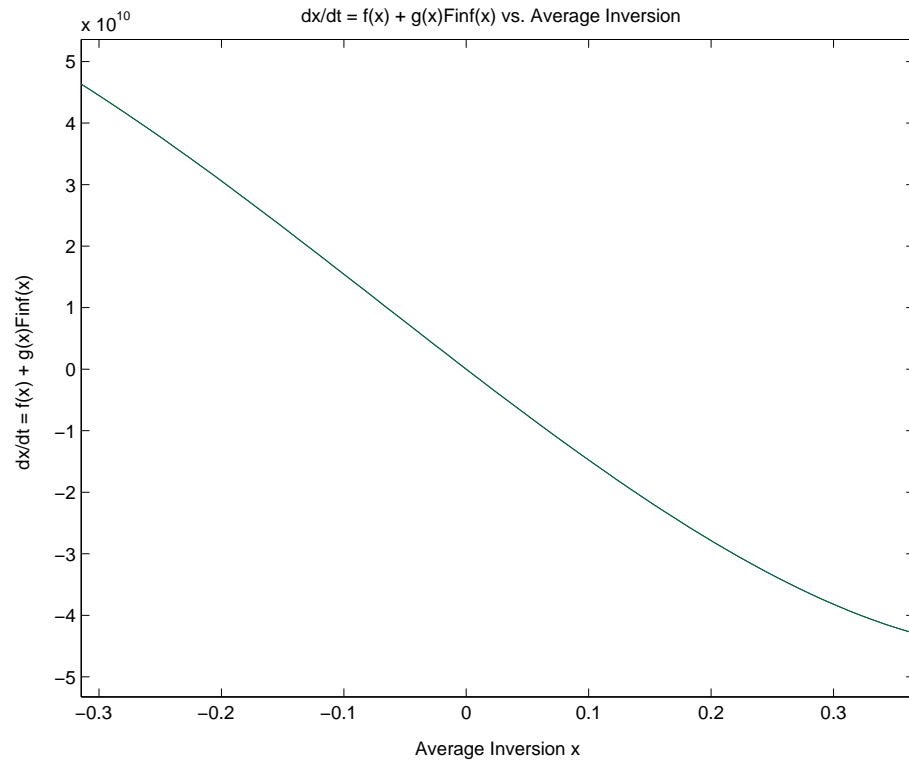


Figure 4.4: $f(x) + \frac{1}{2}Q_{FI}(x)V_x(x)$ Showing a Stable Vector Field to Satisfy Theorem 3.2.1

Condition 2

first, our objective is achieved. The final nonlinear solution, is obtained by tuning and iteration.

4.4 Simulation Results

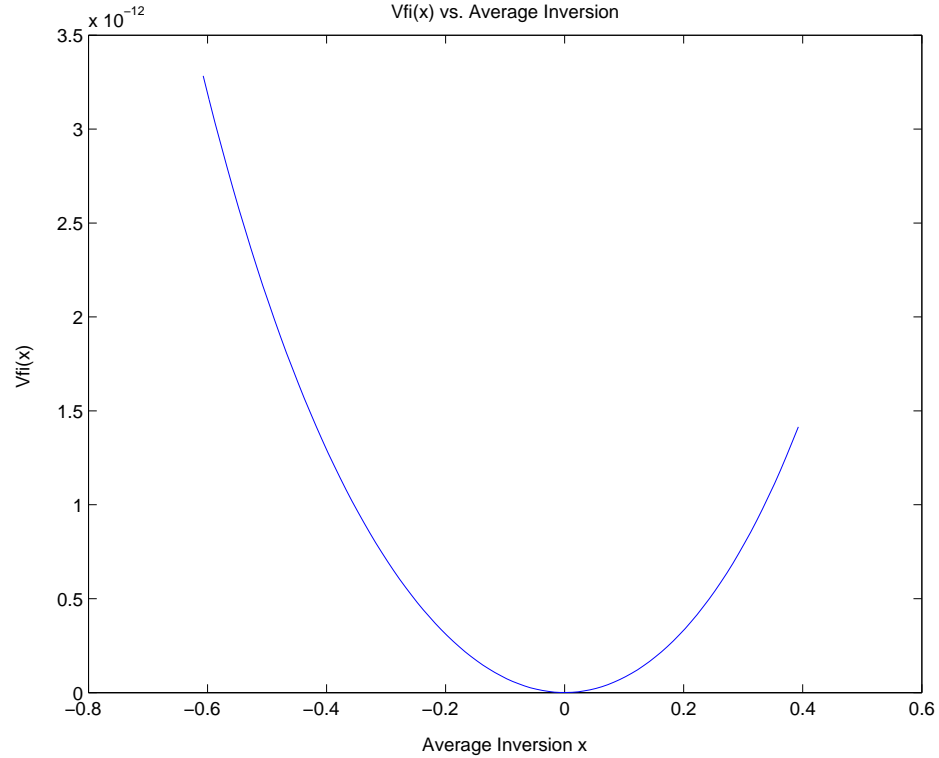
We begin with our EDFA system model, (2.14) with 32 input channels. We follow the data in Tables B.1, B.2 and B.3. We calculate the operating point, $x_0 = 0.60725$. We perform a standard nonlinear shift on the state equation to set $x_0 = 0$, $\Delta w = 0$ and $\Delta u = 0$. Our disturbance is any deviation in signal input power from that which defines the operating point.

We use the linear theory of H_∞ control as a first step in the design process. We defined scaling factors X_w and X_u on the disturbance and pump inputs, respectively, as design parameters. Here, we design for a worst case scenario so the norm of the disturbance for a 100% channel drop is equal to unity. For our system, $\|w\| = 1.8716 * 10^{15} W/J$, which gives $X_w = \frac{1}{1.8716 * 10^{15}} = 5.343 * 10^{-16}$. Thus, $\Delta w = 1$, so our x is limited directly by the L_2 gain, (4.10).

Now, we have a selection for X_w . If we denote G_1 and G_2 as the linear part of $g_1(x)$ and $g_2(x)$, then we can use (4.10) to obtain X_u such that we obtain a proper L_2 gain from $\|\Delta w\|$ to $\|x\|$. We choose a small L_2 gain, $\gamma = 10^{-8}$ and get $X_u = 1.3723 * 10^{-26}$.

By choosing the above parameters, we satisfy Theorem 3.2.2, such that our linear controller, $u = -G_2 P x$, where P is the linear term of $\frac{dV(x)}{dt}$, must yield the designed L_2 gain. Furthermore, from Theorem 3.2.3, there exists a neighborhood around the operating point such that a nonlinear controller asymptotically stabilizes the system and the L_2 gain is valid. The nonlinear controller is exactly that used in Theorem 3.2.1.

If we increase the value of γ , which decreases the amount of attenuation, we can increasingly negate $Q_{FI}(x)$, to achieve an L_2 gain over the entire nonlinear state space. So we begin increasing γ by orders of 10, until we obtain the requirements for Theorem

Figure 4.5: $V_{FI}(x)$ versus Average Inversion

3.2.1. An excellent choice of γ is provided if we choose $\gamma = 10^{-4}$. The intermediate functions are presented in figures 4.5 - 4.8.

In figure 4.5, we see that $V_{FI}(x) \geq 0$ for all x and $V(0) = 0$ which satisfies the first condition of Theorem 3.2.1. Correspondingly, $V_x(x)$ obtains the shape of an unstable vector field as depicted in figure 4.6. As described previously, if we obtain a negative $Q_{FI}(x)$, then its multiplication with $V_x(x)$ will generate a stable looking vector field which would be sufficient to satisfy condition 2 of Theorem 3.2.1. Figure 4.7 shows $Q_{FI}(x) < 0$ is obtained for any average inversion value. A final verification to see that condition 2 of Theorem 3.2.1 is presented in figure 4.8. We can see that our vector field is stable from visual inspection, and as such, we know that we have satisfied all of the requirements of Theorem 3.2.1.

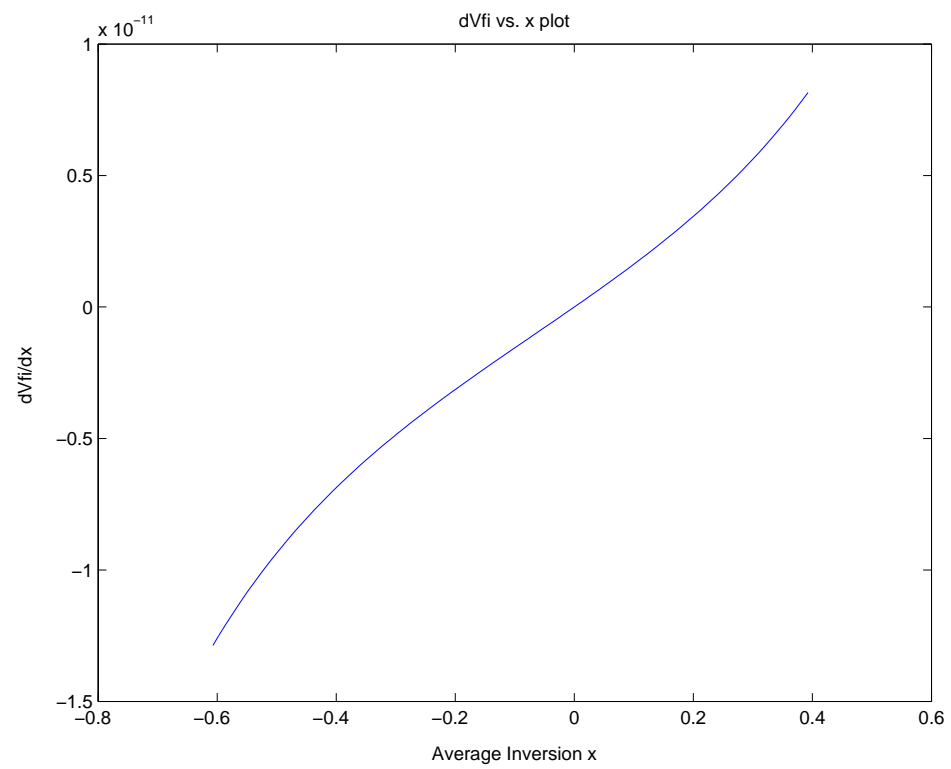
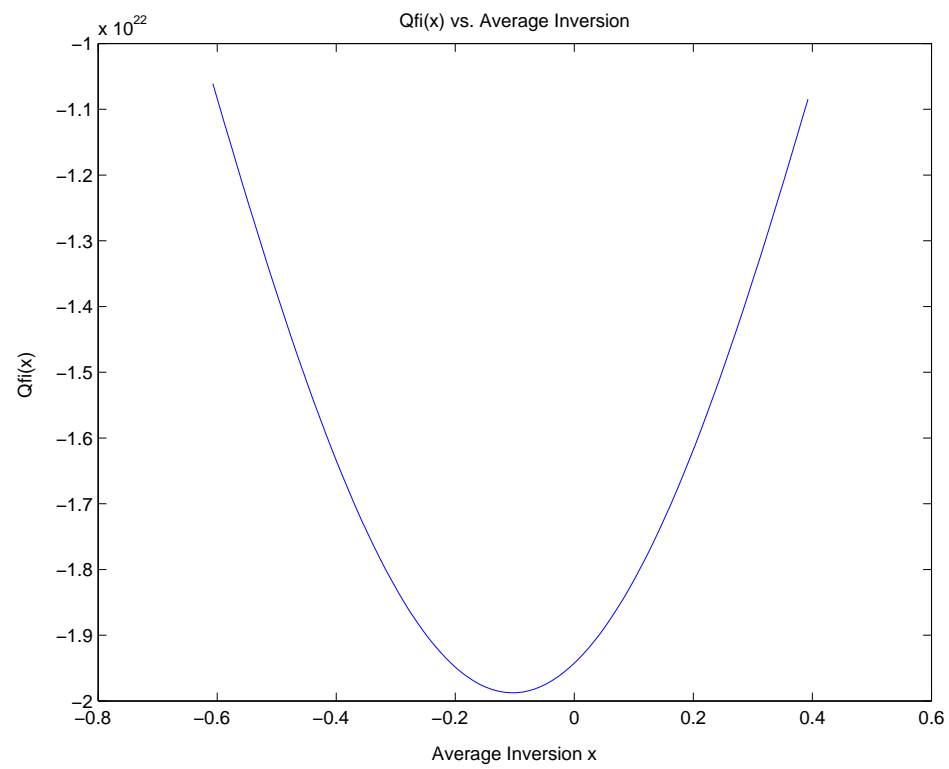


Figure 4.6: $\frac{\partial V_{FI}}{\partial x}(x)$ versus Average Inversion

Figure 4.7: $Q_{FI}(x)$ versus Average Inversion

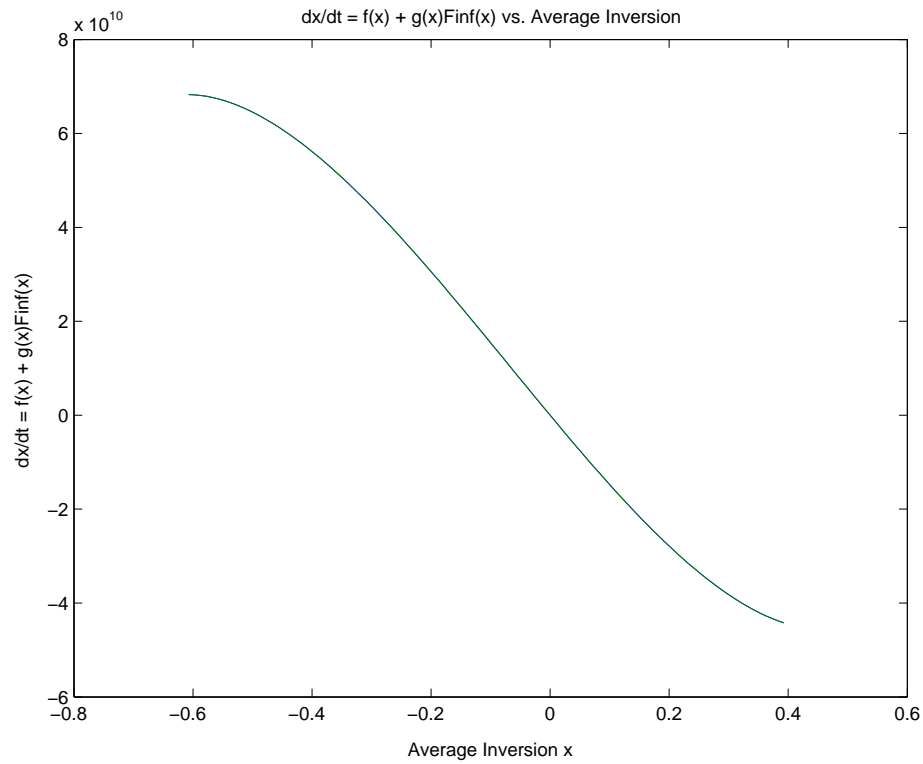


Figure 4.8: $f(x) + \frac{1}{2}Q_{FI}(x)V_x(x)$ Showing a Stable Vector Field to Satisfy Theorem 3.2.1
Condition 2

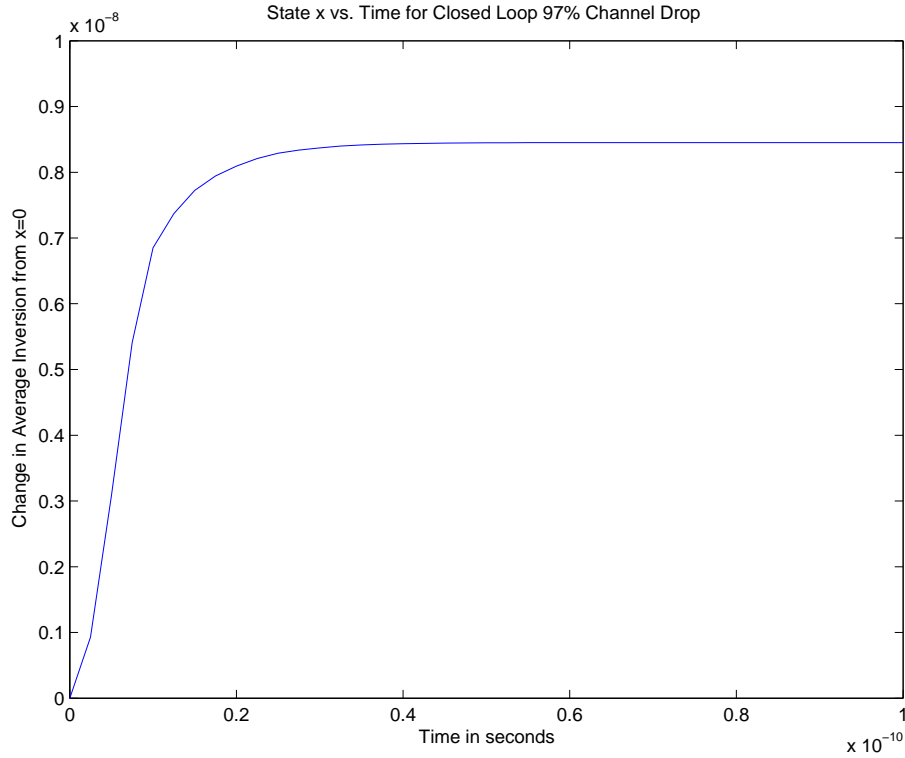


Figure 4.9: Closed Loop System Response of x for 97% channel drop.

The final controller used is:

$$\begin{aligned}
 u = & -1.0954x + 3.4235(10^{-6})x^2 + 2.8757(10^{-5})x^3 \\
 & - 1.0932(10^{-4})x^4 - 9.3091(10^{-4})x^5 \\
 & + 8.9275(10^{-1})x^6 + 1.5442x^7
 \end{aligned} \tag{4.12}$$

Notice that in this particular case, the linear term of the controller dominates the higher order terms since we chose to restrict our state x very tightly. The controller, however, is not necessarily linear for higher values of L_2 gain. For the worst case channel drop, the pump power does not exceed $150mW$ from the operating point value. For our chosen L_2 gain, the pump would operate on an extremely small time scale.

We see in Figure 4.9 that the output power is virtually constant. Notice, however, that since the value x changes so little, the system is still in the linear region. In a real-world application, we could only achieve a performance within hardware limits. We

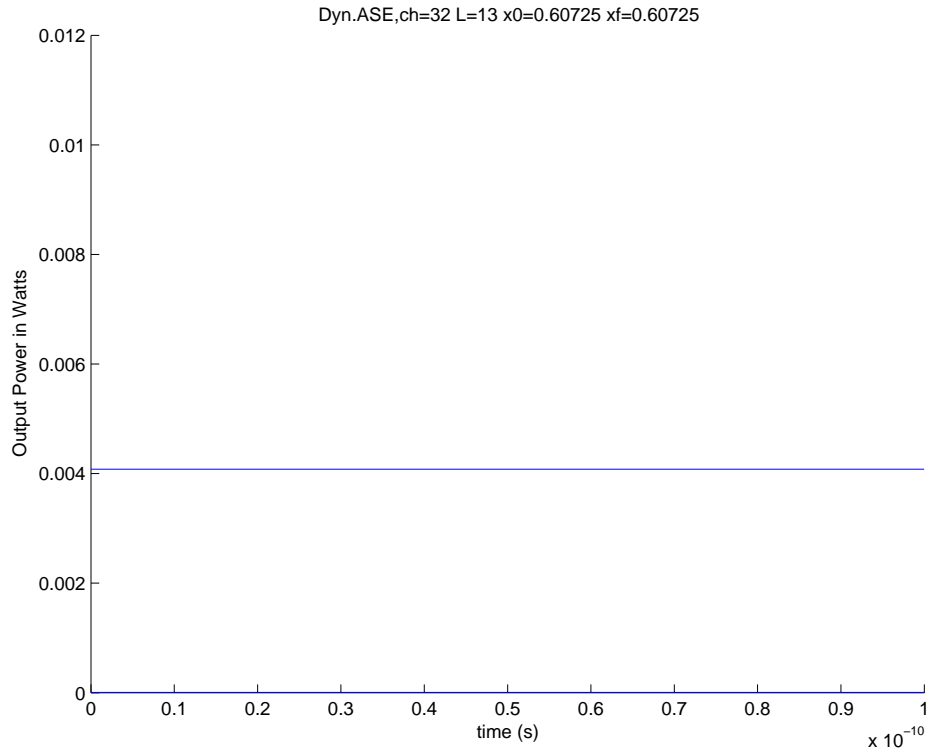


Figure 4.10: Closed Loop System Output Response for 97% channel drop.

could design a controller that operates on a slower time scale at the cost of increasing the L_2 gain. The simulations of these cases yield highly nonlinear controllers where the pump power and response times are very reasonable. Examples are presented in Chapter 5.

On a final note, the above simulations were computed using a Taylor approximated controller for lack of an explicit control function. The approximate controller was computed using Taylor approximations for the system terms. Figure 4.11 depicts the differences between the explicit $f(x)$ term and the Taylor approximated $f(x)$ term for three polynomial terms. We see that the difference can be large away from the operating point. When computing the controller the full $f(x)$ term would generate a more accurate control expression. This is a draw back in using approximation that can not be avoided due to the lack of methodology to solve the HJE explicitly. Future work to find an explicit solution to the HJE would eliminate the need for any approximations. Also, if necessary, one

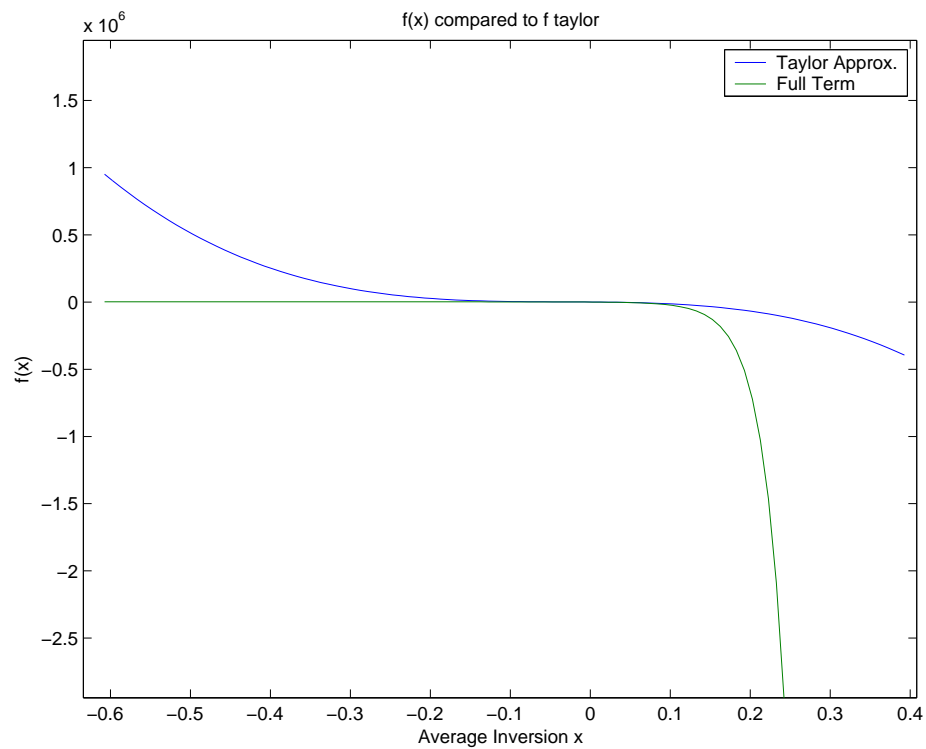


Figure 4.11: $f(x)$ vs. Taylor Approximation to $f(x)$

could increase the number of Taylor terms to increase the accuracy of the approximation.

Chapter 5

Gain Scheduling and L_2 Control Comparison

An overview of gain scheduling is introduced to provide a conceptual understanding of the control scheme goals. Gain scheduling design using PID controllers is then reproduced from [10]. Next, An L_2 nonlinear controller based on real-world pump constraints is derived. Simulations of the transient performances of both of the controlled systems are compared and contrasted in the final section.

5.1 Gain Scheduling Overview

The premise of gain scheduling is to schedule linear controllers based on pre-specified measurable scheduling variables. Given a general nonlinear system, we would choose a number of operating points over which our device would operate. At each operating point, we would linearize the system, and apply standard linear control techniques to achieve a desired response. Of course, the linear controllers would only be valid in a small neighborhood around the operating points. A global scheduler would then decide upon which controller to use based on the chosen scheduling variables. However, as opposed to an abrupt switch in control, usually interpolation or global linear control

representation is used as controllers between operating points.

The methodology to implement gain scheduling is still relatively based around ad hoc methods as there are no complete theories to guarantee that the scheduling scheme will be stable or operate as designed [29]. One good example of this is the reliance on "slow scheduling variables" [29][10]. If one chooses to use scheduling variables that vary too quickly we may not satisfy the design constraints[10], and in fact, we may generate a totally unstable response. Even now, the only sure method of verification is to run through a series of rigorous tests to ensure a desired behaviour. Never the less, gain scheduling provides a systematic structure to control scheduling despite the lack of theoretical analysis of the methodology.

A introductory level tutorial and step by step implementation of gain scheduling design is presented in [29]. Furthermore, a full practical implementation of gain scheduling on a missile is discussed in [30]. A novel implementation of gain scheduling on an EDFA is presented in [10]. The methodology involves the linearization of the EDFA system model derived in [7] and the derivation of a PID control law independent of the open loop pole of the linearized system. As such, no interpolation is required since the exact linear control law for any operating point is obtainable. This approach is introduced in later chapters as a base comparison to the L_2 nonlinear control design. Gain scheduling is an ideal candidate for comparison since it uses linearization techniques like in industry, but it has the added layer of systematic scheduling.

5.2 Gain Scheduling Design

The control scheme outlined in [10] is reproduced for clarity since it will serve as the baseline reference of comparison against the L_2 nonlinear control design. The design objectives and restraints on the gain scheduled PID controller are outlined first. Next, the linear control design from [10] is outlined. The remaining section extends the linear

control design into a gain scheduling scheme which is also from [10].

5.2.1 Design Objectives

The objective of the controller design is to keep the output power of each channel constant and to limit the settling time to less than 1 ms when up to 97% of the input power is dropped or added. The EDFA control design is considered so that the total gain, which is defined as total output power divided by total input power, remains constant after channels dropping or adding. The only real-time information available to this controller is the total input and total output powers since they are the typical measurements used in the industry at amplifier sites [1]. This differs from the L_2 nonlinear controller in that the L_2 controller does have access to the state variable. By maintaining a constant total gain, the gain and the output power of each channel should remain approximately constant.

5.2.2 Linear Control Design

For clarity, the linearized model for the EDFA based on (2.1) is restated, as described in [10]. The model was generated based on the operating conditions x^o , Q_{pump}^o , G^o , Q_k^{ino} , and Q_k^{outo} , $\forall k = 1, 2, \dots, N$. The plant was stated as:

$$\begin{aligned} \frac{dx(t)}{dt} &= A\Delta x(t) + B_1 \mathbf{Q}^{in}(\mathbf{t}) + B_2 u(t) \\ \mathbf{Q}^{out}(\mathbf{t}) &= C_1 \Delta x(t) + D_{11} \mathbf{Q}^{in}(\mathbf{t}) + D_{12} u(t) \\ y(t) &= C_2 \Delta x(t) + D_{21} \mathbf{Q}^{in}(\mathbf{t}) + D_{22} u(t) \end{aligned} \quad (5.1)$$

where each variable corresponds to the representation in Table 5.1. The output of the plant, y , is the total gain of the system. Total gain is denoted as $G(t) = \frac{Q_{total}^{out}}{Q_{total}^{in}}$, where $Q_{total}^{in}(t) = \sum_{i=1}^N Q_i^{in}(t)$ and $Q_{total}^{out}(t) = \sum_{i=1}^N Q_i^{out}(t)$.

The block diagram of the linear model of the EDFA from (5.1) is shown in Fig. 5.1.

Table 5.1: Linearized EDFA Model Parameters[10]

Notation	Expression
A	$-\frac{1}{\tau_o} \left\{ 1 + \frac{\tau_o}{S\rho} \sum_{k=1}^N Q_i^{ino} \exp[((g_k + \alpha_k)x^o - \alpha_k)L](g_k + \alpha_k) \right\}$
B_1	$B_1(k, 1) = \frac{Q_k^{ino} - Q_k^{outo}}{Q_k^{ino} S L \rho}, \forall k = 1, 2, \dots, N$
B_2	$\frac{1}{S L \rho}$
C_1	$C_1(1, k) = Q_k^{outo} (g_k + \alpha_k) L, \forall k = 1, 2, \dots, N$
D_{11}	$D_{11}(i, j) = \begin{cases} \frac{Q_i^{outo}}{Q_i^{ino}} & i = j \\ 0 & \text{otherwise} \end{cases} \quad \forall i, j = 1, 2, \dots, N$
D_{12}	0
C_2	$\frac{\sum_{k=1}^N Q_k^{outo} (g_k + \alpha_k) L}{Q_{total}^{ino}}$
D_{21}	$D_{21}(1, k) = \frac{\exp[((g_k + \alpha_k)x^o - \alpha_k)L]}{Q_{total}^{ino}} - \frac{Q_{total}^{outo}}{(Q_{total}^{ino})^2}, \forall k = 1, 2, \dots, N$
D_{22}	0
$\Delta x(t)$	$x(t) - x^o$
$\mathbf{Q}^{in}(t)$	$[Q_1^{in}(t) - Q_1^{ino}, Q_2^{in}(t) - Q_2^{ino}, \dots, Q_N^{in}(t) - Q_N^{ino}]^T$
$u(t)$	$Q_{pump}(t) - Q_{pump}^o$
$\mathbf{Q}^{out}(t)$	$[Q_1^{out}(t) - Q_1^{outo}, Q_2^{out}(t) - Q_2^{outo}, \dots, Q_N^{out}(t) - Q_N^{outo}]^T$
$y(t)$	$G(t) - G^o$

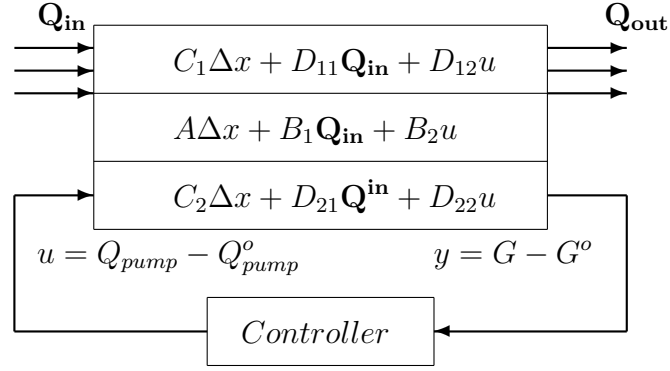


Figure 5.1: Conceptual diagram of the linear model of the EDFA with an controller [10]

The transfer function from [10] is represented as:

$$\begin{aligned}
 G(s) &= \frac{K_p}{s + \omega_{OL}} \\
 K_p &= \frac{\sum_{k=1}^N Q_k^{outo}(g_k + \alpha_k)L}{SL\rho Q_{total}^{ino}} \\
 \omega_{OL} &= \frac{1}{\tau_o} \left\{ 1 + \frac{\tau_o}{S\rho} \sum_{k=1}^N Q_k^{outo}(g_k + \alpha_k) \right\}
 \end{aligned} \tag{5.2}$$

where ω_{OL} is the open loop pole.

[10] applies linear control techniques to achieve the design objectives around an operating point. Frequency domain design along with the root locus method yielded the following PID controller[10].

$$PID : K_{PID}(s) = K_r \frac{(1 + \tau_1 s)(1 + \tau_2 s)}{\tau_1 s(1 + 0.1\tau_2 s)} \tag{5.3}$$

where the values of τ_1 , τ_2 and K_r are provided in Table 5.2. τ_1 and τ_2 were designed using frequency domain analysis such that a minimum phase margin of 50 degrees was provided. Furthermore, [10] chooses to place the closed loop poles far away from the origin at $7.6\omega_{OL}$, $7.6\omega_{OL}$, and $491\omega_{OL}$, which generates a short settling time. The resultant parameter values are rewritten in Table 5.2.

Table 5.2: The PID controller's parameters

Parameters	K_r	τ_1	τ_2
PID	$\frac{33.8\omega_{OL}}{K_p}$	$\frac{1}{5\omega_{OL}}$	$\frac{3}{50\omega_{OL}}$

5.2.3 Gain Scheduling Extension

The reason for implementing gain scheduling is that one linearized controller is not sufficient to properly control the EDFA system, (2.1). The EDFA system is highly nonlinear in nature, meaning that the Jacobian at various operating points can change significantly, even for small regions in the state space. Hence, it becomes necessary to schedule multiple controllers based on the current operating point. From the work developed in [10] in the previous subsection, a controller that is described based on any operating point already exists. As such, interpolation is not necessary. The predefined scheduling methodology from [10] is restated.

The parameters $Q_k^{in}(t)$, $Q_k^{out}(t)$ and x are not available for this control law, so [10] derives estimates on the plant parameters K_p and ω_{OL} based on $Q_{total}^{in}(t)$, $Q_{total}^{out}(t)$ and $G(t)$. These variables make possible to calculate an approximate representation of a linearized plant at different operating values. The expressions are stated as [10]:

$$K_p = \frac{\overline{g + \alpha\rho}G^o}{S} \quad (5.4)$$

$$\omega_{OL} = \frac{1}{\tau_o} \left\{ 1 + \frac{\tau_o}{S\rho} \overline{g + \alpha} Q_{total}^{ino} G^o \right\} \quad (5.5)$$

where $\overline{g + \alpha}$ is the weighted average of N channels' $g + \alpha$ defined as:

$$\overline{g + \alpha} = \sum_{k=1}^N \frac{Q_k^{outo}}{Q_{total}^{outo}} (g_k + \alpha_k) \quad (5.6)$$

The value of (5.6) is approximated to the mean of its possible range in [10]. Hence, as seen from (5.4) and (5.5), the plant can be represented by the parameters, $Q_{total}^{in}(t)$ and $G(t)$. These are the scheduling variables used in [10]. They determine the controller

to use in every given situation. The resultant nonlinear controller from [10] is:

$$\begin{aligned} \dot{x}_c &= f(x_c(Q_{total}^{in}, G), u_c(Q_{total}^{in}, G), Q_{total}^{in}, G) \\ y_c &= g(x_c(Q_{total}^{in}, G), u_c(Q_{total}^{in}, G), Q_{total}^{in}, G) \end{aligned} \quad (5.7)$$

Gain scheduling is not an exact methodology in that it relies heavily on trial and error. Specifically, performance and stability are not known explicitly before implementation. Currently, only experimentation can determine if gain scheduling accomplishes its intended goal. The results described here from [10] satisfy their objective.

Another problem encountered in [10] involves fast changing parameters, $Q_{total}^{in}(t)$ and $G(t)$. Through experimentation, [10] determines that the above control design is prone to failure on its own. Instant switching can cause the gain scheduling controller to switch intensively to cause instability. A remedy to this situation is provided in [10] and restated below for completeness.

1. Upon detection of any change in $Q_{total}^{in}(t)$ or $G_{ref}(t)$ above certain threshold, the gain scheduling starts.
2. Define the steady state before the gain scheduling as the old state and the future steady state the system will eventually reach with the given new $Q_{total}^{in}(t)$ and $G_{ref}(t)$ as the new state. The controller designed for the old state will be used for the next 200 μs .
3. After 200 μs , an intermediate controller is created from linearly time-weight interpolating the τ 's and the K_r of the two controllers for the old and new states in the next 800 μs . This is equivalent to (5.8), where t is the time (in μs) measured 200 μs after the gain scheduling starts.

$$\begin{aligned} \tau &= \frac{t}{800}\tau_{new} + \frac{800-t}{800}\tau_{old} \\ K_r &= \frac{t}{800}K_{rnew} + \frac{800-t}{800}K_{roid} \end{aligned} \quad (5.8)$$

4. After linear time-weight interpolation (i.e. 1 ms after the scheduling starts), the controller for the new state is left to operate until another change is detected.

With the above modification in place, the PID controllers under gain scheduling function as intended. This control scheme is used to control the EDFA model (2.1) according to the design constraints outlined.

5.3 L_2 Control Design

The design objectives are outlined, taking note that the system outputs and the control objectives are modified from the PID gain scheduling case [10]. The controller is derived following the methodology outlined in Chapter 4. The controller is made to reflect the real-world situation where the reaction time of the pump is limited.

5.3.1 Design Objectives

In the case of L_2 nonlinear control scheme, we control the average inversion since we can compute this in real-time using the input and output power measurements of a specific channel. Moreover, from (2.14), by keeping the average inversion constant, we will keep the output powers of each channel constant.

An upper performance bound must be set for the controller. From experimentation, between 1 to 10 microseconds should be sufficient for a pump to deliver a significant amount of power to the Erbium Doped fiber. Accordingly, any controller design should yield a transient pump signal that does not violate generating a large power change faster than the above specified time period.

5.3.2 L_2 Controller Design with Parameters Constrained to Physical Limitations

We will now outline the fundamental design constraints for the nonlinear L_2 controller. In the case of the EDFA, the main constraint is the pump's ability to deliver power over a specified time scale. By simulation, we discovered that a nonlinear L_2 gain of 0.03 would yield an approximate $15\mu s$ response time for the pump. The design involves choosing the scaling terms X_w and X_u such that they give an L_2 gain equal to 0.003 for the linearized system, and then increasing the L_2 gain to 0.03 to satisfy the nonlinear conditions.

We begin with our EDFA system model, (2.14), and calculate the operating point based upon the data provided in Tables B.1, B.2 and B.3. We calculate the the operating point, $x_0 = 0.60725$ for 32 channels and $x_0 = 0.68337$ for 2 channels. We perform a standard nonlinear shift on the state equation to set $x_0 = 0$. Note, we also get $\Delta w = 0$ and $\Delta u = 0$ to represent the signal input powers and pump input powers that define the operating point.

We use the linear theory of H_∞ control as a first step in the design process. We choose the scaling factors X_w and X_u on the disturbance and pump parameters, respectively. Here, we design for a worst case scenario, so we scale the norm of the disturbance for a 100% channel drop to equal unity. For our system, we calculate $\|w\| = 1.8716 * 10^{15}$ for 32 channels, and $\|w\| = 4.6447 * 10^{14}$ for 2 channels. We calculate $X_w = \frac{1}{\|w\|}$. Thus, $\Delta w = 1$, so our x is limited directly by the L_2 gain.

If we denote G_1 and G_2 as the linear part of $g_1(x)$ and $g_2(x)$, then we can use (4.10) to obtain X_u . We choose the L_2 gain, $\gamma = 0.003$ and get $X_u = 4.1169 * 10^{-21}$ for 32 channels and $X_u = 4.2555 * 10^{-21}$ for 2 channels. From [14] we know that there exists a neighborhood around the operating point such that a nonlinear controller is asymptotically stable.

If we increase the value of γ , which decreases the amount of attenuation, we can

increasingly negate $Q_{FI}(x)$ to achieve an L_2 gain over a larger neighborhood. So we increase γ until we obtain the requirements for Theorem 3.2.1. Our conditions are satisfied if we choose $\gamma = 0.03$. We do not need to obtain a global solution to the L_2 control problem, since simulations show that the controller functions properly in the worst case channel drop. The final controllers used are:

$$\begin{aligned} u_2 &= -9.8909(10^{-1})x + 1.7115x^2 + 1.2308(10^1)x^3 - 2.51(10^2)x^4 \\ &\quad - 1.8283(10^3)x^5 + 1.4708(10^3)x^6 + 4.4092(10^3)x^7 \end{aligned} \quad (5.9)$$

$$\begin{aligned} u_{32} &= -1.0237x + 7.8867(10^{-1})x^2 + 3.1106x^3 - 9.95(10^1)x^4 \\ &\quad - 6.8735(10^2)x^5 + 2.6259(10^2)x^6 + 7.586(10^2)x^7 \end{aligned} \quad (5.10)$$

5.4 Gain Scheduling and L_2 Control Simulation Comparison

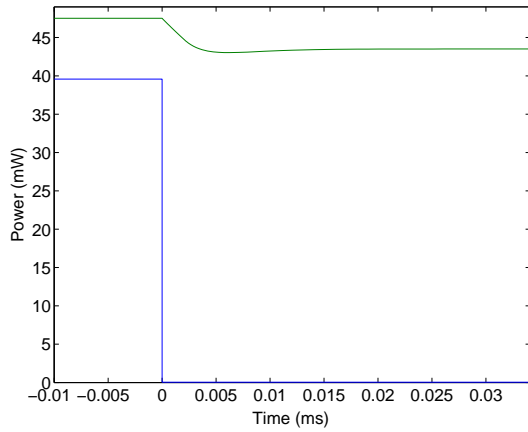
The channel numbers and their input powers are shown in Table B.1. The parameter data for the EDFA is listed in Table B.2. The signal and pump wavelengths with absorption and emission ranges are provided in Table B.3.

We will simulate a 50 percent drop in both the 2 channel case and the 32 channel case. In addition, an extreme power drop of 97 percent will be simulated for the 32 channel case. The channels with the lowest wavelengths are always dropped.

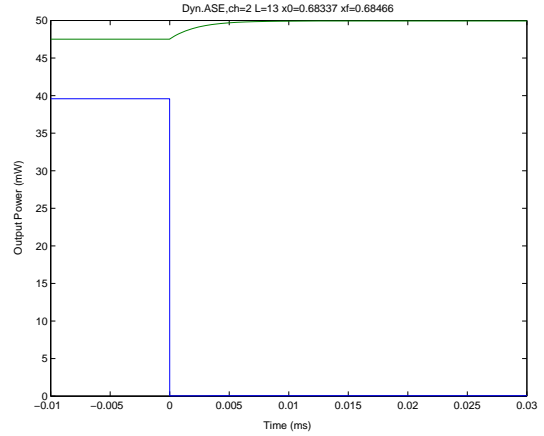
The simulation results for these three cases are presented on Fig. 5.2, Fig. 5.3 and Fig. 5.4 respectively, for both PID [28] and L_2 control. Note that the channels are dropped at $t = 0$ seconds.

5.4.1 Simulation Results Analysis

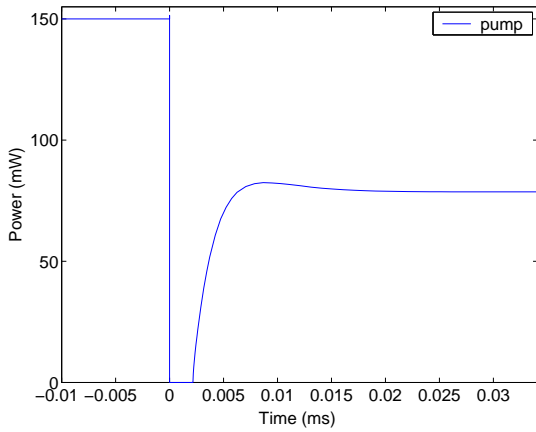
In all three simulated situations, the L_2 nonlinear controller clearly outperforms the gain scheduled PID controller as shown in Fig. 5.2, Fig. 5.3 and Fig. 5.4. With the L_2



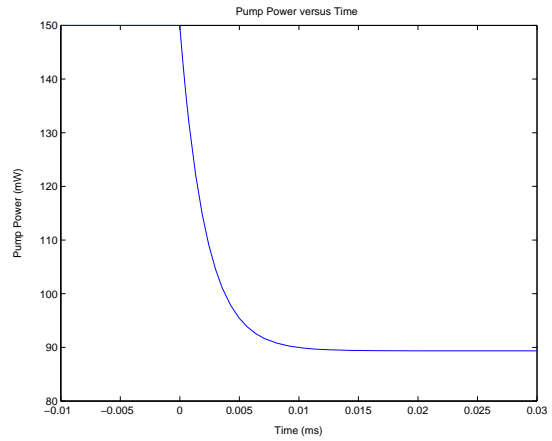
(a) p^{out} of the two channels with the gain scheduled PID controller



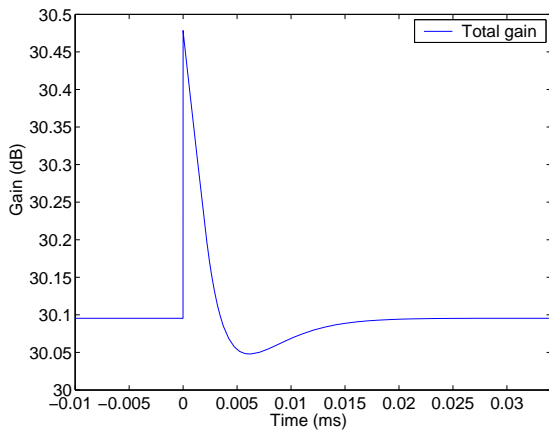
(b) p^{out} of the two channels with the L_2 non-linear controller



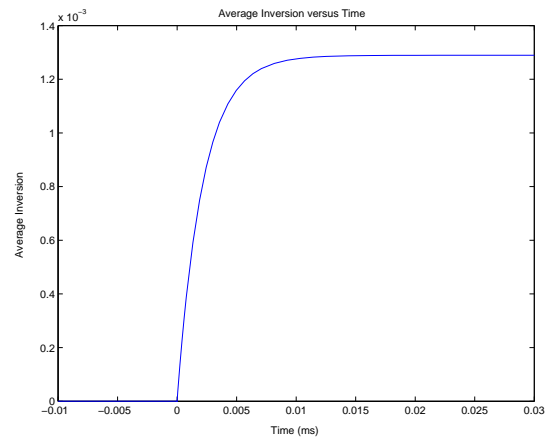
(c) p_{pump} with the gain scheduled PID controller



(d) p_{pump} with the L_2 nonlinear controller

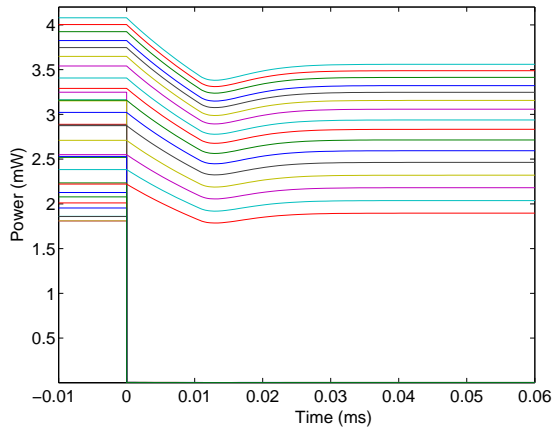


(e) total gain, G , with the gain scheduled PID controller

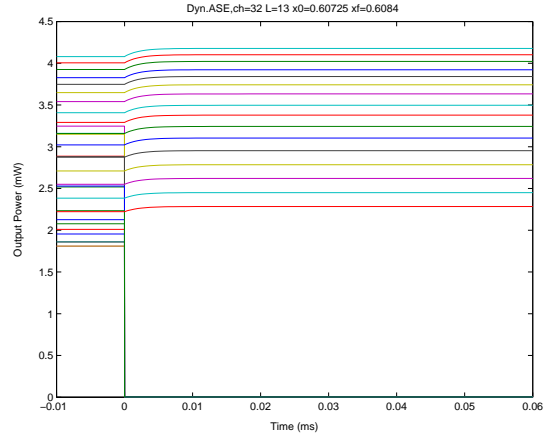


(f) average inversion level, x , with the L_2 non-linear controller

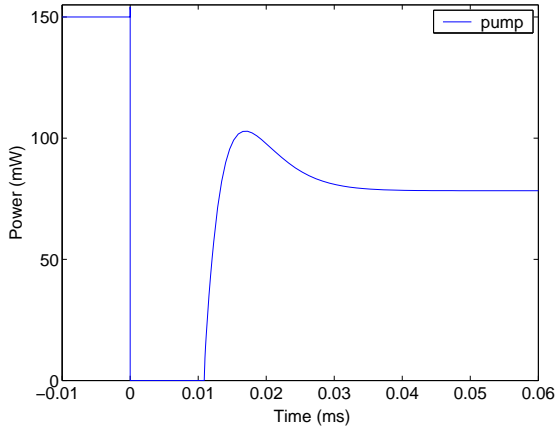
Figure 5.2: System response with one channel dropped from two channels



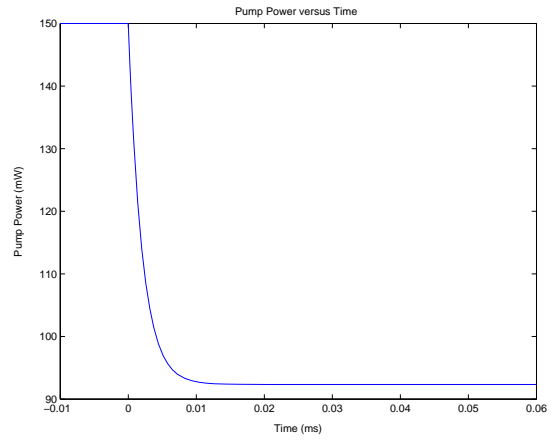
(a) p^{out} of the 32 channels with the gain scheduled PID controller



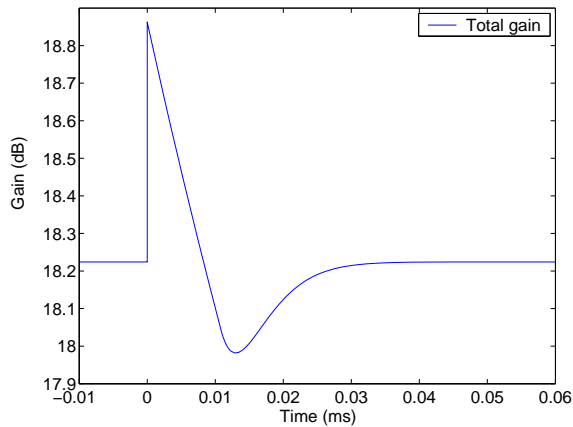
(b) p^{out} of the 32 channels with the L_2 nonlinear controller



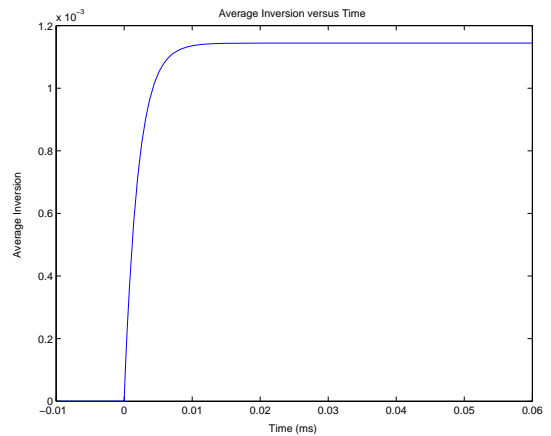
(c) p_{pump} with the gain scheduled PID controller



(d) p_{pump} with the L_2 nonlinear controller

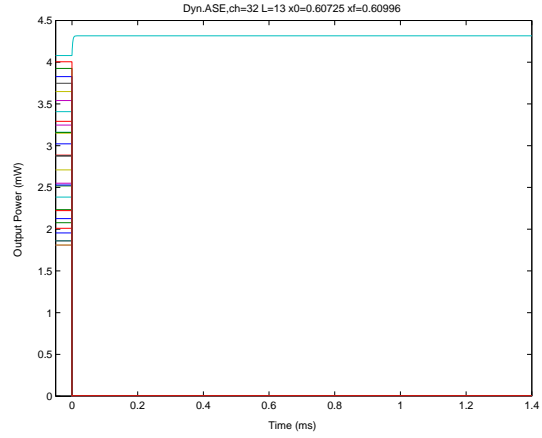
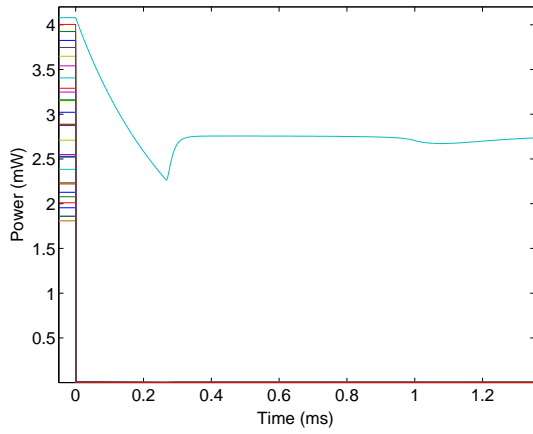


(e) total gain, G , with the gain scheduled PID controller



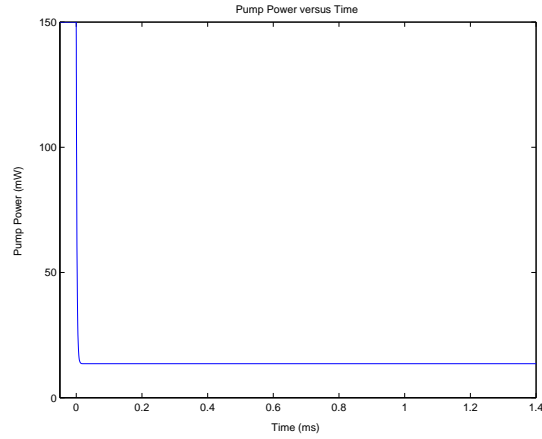
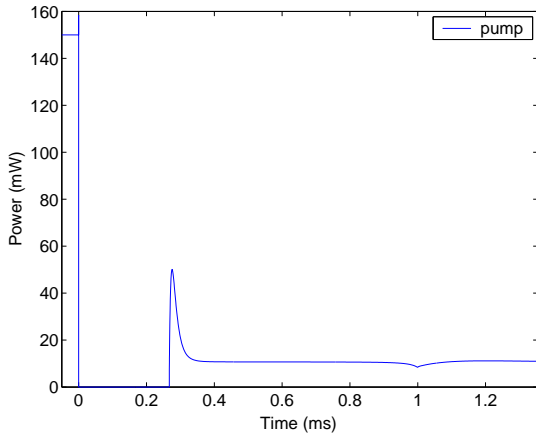
(f) average inversion level, x , with the L_2 nonlinear controller

Figure 5.3: System response with 16 channel dropped from 32 channels



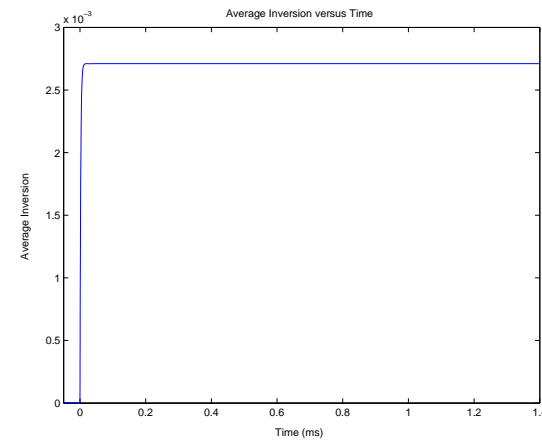
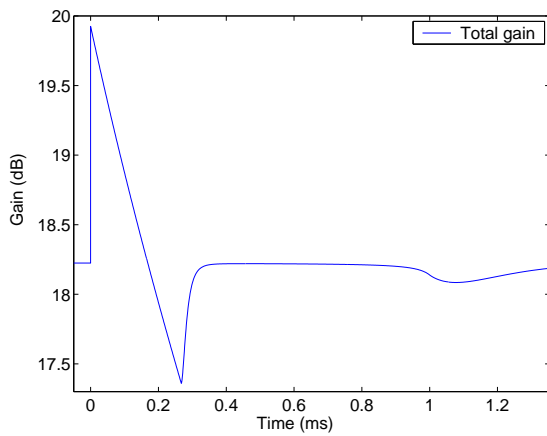
(a) p^{out} of the 32 channels with the gain scheduled PID controller

(b) p^{out} of the 32 channels with the L_2 nonlinear controller



(c) p_{pump} with the gain scheduled PID controller

(d) p_{pump} with the L_2 nonlinear controller



(e) total gain, G , with the gain scheduled PID controller

(f) average inversion level, x , with the L_2 nonlinear controller

Figure 5.4: System response with 31 channels dropped from 32 channels

nonlinear controller, the system has shorter transient time ($15 \mu\text{s}$ compared with $20 \mu\text{s}$ up to 1.2 ms for the scheduled PID controller) and much smoother response. On the contrary, the system with the gain scheduled PID controller generates spikes in the total gain and the pump power at the instance of channels dropping. This is because the PID controller acts upon the change of the total gain, which varies instantaneously when the input channels drop. Notice the pump power stays at zero for a short period in the PID controlled cases to reduce the average inversion as fast as possible.

Two more observations can be made from the simulation results. First, it should be noted that the L_2 nonlinear controller yields similar responses whereas the scheduled PID controller shows great variation. This is evident in Fig. 5.4. The response of the L_2 nonlinear controller is identical to the other two (Fig. 5.2 and Fig. 5.3). The open loop pole of the plant with only one input channel is much smaller than the previous plant with 32 input channels which causes longer transient time and less smooth response in the PID control. Also, the designed controllers are disparate so the response is not as smooth. Secondly, the final values of the pump power and channel output power are different in the two control schemes. This is reasonable because the objective of the scheduled PID controller is to clamp the total gain, whereas the L_2 nonlinear controller tries to minimize the change of the average inversion, x . The channel output powers are vastly different from the initial values in the gain scheduled PID cases because the total gain is the weighted average of the channel gains.

5.4.2 Extreme Case for Gain Scheduled PID Control

There are two major drawbacks for the gain scheduled PID controller design. The first drawback is the response time is limited by the open loop pole of the plant. The second drawback is the estimation error of the open loop pole and the gain of the plant may result in large error.

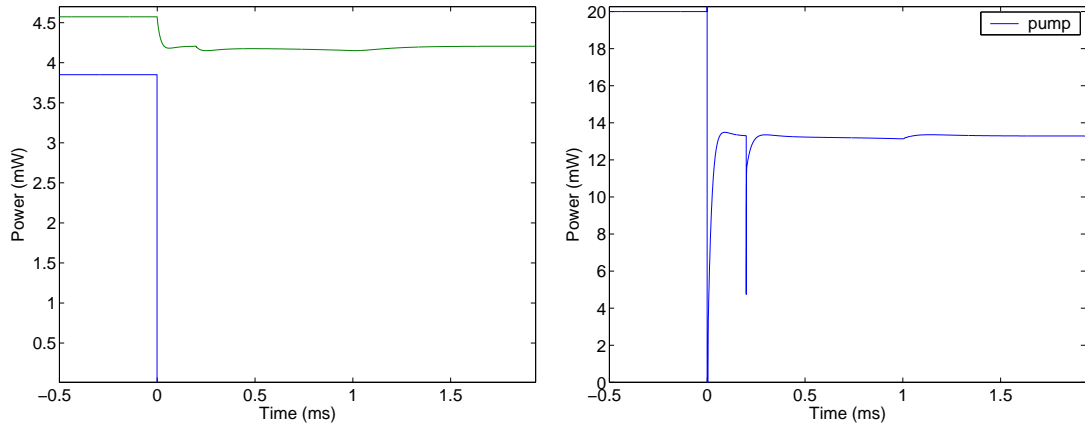
An extreme case where both flaws happen at the same time is simulated. To show

the effect of a small open loop pole of the plant, a pump power of 20 mW is used to amplify two input channels with 42.6 μ W each. A 100% error is intentionally included in the approximation of the open loop pole and the gain of the plant. The pole is estimated smaller and the gain is estimated higher. All the other parameters are the same as before. The simulation results are shown on Fig. 5.5. The performance of the system is less desirable in comparison with Fig. 5.2. The settling time for the simulation on Fig. 5.2 is less than 0.03 ms, whereas the settling time for the current simulation is 1.5 ms. There are also two spikes in the pump power and a patchy curve in the total gain graph corresponding to the changes of the controller in the gain scheduling process. However, the controller still manages to stabilize the system and clamp the original total gain value.

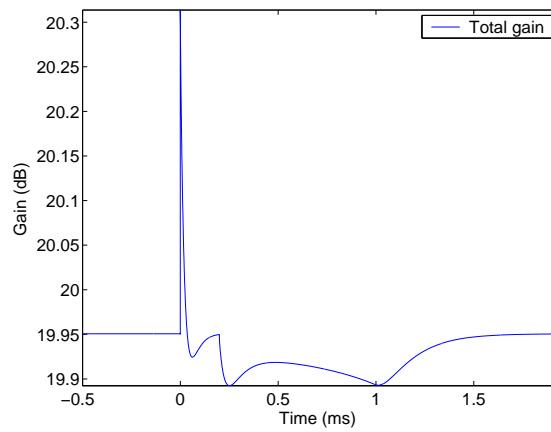
5.4.3 Extreme Case for L_2 Control

There can be potential pitfalls in designing a nonlinear L_2 controller that does not globally satisfy all of the conditions of Theorem 3.2.1. We will now show a case involving 32 input channels with an L_2 gain $\gamma = 0.1$, which is less restrictive on the state than before, and 97% percent drop. We satisfy the conditions of Theorem 3.2.1 within a neighborhood of the operating point but not globally.

The simulation of the 97% drop case yields an unexpected result (Fig. 5.7). The average inversion increases dramatically by changing more than 0.3, which violates the chosen L_2 gain. The reason for this response is that the 97% drop causes a large change in the average inversion such that the state variable leaves the neighborhood around the operating point where the conditions of Theorem 3.2.1 are valid. A simple check would be to test the worst case scenario, which is a 100% channel drop in this case, and verify if the L_2 gain is still satisfied.

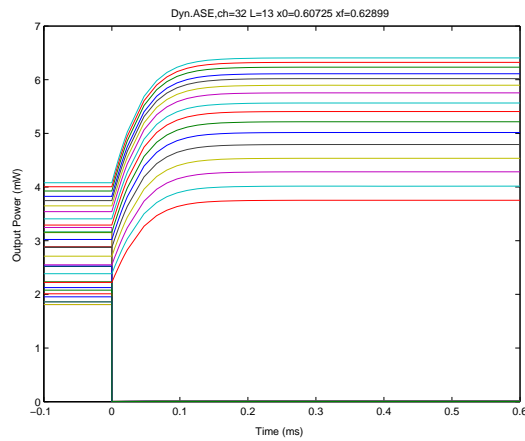


(a) p^{out} of the two channels with the gain scheduled PID controller (b) p_{pump} with the gain scheduled PID controller

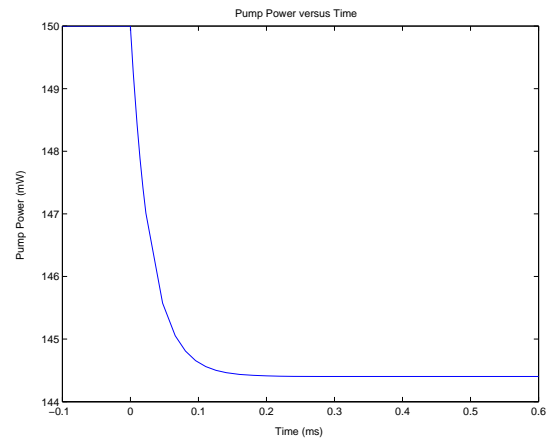


(c) total gain, G , with the gain scheduled PID controller

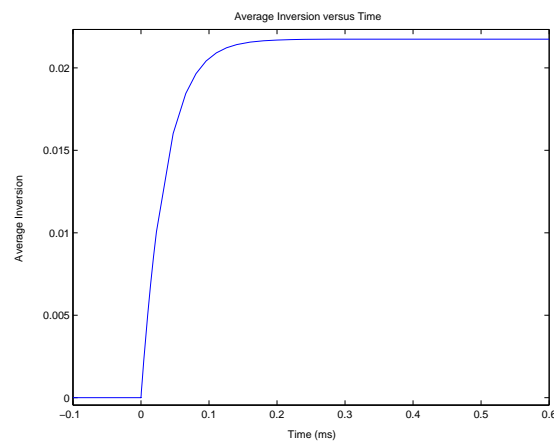
Figure 5.5: System response with one channel dropped from two channels with 20mW pump power and 100% estimation error



(a) p^{out} of the 32 channels with the L_2 controller

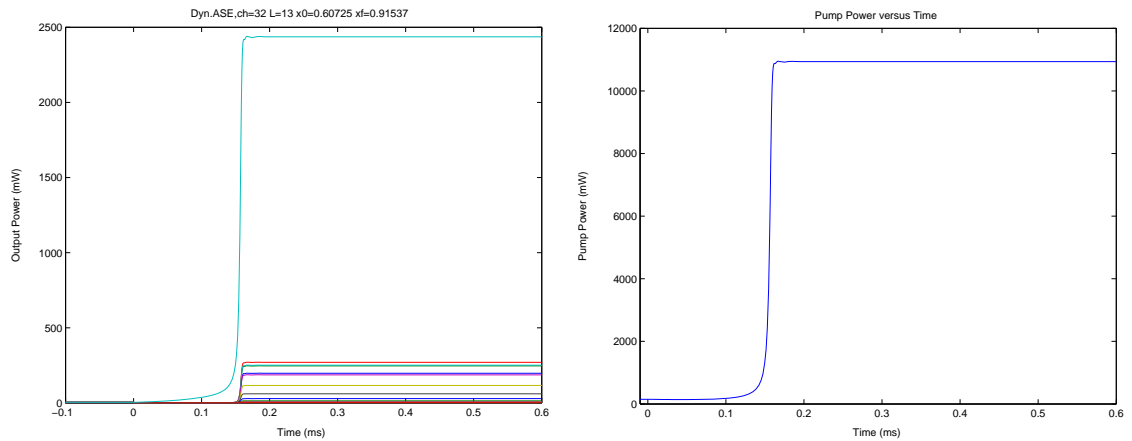
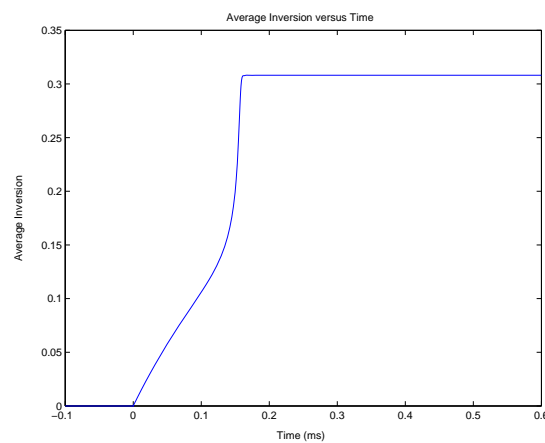


(b) p_{pump} of the L_2 Controller



(c) Average inversion over time

Figure 5.6: Extreme 32 Channel Case with High L_2 Gain and 50 percent channel drop.

(a) p^{out} of the 32 channels with the L_2 controller(b) p_{pump} of the L_2 Controller

(c) Average inversion over time

Figure 5.7: Extreme 32 Channel Case with High L_2 Gain and 97 percent channel drop.

Chapter 6

Robustness Design

The L_2 control design developed in previous sections assumes a perfect knowledge of the state variables as well as inputs and outputs. The state variable of the EDFA system (2.14) may also not be known exactly since the state is a function of the parameters values, such as α_k and g_k , which may not be perfectly accurate. The EDFA system model with uncertainties in its parameters will be different from the physical system. Uncertainties in the system parameters can also be represented as uncertainties in the state variable, x . In fact, we can generalize a say that state uncertainty could potentially represent unknown factors outside of the model. It should also be noted that the initial operating point as calculated from EDFA system model (2.14) could be different than the physical system.

It is not simply enough to know that our system is stable. Robustness analysis allows a designer to specifically design the performance of a system despite specific types of uncertainty. We want to control the performance by limiting specific uncertainties. For highly nonlinear systems, small uncertainties can generate enormous problems. By using robustness analysis in general, we quantify uncertainty in the system.

We use the methods outlined in [15], [12], to represent input multiplicative uncertainty as a disturbance to the ideal system. Furthermore, we derive an input affine approxi-

mation to any general nonlinear function for state uncertainties. The resultant system is then used to derive a robust L_2 controller for the EDFA. A series of state and input multiplicative uncertainty cases are tested and compared to their previous non-robust counterpart.

The sections are organized as follows. First, the state uncertainty theory is derived. This is accompanied by a representation of state uncertainty in the form of parametric uncertainty for α and g . Next, we combine the results of [15], [12], and the state uncertainty with the EDFA model with ASE derived herein to produce the robust EDFA model framework. Finally, the results of different uncertainty cases are presented through various simulations.

6.1 State Uncertainty Derivation

The state in the EDFA system is extremely important for calculating the appropriate action for the nonlinear L_2 controller. Unfortunately, the state is not directly available from the system, so it must be calculated in real-time. This requires precise knowledge of the input and output power of at least one channel, along with the precise value of the EDFA parameters. In this respect, it becomes practical to model a state uncertainty, which would represent a deviation from the ideal state value as provided by the state model.

Definition 11. Let uncertainty in the state variable, x , be denoted as x_Δ

The first step is to assume this state deviation can occur in any term in our system model. We represent this as a general, nonlinear term we can call $f_{NL}(x)$. So, with state uncertainty included, we obtain $f_{NL}(x + x_\Delta)$. This representation of uncertainty is not input affine since it is in the context of a general nonlinear function. However, it is necessary to adhere to the same structure as (3.6). We can approximate the term using

a Taylor expansion about a point, $x = a$,

$$f_{NL}(x) = f_{NL}(a) + f'_{NL}(a)(x - a) + \frac{f''_{NL}(a)}{2!}(x - a)^2 + \dots \quad (6.1)$$

If we neglect the higher order terms in (6.1), we get

$$f_{NL}(x) = f_{NL}(a) + f'_{NL}(a)(x - a) \quad (6.2)$$

If we substitute $x + x_\Delta$ into (6.2) as the argument in the equation, and let $a = x$, we obtain

$$f_{NL}(x + x_\Delta) = f_{NL}(x) + f'_{NL}(x)x_\Delta \quad (6.3)$$

From (6.3), we now have a method to represent nonlinear state uncertainty in the form of an input affine structure. Of course, (6.3) is only valid in a sufficiently small neighborhood around the operating point. This is restated in the assumption:

Assumption 10. State uncertainty, x_Δ , is represented as an input affine linear approximation within the system model by $f_{NL}(x + x_\Delta) = f_{NL}(x) + f'_{NL}(x)x_\Delta$. As such, it is only valid for a sufficiently small neighborhood around the operating point.

For a general extended state space description of a plant, we can rewrite the terms taking state uncertainty into account, and group them together into the disturbance vector.

$$\begin{aligned} \dot{x} &= f(x) + g_1(x)w + g_2(x)u \\ \Rightarrow \dot{x} &= f(x) + f'(x)x_\Delta + g_1(x)w + g'_1(x)wx_\Delta + g_2(x)u + g'_2(x)ux_\Delta \\ \Rightarrow \dot{x} &= f(x) + \begin{bmatrix} g_1(x) & g'_1(x) & f'(x) & g'_2(x) \end{bmatrix} \begin{bmatrix} w \\ wx_\Delta \\ x_\Delta \\ ux_\Delta \end{bmatrix} + g_2(x)u \end{aligned}$$

Thus, we have augmented the disturbance vector to include state uncertainty as a disturbance.

Table 6.1: Enumerated EDFA System Terms

Terms	Expression
term 1	$\frac{1}{\zeta\tau_o L} g_k m \Delta \nu_k L x$
term 2	$-\frac{1}{\zeta\tau_o L} u_k \left[\frac{-g_k m \Delta \nu_k x}{(\alpha_k + g_k)x - (\alpha_k + \ell_k)} (1 - e^{u_k \{(\alpha_k + g_k)x - (\alpha_k + \ell_k)\} L}) \right]$
term 3	$-\frac{1}{\zeta\tau_o L} u_k (e^{u_k \{(\alpha_k + g_k)x - (\alpha_k + \ell_k)\} L} - 1)$
term 4	$-\frac{x}{\tau_o}$

6.2 State Uncertainty for Parametric Representation

One important reason for including x_Δ as a disturbance comes from the idea that we can associate uncertainty in the parameter values of the EDFA with an uncertainty in x . The intuition is clear as one just has to image that a deviant value of one of the parameters in the EDFA system equations would produce a change in the state computation with respect to the physical device. However, the intuition on its own is not sufficient to justify assuming deviations in x can represent parametric uncertainties. A more rigorous mathematical construction must be formed to justify this idea.

To prove the structural link between parametric uncertainty and state uncertainty, we first have to write out every term in the EDFA system model (2.14) with parametric uncertainty included, and separately, write out the EDFA system terms with state uncertainty. We then compare the parametric uncertainty terms with the state uncertainty terms to see the mathematical relationship.

We begin with the most important parameters in the EDFA system equations (2.14), α_k and g_k , the absorption and emission coefficients. Not only are these parameters the most important in modeling the EDFA, but upon inspection with (2.14), they almost always have a direct multiplicative association with the state, x . We enumerate the terms in the state equation of the EDFA model with ASE, as show in Table 6.1.

Notice specifically that g_k directly multiplies x in every term except term 4. Also

Table 6.2: Subdivision of Term 2

Terms	Expression
term 2.1	$-g_k m \Delta \nu_k x$
term 2.2	$(\alpha_k + g_k)x - (\alpha_k + \ell_k)$
term 2.3	$1 - e^{u_k \{(\alpha_k + g_k)x - (\alpha_k + \ell_k)\}L}$

notice that terms 3 and 4 are usually very small for high average inversion levels, which is the normal operation of the EDFA.

We represent the parametric uncertainties as $g_{k\Delta}$ and $\alpha_{k\Delta}$. The state uncertainty is represented as x_Δ . Furthermore, let LS represent the term with parametric uncertainty applied, while RS represent the term with state uncertainty applied.

For term 1,

$$\begin{aligned}
 LS &= \frac{1}{\zeta \tau_0 L} (g_k + g_{k\Delta}) m \Delta \nu_k L x = \frac{1}{\zeta \tau_0 L} g_k m \Delta \nu_k L x + \frac{1}{\zeta \tau_0 L} g_{k\Delta} m \Delta \nu_k L x \\
 RS &= \frac{1}{\zeta \tau_0 L} g_k m \Delta \nu_k L (x + x_\Delta) = \frac{1}{\zeta \tau_0 L} g_k m \Delta \nu_k L x + \frac{1}{\zeta \tau_0 L} g_k m \Delta \nu_k L x_\Delta
 \end{aligned}$$

where for $LS = RS$, we get

$$\frac{x_\Delta}{x} = \frac{g_{k\Delta}}{g_k} \quad (6.4)$$

for term 2, the equation is much more complex, but we can break it down into 3 smaller terms. The subdivided terms are given in Table 6.2.

for term 2.1, we get the same result as (6.4).

for term 2.2,

$$\begin{aligned}
 LS &= (\alpha_k + g_k + \alpha_{k\Delta} + g_{k\Delta})x - (\alpha_k + \alpha_{k\Delta} + \ell_k) \\
 &= (\alpha_k + g_k)x + (\alpha_{k\Delta} + g_{k\Delta})x - (\alpha_k + \ell_k) - \alpha_{k\Delta} \\
 RS &= (\alpha_k + g_k)(x + x_\Delta) - (\alpha_k + \ell_k) = (\alpha_k + g_k)x + (\alpha_k + g_k)x_\Delta - (\alpha_k + \ell_k)
 \end{aligned}$$

for $LS = RS$, we get

$$\frac{x_\Delta}{x} = \frac{\alpha_{k\Delta} + g_{k\Delta}}{\alpha_k + g_k} - \frac{\alpha_{k\Delta}}{x(\alpha_k + g_k)} \quad (6.5)$$

for term 2.3, we get the same result as term 2.2.

for term 3, we get the same result as terms 2.2 and 2.3.

We choose to neglect term 4 since it is very small with respect to the other terms with high average inversion. Notice that the second term in the right half side of (6.5) can also be neglected if we assume that the absorption uncertainty, $\alpha_{k\Delta}$, is much smaller than the absorption and emission variables, α_k and g_k . This in fact should be true since the channel wavelengths have higher emission coefficients in general. With this assumption, (6.4) and (6.5) are simply representations of percentage deviations from the parameter values. We could also make the assumption that all of the parameters are deviant by the same percentage. Hence, for any k , we equate (6.4) and (6.5) to get

$$\frac{x_\Delta}{x} = \frac{g_{k\Delta}}{g_k} = \frac{\alpha_{k\Delta} + g_{k\Delta}}{\alpha_k + g_k} \quad (6.6)$$

Notice that the above result is a nice, simplified representation, and that we could have also included the second term in (6.5) if needed. However, the intuition would not have been as elegant, and the term is small enough to be neglected. Note that it may be possible to represent other EDFA parameters as state uncertainty as well.

It is also important to note the trivial case of extreme robustness when x is made to be extremely restricted. Imagine that using L_2 control, we restrict x very tightly by giving the system a very small L_2 gain. Clearly, given any disturbance, our controller will be able to minimize variation in x to an extremely small range. The smaller the restriction on x , the more robust the system. Unfortunately, controllers are always restricted to physical constraints that prevent an unlimited restriction. Never the less, it is clear that given a controller that can operate on a faster time scale to dispense more power, we would be able to achieve greater robustness.

6.3 Robust Modeling of EDFA with ASE

Now we can combine input multiplicative uncertainty with state uncertainty to create an EDFA system model that will reject unwanted physical effects. All uncertainties will be combined into one augmented disturbance vector. In addition to the usual L_2 performance output, z , robust performance outputs will be included.

We begin by including the input multiplicative uncertainty into the EDFA model. We represent uncertainty on every individual signal input power as well as the pump power. Let $w^u = w + w_\Delta$ and $u^u = u + u_\Delta$, where w is the nominal input vector of channel powers, w_Δ is the uncertainty on the input channels, u is the nominal pump input power, and u_Δ is the uncertainty on the pump input. We substitute w^u and u^u into the state equation of (3.1) to obtain

$$\begin{aligned} \dot{x} &= f(x) + g_1(x)(w + w_\Delta) + g_2(x)(u + u_\Delta) \\ \Rightarrow \dot{x} &= f(x) + \begin{bmatrix} g_1(x) & g_1(x) & g_2(x) \end{bmatrix} \begin{bmatrix} w \\ w_\Delta \\ u_\Delta \end{bmatrix} + g_2(x)u \end{aligned} \quad (6.7)$$

Next, we apply the state uncertainty as derived in (6.3). We represent uncertainty on the state x as $x^u = x + x_\Delta$, where x is the nominal state and x_Δ is the state uncertainty. We substitute x^u as the argument in (6.7) and let $g_1^*(x) = \begin{bmatrix} g_1(x) & g_1(x) & g_2(x) \end{bmatrix}$ to

obtain

$$\begin{aligned}
\dot{x} &= f(x + x_\Delta) + g_1^*(x + x_\Delta) \begin{bmatrix} w \\ w_\Delta \\ u_\Delta \end{bmatrix} + g_2(x + x_\Delta)u \\
\Rightarrow \dot{x} &= f(x) + f'(x)x_\Delta + (g_1^*(x) + g_1^{*'}(x)x_\Delta) \begin{bmatrix} w \\ w_\Delta \\ u_\Delta \end{bmatrix} + (g_2(x) + g_2'(x)x_\Delta)u \\
\Rightarrow \dot{x} &= f(x) + \begin{bmatrix} g_1^*(x) & g_1^{*'}(x) & f'(x) & g_2'(x) \end{bmatrix} \begin{bmatrix} w \\ w_\Delta \\ u_\Delta \\ wx_\Delta \\ w_\Delta x_\Delta \\ u_\Delta x_\Delta \\ x_\Delta \\ ux_\Delta \end{bmatrix} + g_2(x)u \quad (6.8)
\end{aligned}$$

In examination of the robust final system structure, (6.8), we note that $w_\Delta x_\Delta$ and $u_\Delta x_\Delta$ are actually uncertainties multiplying uncertainties, meaning that their influence would be very small. As such, these are neglected in the simulations.

Assumption 11. $w_\Delta x_\Delta$ and $u_\Delta x_\Delta$ are neglected.

We rewrite (6.8) with assumption 11 as

$$\dot{x} = f(x) + \hat{g}_1(x)\hat{w} + g_2(x)u \quad (6.9)$$

Furthermore, it is important to note that wx_Δ and ux_Δ represent two multiplied signal values. However, these disturbances are treated as just one signal each, mixed together. Any controller that is designed based on the system structure of (6.8) will not have the "intelligence" to know that the multiplied disturbances have this unique structure. Hence,

the control law will be designed to take any disturbance values, without structure, into account. This will yield a more conservative controller than is needed, but the controller will still be valid.

Definition 12. Let $w_x = wx_\Delta$ and $u_x = ux_\Delta$. w_x and u_x are treated as individual signals without structure.

Now that the state equation, (6.8), is structured, and we know that our output equation will be in the form of the Full Information problem, we are only left to design the output performance equation, z' . For the non-robust performance variable, we chose to use x and u as the variables to attenuate. These variables will still be used. In addition, we must consider including the disturbance variables, w . Note that these disturbances also include channel powers and the uncertainties that they generate.

We can represent the output performance equation, z' as:

$$z' = \begin{bmatrix} \alpha_x x \\ 0 \\ 0 \end{bmatrix} + \begin{bmatrix} 0 \\ \alpha_w I \\ 0 \end{bmatrix} \hat{w} + \begin{bmatrix} 0 \\ 0 \\ \alpha_u \end{bmatrix} u \quad (6.10)$$

where α_x , α_w and α_u are all scalars in the performance output. It will be shown that α_w will be taken as 0 later in the section. For now, we will treat (6.10) in its general form.

The first observation to make is that we chose to scale the disturbance vector, \hat{w} , by a scalar and not a matrix. In fact we could choose to scale this by a matrix, but this would unnecessarily complicate matters. The designer would usually scale the disturbances according to a worst case disturbance that they wish to attenuate. Hence, only one scalar is necessary. Secondly, we notice that the state also has a scalar multiplying it. Although this is valid, this also introduces unnecessary complication since the impact of the state is relative to the sizes of the \hat{w} element and the u element. Since we are scaling \hat{w} and u , the impact of x changes relative to these values, and we do not need to explicitly scale this term. Hence, here we consider $\alpha_x = 1$, and without loss of generality, we still assume $\alpha_u = 1$.

Notice that in (6.10) we do not repeat any rows of z' even though certain rows of (6.10) are identical to the non-robust performance equation. If a row is included in the z' equation, then it will be attenuated, and no extra copies need to be made.

As a final note, let us consider the idea to use unstructured uncertainty to model ASE in the original ASE model (2.1). We can use the knowledge that we have obtained from the derivation of the EDFA model with ASE (2.14). Notice that each ASE term in (2.14) is only a function of x and not a function of the input u or channel powers. Also note that ASE can be thought of as a disturbance in the rate equation. To restrict ASE, one would have to restrict the state, x , which we are already restricting in our L_2 designs. As long as we employ a restriction on x using L_2 nonlinear control, we are imposing a restriction on ASE.

With the performance output equation included in the extended state space model, we get:

$$\begin{aligned} \dot{x} &= f(x) + \hat{g}_1 \hat{w} + g_2(x)u \\ z' &= \begin{bmatrix} x \\ 0 \\ 0 \end{bmatrix} + \begin{bmatrix} 0 \\ \alpha_w I \\ 0 \end{bmatrix} \hat{w} + \begin{bmatrix} 0 \\ 0 \\ 1 \end{bmatrix} u \\ y &= \begin{bmatrix} x \\ 0 \end{bmatrix} + \begin{bmatrix} 0 \\ I \end{bmatrix} \hat{w} \end{aligned} \tag{6.11}$$

In this final model form, we notice that the model is much more complex than the previous model. The disturbance term has been significantly augmented with complex nonlinear terms. Also, we can see that $k_{11} \neq 0$ which could potentially cause computational problems.

After careful scrutiny, a fascinating solution presented itself to greatly simplify the structure of the above system and also shed some light on the problem. After attempting to evaluate the equations for $A_{FI}(x)$, $R_{FI}(x)$ and $Q_{FI}(x)$, it was discovered that $A_{FI}(x)$ and $R_{FI}(x)$ were identical to the non-robust extended model and $Q_{FI}(x)$ had a very

similar structure. This result was unexpected. It became apparent that so long as k_{11} had a simplified structure like that chosen above, $k_{11} = \alpha_w I$, we could actually rewrite system (6.11) into a simpler system where $k_{11} = 0$! We know,

$$\|z'\|^2 \leq \gamma^2 \|\hat{w}\|^2$$

Next, we can expand z' according to its representation in terms of x , \hat{w} and u :

$$\|x\|^2 + \alpha_w^2 \|\hat{w}\|^2 + \|u\|^2 \leq \gamma^2 \|\hat{w}\|^2 \quad (6.12)$$

and if we rewrite equation (6.12), we get

$$\|x\|^2 + \|u\|^2 \leq (\gamma^2 - \alpha_w^2) \|\hat{w}\|^2 \quad (6.13)$$

which is exactly the relationship that we would get for our system when $k_{11} = 0$, but with a lower L_2 gain, $\gamma'^2 = \gamma^2 - \alpha_w^2$. This makes a lot of sense since including \hat{w} in the output performance, z' , does not translate into a physical reduction on \hat{w} because \hat{w} is an external signal. The effect of wanting to restrict the \hat{w} results in a more restrictive L_2 gain on the other variables. So in effect, we can actually neglect α_w by setting it equal to 0. This is a very nice and intuitive result.

6.4 Robustness Simulation Results

In the previous section we outlined an extended state space model for the EDFA with ASE that included robustness (6.11). To test the results of an L_2 nonlinear controller on the system, we use the parameters in Appendix B. We begin by deriving a controller using the methodology from chapter 4. We then test the uncertainty cases with no input power variation. Finally, we explore the scenario of having channel drops occur with uncertainties present in the system.

6.4.1 Controller Derivation

We follow the same procedure as outlined in Chapter 4 to derive the L_2 nonlinear controller. We begin with our EDFA system model, (2.14), and calculate the operating point based upon the data provided in Tables B.1, B.2 and B.3. We calculate the the operating point, $x_0 = 0.60725$ for 32 channels and $x_0 = 0.68337$ for 2 channels. We perform a standard nonlinear shift on the state equation to set $x_0 = 0$. Note, we also get $w = 0$ and $u = 0$ to represent the signal input powers and pump input powers that define the operating point.

We use the linear theory of H_∞ control as a first step in the design process. We choose the scaling factors X_w and X_u on the disturbance and pump parameters, respectively. Here, we design for a worst case scenario, so we scale the norm of the disturbance for a 100% channel drop to equal unity. For our system, we calculate $\|w\| = 1.8716 * 10^{15}$ for 32 channels, and $\|w\| = 4.6447 * 10^{14}$ for 2 channels. We calculate $X_w = \frac{1}{\|w\|}$. Thus, $\Delta w = 1$, so our x is limited directly by the L_2 gain.

If we denote G_1 and G_2 as the linear part of $g_1(x)$ and $g_2(x)$, then we can use (4.10) to obtain X_u . We choose the L_2 gain, $\gamma = 0.003$, which is the same γ value used in the comparison with the PID gain scheduling controller. We are interested in three test cases for the robustness analysis: input multiplicative uncertainty, state uncertainty, both input multiplicative and state uncertainty. Moreover, each simulation must be compared to a baseline reference, which we choose to be the L_2 system with no robustness, so this represents another test case. Notice that we will use precisely the same γ values for each test case so that it functions as a baseline comparison. This will allow us to interpret the performance differences between the simulations according to this γ value.

We need four X_u scalings for the four test cases. This must be done for the 2 and 32 channels. The resultant values are tabulated in Table 6.3.

If we increase the value of γ , which decreases the amount of attenuation, we can increasingly negate $Q_{FI}(x)$ to achieve an L_2 gain over a larger neighborhood. So we in-

Table 6.3: X_u Scaling Values for Robustness Test Cases

X_u Scaling Case	2 Channels	32 Channels
No Uncertainty	4.2555(10^{-21})	4.1168(10^{-21})
Input Uncertainty	3.0091(10^{-21})	2.9110(10^{-21})
State Uncertainty	2.3488(10^{-37})	8.3177(10^{-38})
Input and State Uncertainty	2.3488(10^{-37})	8.3177(10^{-38})

crease γ until we obtain the requirements for Theorem 3.2.1. Our conditions are satisfied if we choose $\gamma = 0.03$ in each case. We do not need to obtain a global solution to the L_2 control problem, since simulations show that the controller functions properly in the

worst case channel drop. The final controllers used are:

$$\begin{aligned}
u_2 &= -9.8909(10^{-1})x + 1.7115x^2 + 1.2308(10^1)x^3 - 2.51(10^2)x^4 \\
&\quad -1.8283(10^3)x^5 + 1.4708(10^3)x^6 + 4.4092(10^3)x^7 \\
u_{2Mult} &= -1.0206x + 1.1352x^2 + 4.9244x^3 - 2.6415(10^2)x^4 \\
&\quad -2.3260(10^3)x^5 + 1.7616(10^3)x^6 + 5.6130(10^3)x^7 \\
u_{2State} &= -1.1010x - 4.2862(10^{-1})x^2 - 1.6872(10^1)x^3 - 3.4679(10^2)x^4 \\
&\quad -4.1334(10^3)x^5 + 2.8906(10^3)x^6 + 9.9909(10^3)x^7 \\
u_{2StateANDMult} &= -1.1010x - 4.2862(10^{-1})x^2 - 1.6872(10^1)x^3 - 3.4679(10^2)x^4 \\
&\quad -4.1334(10^3)x^5 + 2.8906(10^3)x^6 + 9.9909(10^3)x^7 \\
u_{32} &= -1.0237x + 7.8867(10^{-1})x^2 + 3.1106x^3 - 9.95(10^1)x^4 \\
&\quad -6.8735(10^2)x^5 + 2.6259(10^2)x^6 + 7.586(10^2)x^7 \\
u_{32Mult} &= -1.0458x + 4.8826(10^{-1})x^2 + 5.4567(10^{-2})x^3 - 1.0526(10^2)x^4 \\
&\quad -8.0458(10^2)x^5 + 2.9699(10^2)x^6 + 8.8965(10^2)x^7 \\
u_{32State} &= -1.1010x - 3.1001(10^{-1})x^2 - 9.0484x^3 - 1.3708(10^2)x^4 \\
&\quad -1.2159(10^3)x^5 + 4.2958(10^2)x^6 + 1.3501(10^3)x^7 \\
u_{32StateANDMult} &= -1.1010x - 3.1001(10^{-1})x^2 - 9.0484x^3 - 1.3708(10^2)x^4 \\
&\quad -1.2159(10^3)x^5 + 4.2958(10^2)x^6 + 1.3501(10^3)x^7
\end{aligned} \tag{6.14}$$

Notice that the controllers for the state uncertainty case and the combined state and input uncertainty case are equivalent. This is due to a dominant state uncertainty term in the augmented disturbance vector. The state uncertainty term dominates the input uncertainty terms, and as such, two similar controllers are derived.

6.4.2 Simulation of Uncertainty Cases

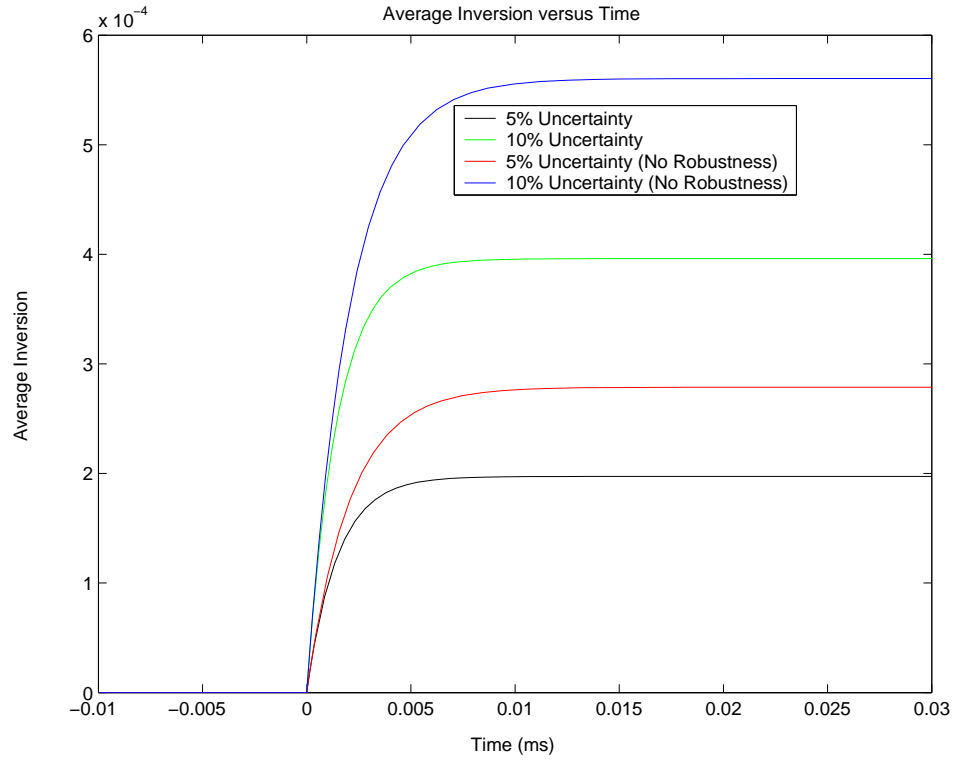
This section will only focus on robustness uncertainties without input channel variation. In other words, only system and input uncertainties will be simulated given operation precisely at the nominal operating point. There are three main test cases that we will simulate in this section. The first case will only simulate the unstructured input uncertainty without state uncertainty. The second case will focus on only the state uncertainty without the input uncertainty. The third case will consider both uncertainties simultaneously. However, we must gauge the response of these simulations against the non-robust system outlined in chapter 4. Hence, we will also implement the same uncertainties against the non-robust system to compare the performance of each controller.

We simulate the robust responses of the closed loop systems using the same parameters as outlined in Table B.2 and Table B.3. We simulate all test cases using the inputs defined in Table B.1. For simulation purposes, uncertainties are introduced into the signals at time $t = 0$ seconds. In each case herein, we use a step signal to provide uncertainty.

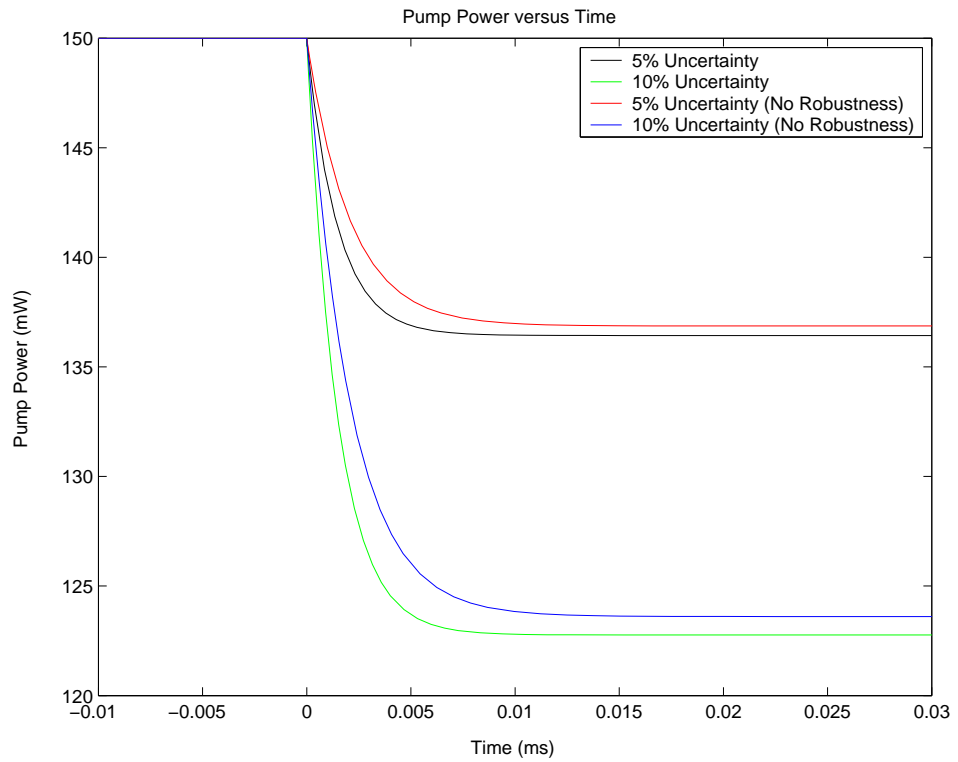
We begin by analyzing the input signal uncertainty case. We introduce a 5% and 10% signal reduction at $t = 0$ seconds. Conceptually, this is like discovering that the input signals are in fact 5% and 10% smaller than initially thought. The results are presented in figures 6.1 and 6.2 for the 2 channel and 32 channel cases, respectively.

We see in figure 6.1 that the average inversion is more restricted using the robust controller as compared to the controller with no robustness. The effect is seen for both the 5% and the 10% uncertainty cases. Note that all of the responses are similar in their shape, with only the amount of variance from the operating point, $x = 0$, being different. We expect to see a larger variance for the 10% uncertainty than the 5% uncertainty in both test cases because we are restricting a larger uncertainty. This is verified in simulation. Finally, notice in figure 6.2 that we see very similar results for the 32 channel case.

In figure 6.1 we see that the pump power must change more rapidly in the robust

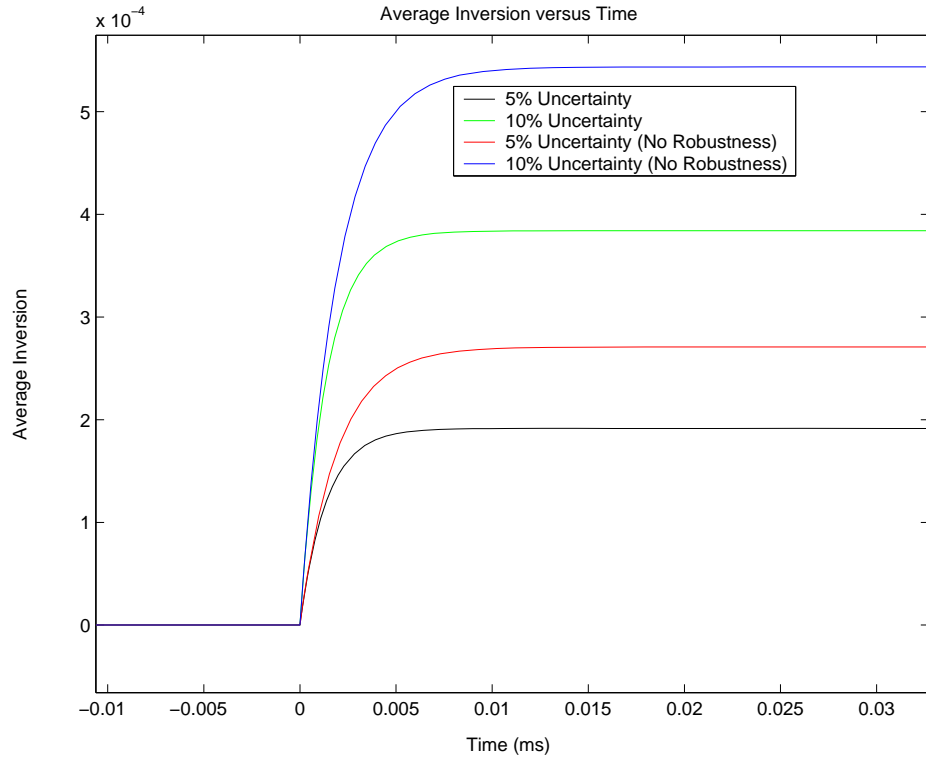


(a) Average Inversion versus Time for 2 Channels

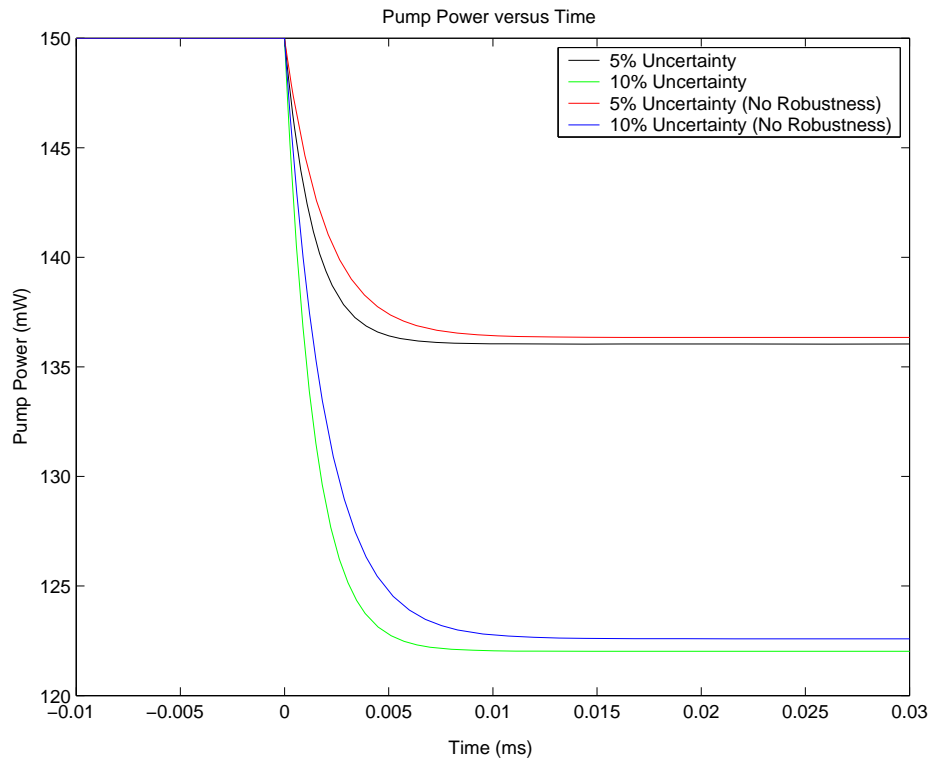


(b) p^{out} versus Time for 2 Channels

Figure 6.1: Input Multiplicative Test Case for 2 Channels with 5% and 10% Input Uncertainty



(a) Average Inversion versus Time for 32 Channels



(b) p^{out} versus Time for 32 Channels

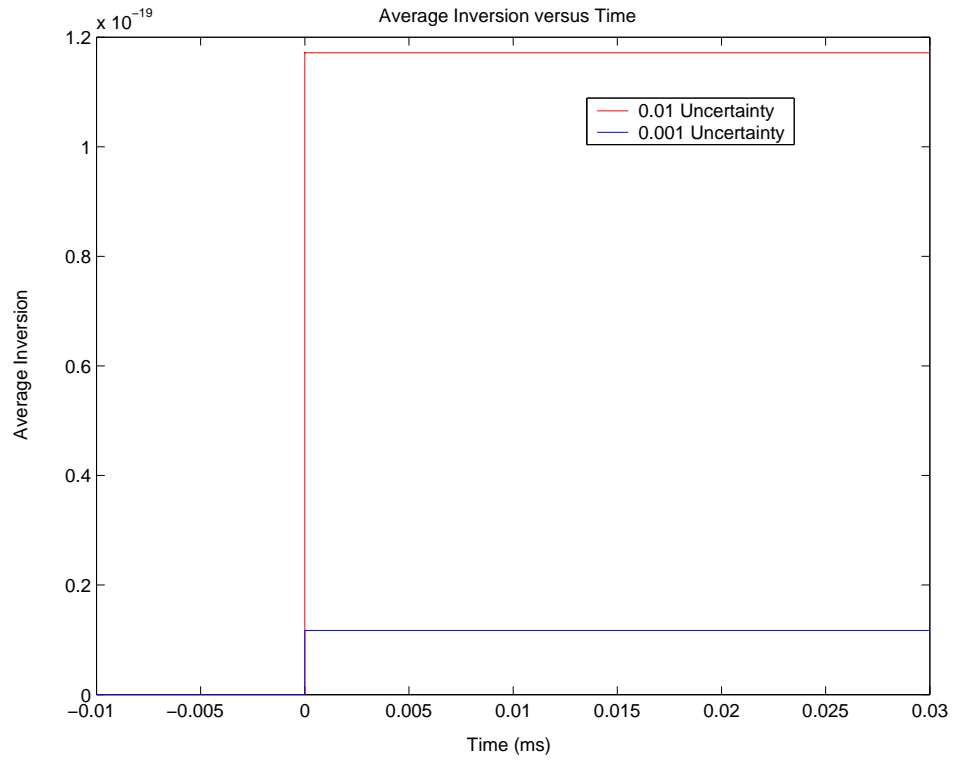
Figure 6.2: Input Multiplicative Test Case for 32 Channels with 5% and 10% Input Uncertainty

controller. We can see a slightly steeper increase in slope for the pump compensated plots. The final power values of the test cases show an approximate 1mW difference between the robust and non-robust controllers. This means that the pump must be able to vary more power in a shorter period of time. The small difference in pump power compensation compared with the large impact on the state variable restrictions offers encouraging results about the usefulness of this control scheme. The 10% uncertainty cases needs a much larger drop in pump power as compared with the 5% uncertainty case. Once again, this is due to the larger uncertainty requiring a larger pump power variation response. Also, we see a similar response when we examine the 32 channel case in figure 6.2.

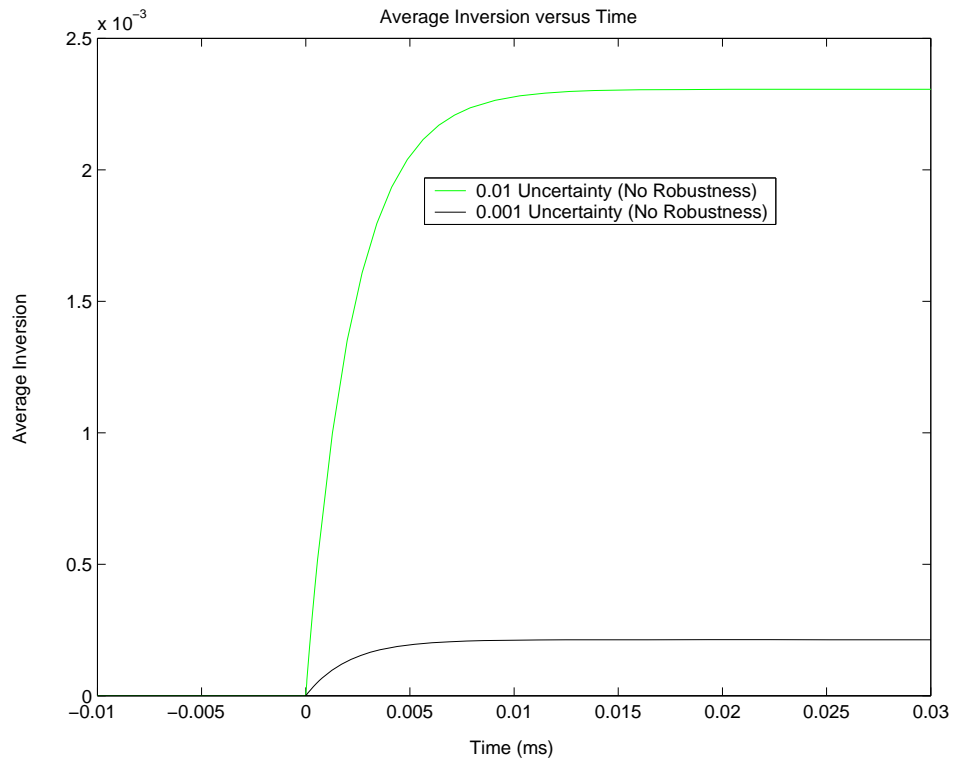
Next we examine the state uncertainty test cases for both the robust L_2 nonlinear controller and the L_2 nonlinear controller without robustness. The state uncertainty case represents imprecision in the EDFA parameters. State uncertainty also represents any unknown factors that cause the state to deviate from its modeled behaviour. Hence, state uncertainty can be an important factor for the EDFA system model.

We choose to use state uncertainties of 0.01 and 0.001 for an extreme and modest case, respectively. The uncertainty is chosen to subtract from the equilibrium state value. This would cause the controlled system to respond by increasing the state. The results of the state variable plots and the pump power plots are shown in figures 6.3 - 6.6.

If we first examine the 2 channel state variable plot in figure 6.3, we immediately notice that the state moves to $x = 1.2(10^{-19})$. This is extremely small as compared with the non-robust controller in figure 6.3. The time scale for the controller is also extremely small which generates the angular looking responses. The reason for this extreme reaction is that the state uncertainty term, $f'(x)$, in the disturbance vector from (6.8) dominated the remaining terms substantially. This response would clearly not be feasible for a physical implementation but it serves the purpose of showing the significant impact state uncertainty has on the system using the chosen gain of $\gamma = 0.03$. A physical realization



(a) Average Inversion versus Time for 2 Channels



(b) Average Inversion versus Time for 2 Channels

Figure 6.3: State Uncertainty Test Case for 2 Channels with 0.01 and 0.001 State Uncertainty

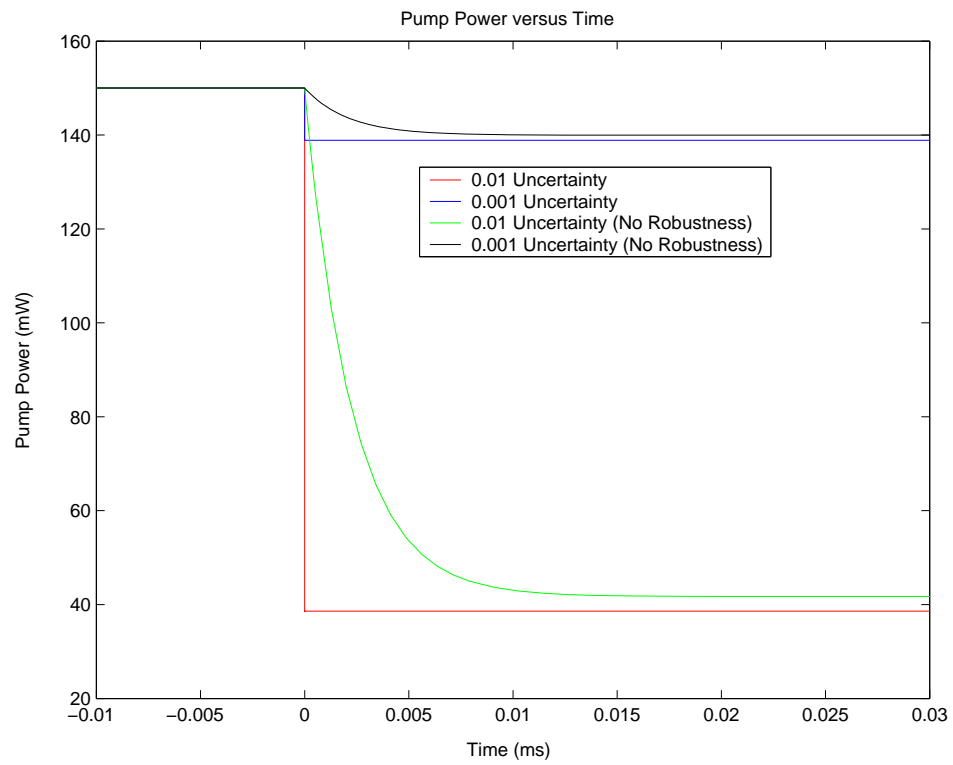
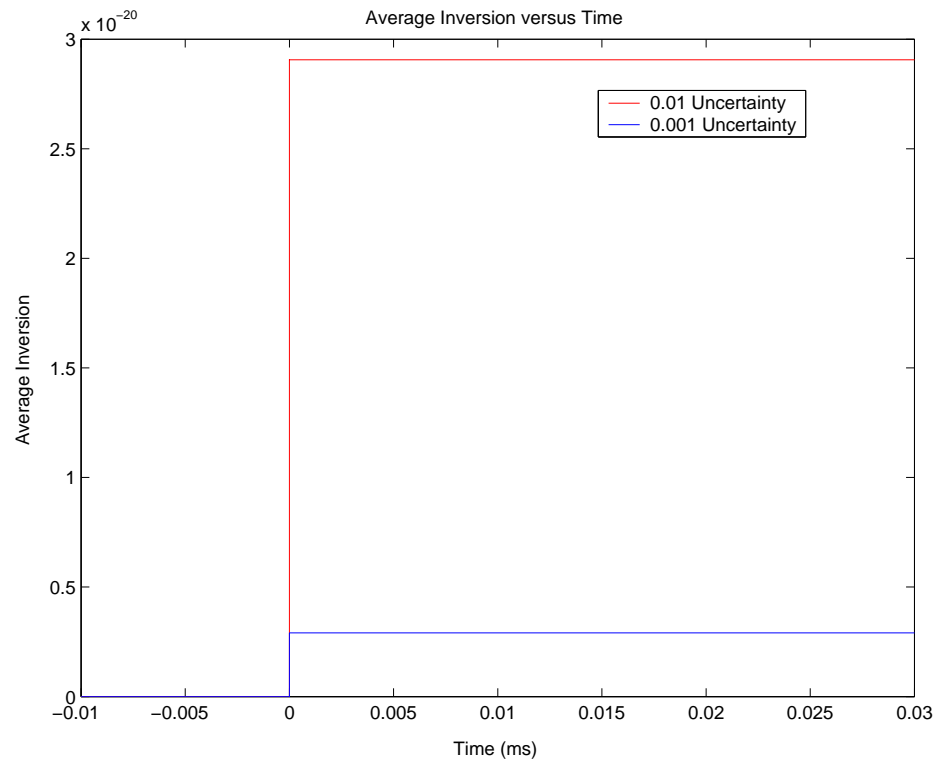
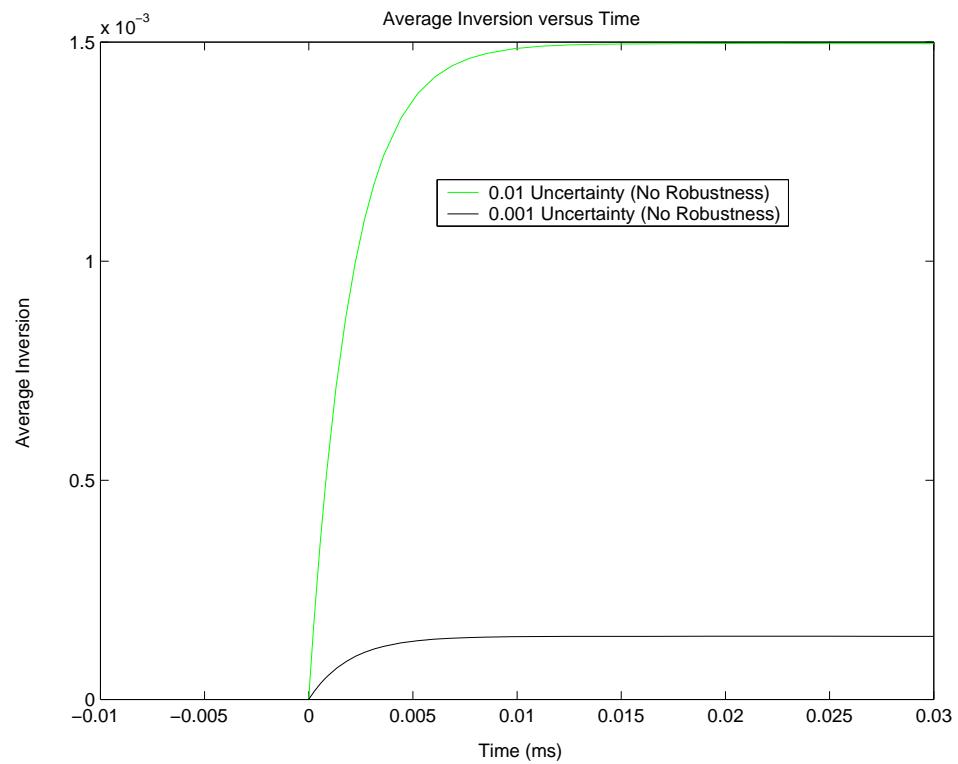


Figure 6.4: State Uncertainty Test Case for 2 Channels with 0.01 and 0.001 State Uncertainty



(a) Average Inversion versus Time for 32 Channels



(b) Average Inversion versus Time for 32 Channels

Figure 6.5: State Uncertainty Test Case for 32 Channels with 0.01 and 0.001 State Uncertainty

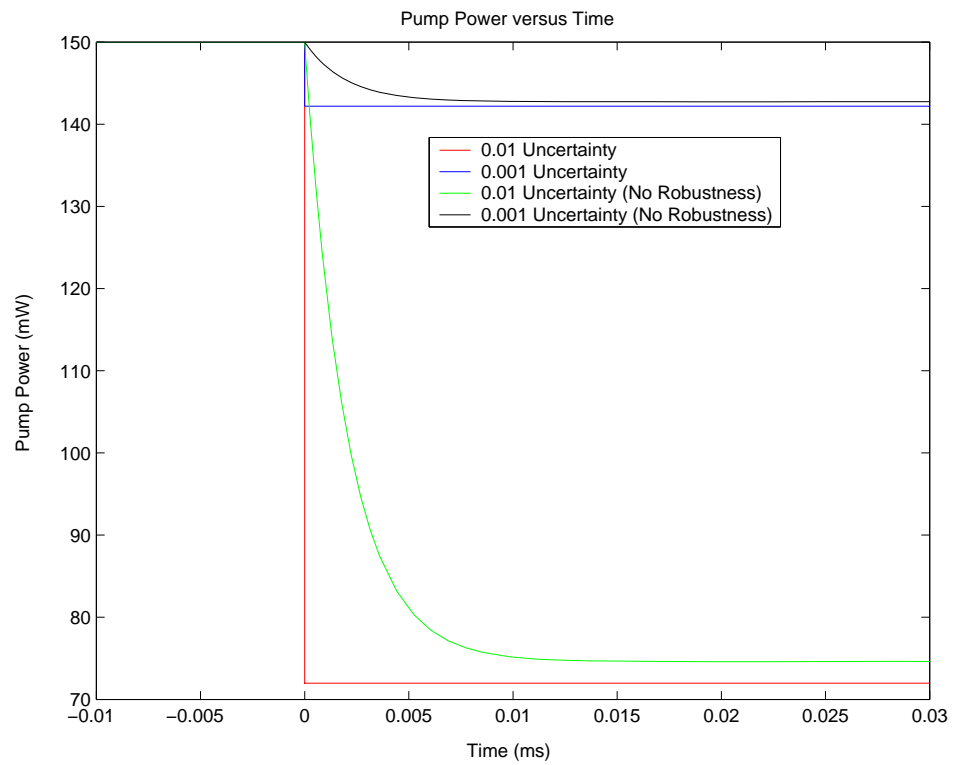


Figure 6.6: State Uncertainty Test Case for 32 Channels with 0.01 and 0.001 State Uncertainty

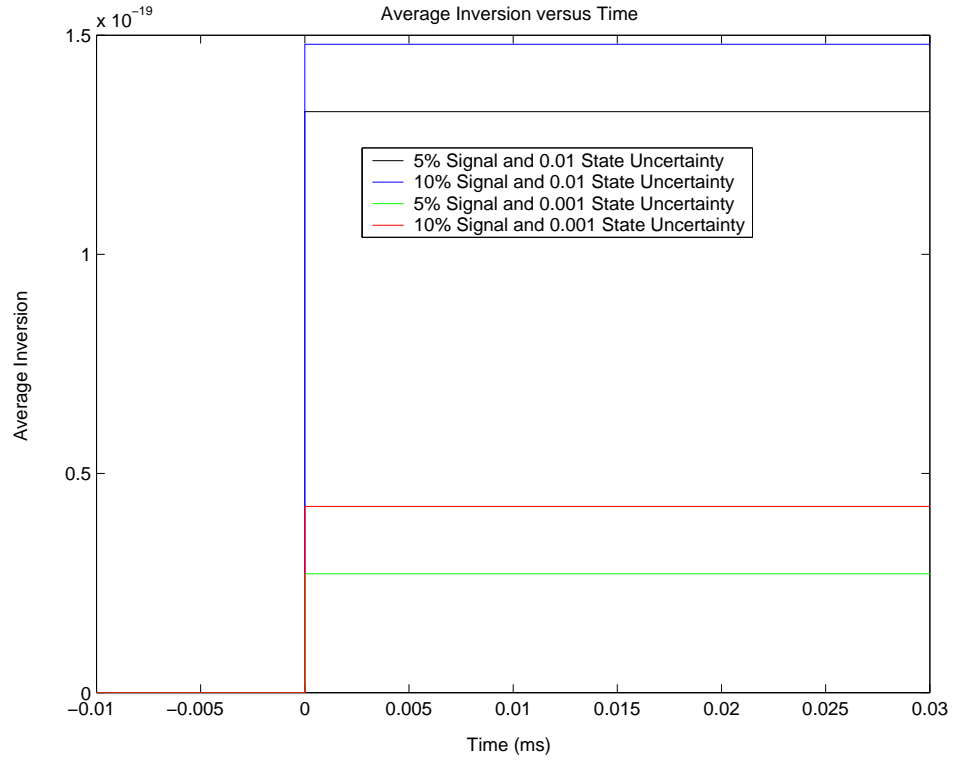
would involve increasing the L_2 gain up until a reasonable uncertainty response can be generated from the pump.

If we examine the L_2 controlled system with no robustness we see a much more reasonable time response for the state as shown in figure 6.3. As such, when we compare these results to those of the robust controller, we see a substantial difference. This further justifies the need to include robust control mechanisms in the EDFA system. We see similar responses for the 32 channel cases in figure 6.5.

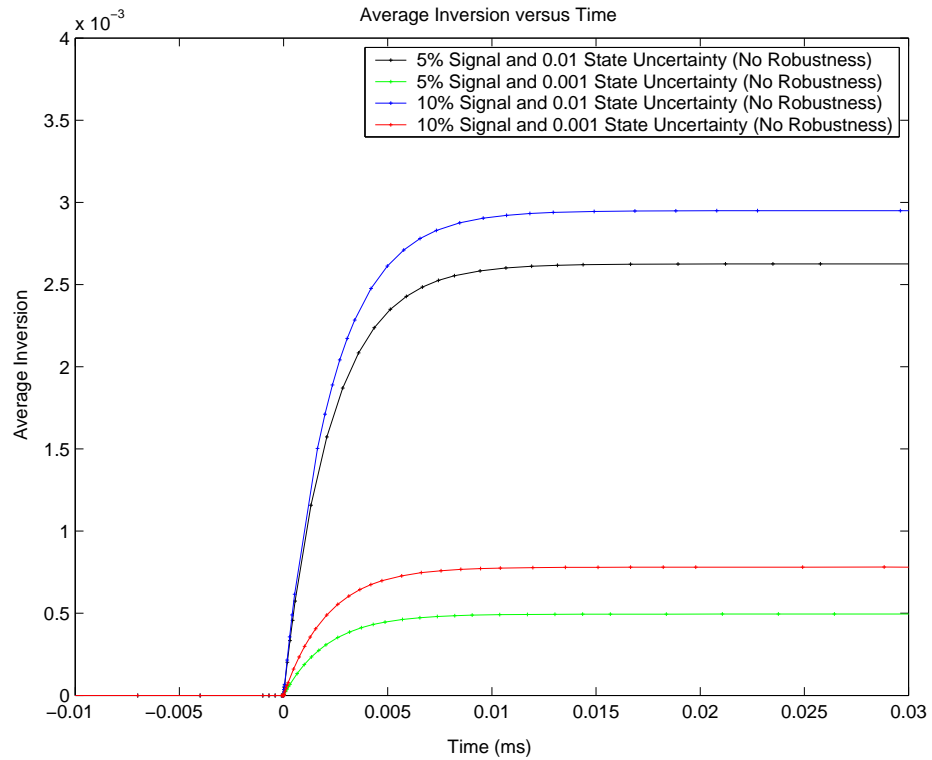
In the pump power transient simulations shown in figures 6.4 and 6.6 we see relatively small differences in final power values between the different controllers. It is clear again that the robust controller operates on a much smaller time scale than its predecessor. In each case, the robust controller requires a slightly larger power drop to achieve its results. However, this is entirely reasonable for the results that it achieves.

We can take the above input uncertainty and state uncertainty tests and combine them together. Thus, we permute 0.01 and 0.001 state uncertainty with 5% and 10% input uncertainty. The controller we use will be identical to the state uncertainty case because of the dominance of the state uncertainty disturbance term from (6.8). The simulations are depicted in figures 6.7 - 6.10.

We see that all of the simulations yield similar responses as those in their uncombined test cases. The results are cumulative in that two uncertainties combined generate a more significant pump compensation than either of the individual uncertainties. An interesting observation is that the extreme case of 10% input uncertainty with 0.01 state uncertainty causes an enormous pump power drop. The response is close to the 0 power mark which is the limit of the pump response. This leaves little room for other disturbances such as channel drops in addition to the uncertainties since the pump can not move beyond the 0 boundary. If the requirement required the pump to move into negative pump power, this would be equivalent to not being able to achieve the specified response. We can now consider the effect of including channel drops in addition to state and input uncertainty.



(a) Average Inversion versus Time for 2 Channels



(b) Average Inversion versus Time for 2 Channels

Figure 6.7: State Uncertainty and Multiplicative Uncertainty Test Case for 2 Channels with 0.01 and 0.001 State Uncertainty and 5% and 10% Input Uncertainty

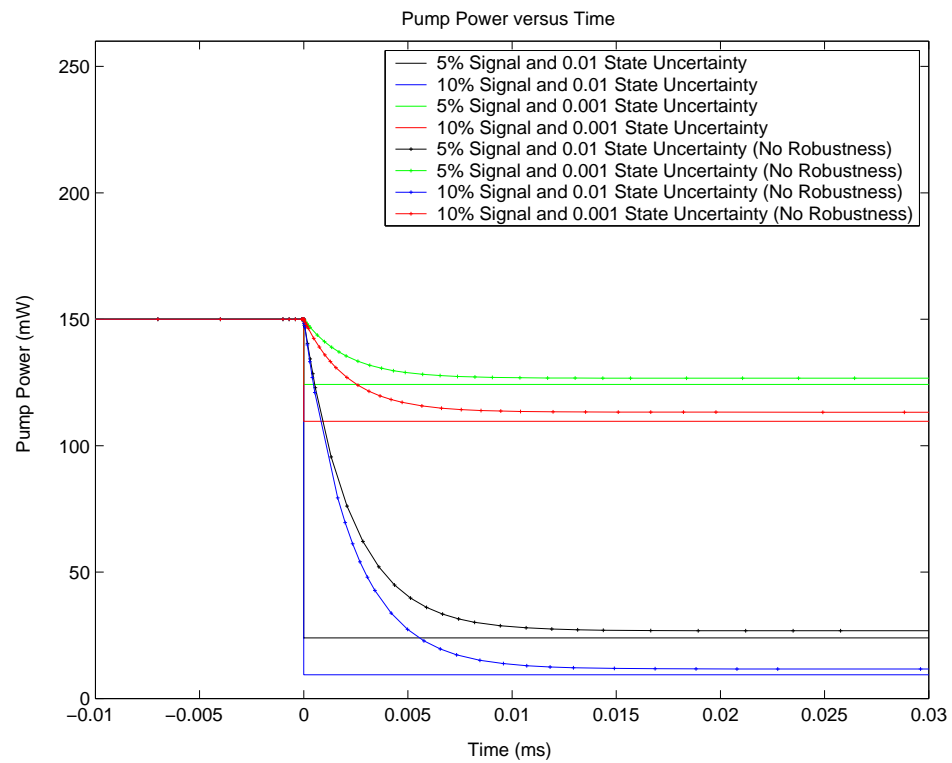
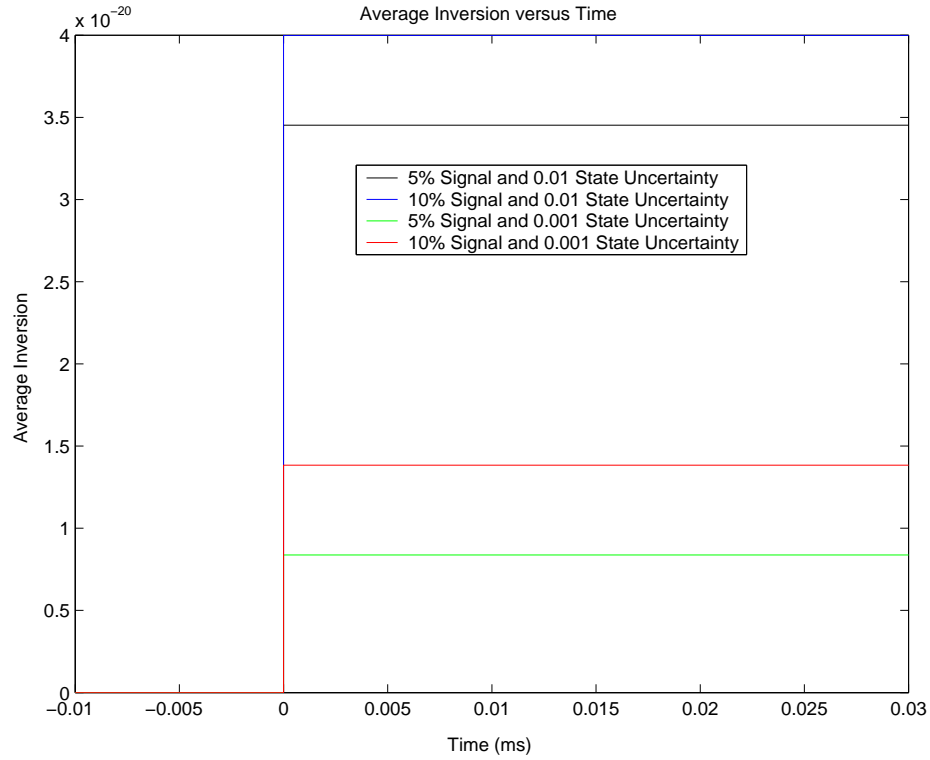
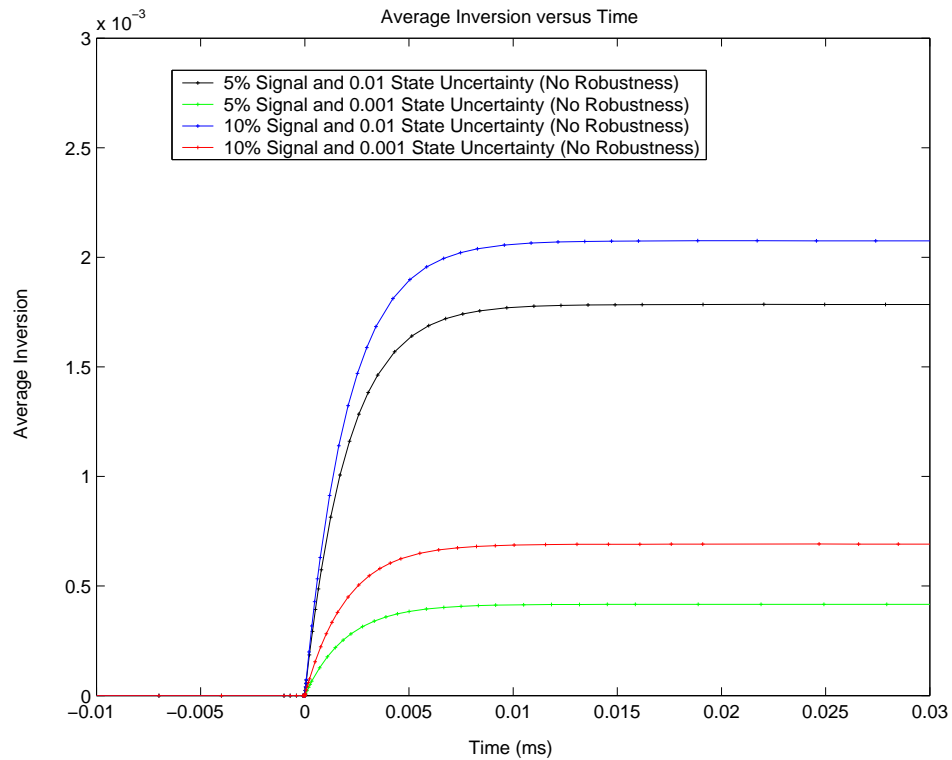


Figure 6.8: State Uncertainty and Multiplicative Uncertainty Test Case for 2 Channels with 0.01 and 0.001 State Uncertainty and 5% and 10% Input Uncertainty



(a) Average Inversion versus Time for 32 Channels



(b) Average Inversion versus Time for 32 Channels

Figure 6.9: State Uncertainty and Multiplicative Uncertainty Test Case for 32 Channels with 0.01 and 0.001 State Uncertainty and 5% and 10% Input Uncertainty

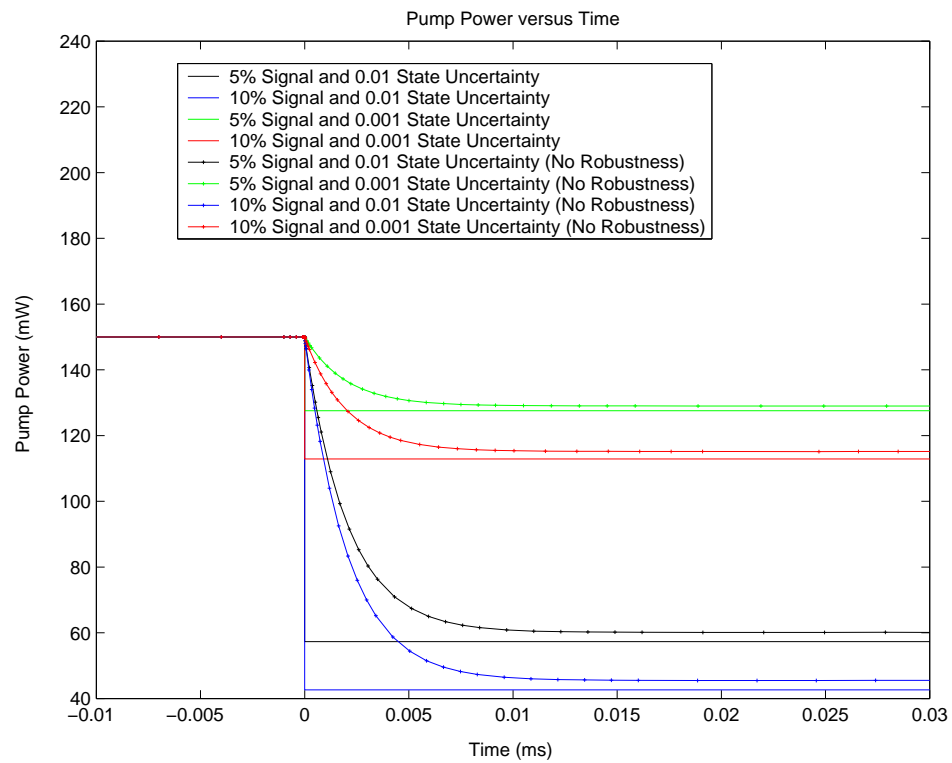


Figure 6.10: State Uncertainty and Multiplicative Uncertainty Test Case for 32 Channels with 0.01 and 0.001 State Uncertainty and 5% and 10% Input Uncertainty

6.4.3 Simulation of Uncertainty with Channel Drops

The physical implementation of the EDFA will experience channel drops in addition to state and input uncertainties. This necessitates the simulation of the closed loop EDFA system with channel drops in addition to uncertainties. As such, we will choose the two mildest uncertainty values of 0.001 state uncertainty and 5% input uncertainty as our baseline reference. We saw before that 0.01 state uncertainty and 10% input uncertainty already generate significant system response, so these will be neglected for now. These test situations will determine the behaviour of the closed loop system in response to channel drops of 50%, 97% and 100% input power.

We simulate the robust responses of the closed loop systems using the same parameters as outlined in Tables B.1, B.2 and Table B.3. For simulation purposes, uncertainties are introduced into the signals at time $t = 0$ seconds. In each case herein, we use a step signal to provide uncertainty. Of course, once again, we choose $\gamma = 0.03$ as the L_2 gain for each controller.

We begin by examining the case of 5% input uncertainty with 50% and 100% channel drops for the 2 channel case in figure 6.11. We see that the robust controller restricts the change in average inversion better than the L_2 controller without robustness. The 100% channel drop causes a larger state change than the 50% channel drop. These results are depicted again for the 32 channel case with 50%, 97% and 100% channel drop cases in figure 6.12.

The transient pump powers are depicted in figures 6.11 and 6.12. The final pump powers between the robust and non-robust controllers differ by only a small amount. Also, the robust controller responds quicker than the L_2 controller without robustness to compensate for the disturbances. It is interesting to note that in the 2 channel case, the 100% drop case results in both controllers falling to almost 0mW pump power. In the 32 channel case, we see that in fact the pump power for the 100% drop case exceeds the 0mW boundary. This situation represents a failure for the pump to compensate for the

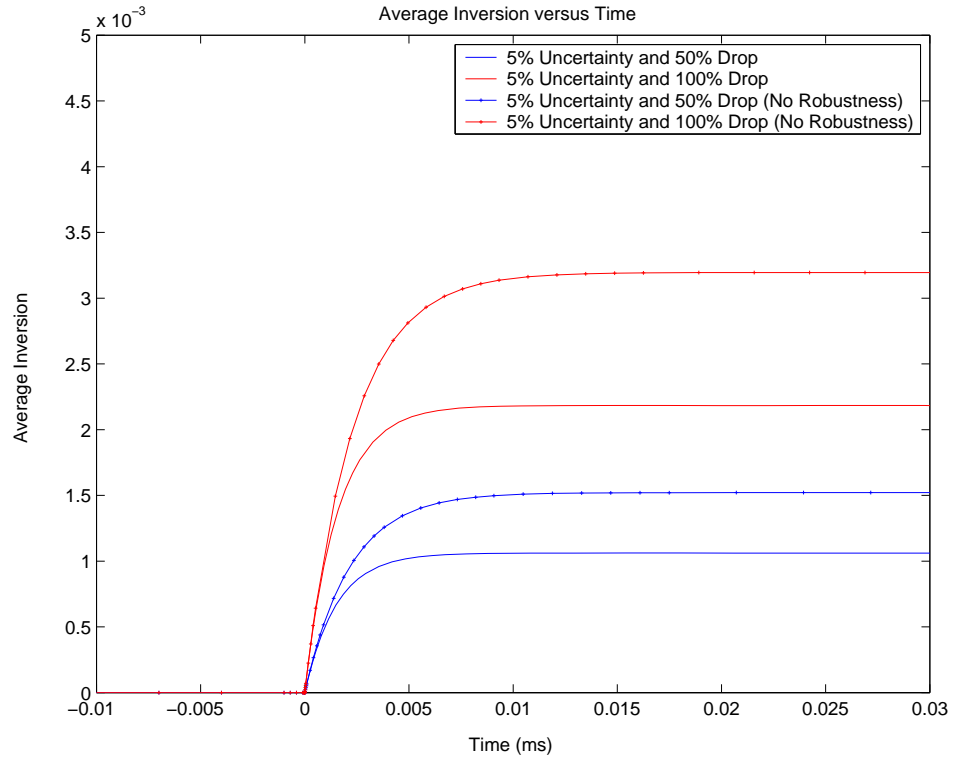
disturbance according to its design. Since it can not drop to less than 0mW of power, the pump essentially saturates at the 0mW position and remains there. Thus, we see the robust controller derived here would compensate most drop channels except such an extreme case.

The case with only state uncertainty is similar to previous sections as shown in figure 6.13. The results are predictable in that the 100% channel drop causes a larger state variance than the 50% channel drop. Once again, the state uncertainty term $f'(x)$ dominates the other terms thereby causing a very fast and small state disturbance. This results in an angular looking transient plot. The controller with no robustness also shows a predictable behaviour but with a much larger response time. These results are also visible in the 32 channel cases in figure 6.15.

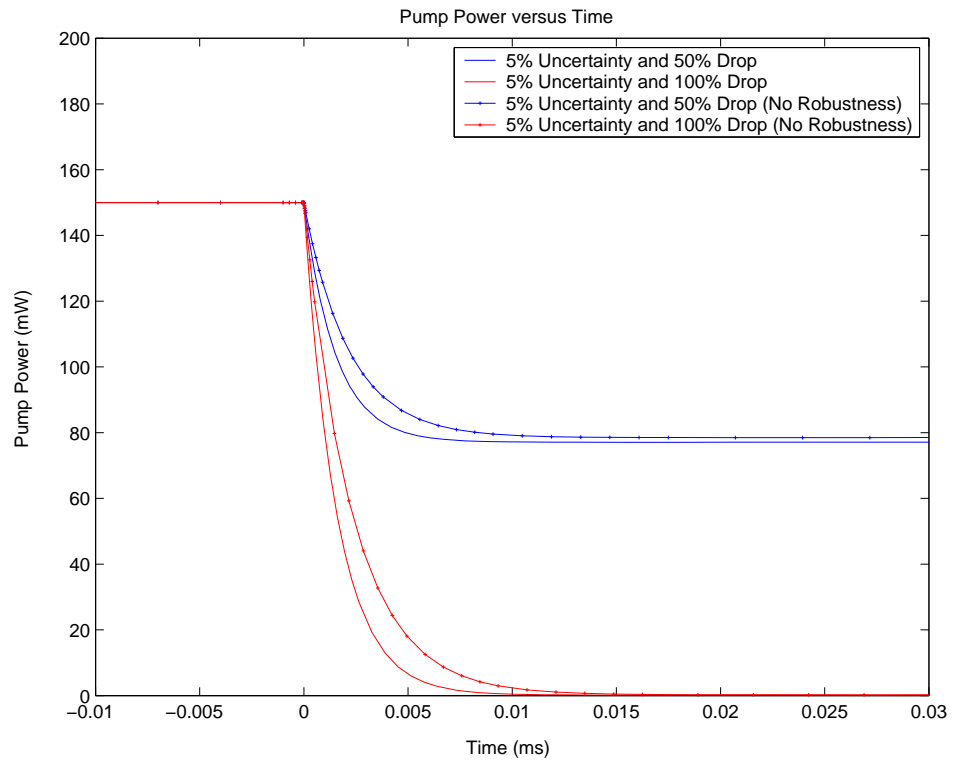
If we examine the pump power plots in figures 6.14 and 6.16 we notice the pump saturation again. We see that in the most extreme drop cases of 100%, the pump can not respond with enough power to compensate the disturbance. These situations must be tested by simulation to determine in advance if this could happen. These results tell us that there are limits to the compensation ability of the controllers. Either a new design where there was more restriction on the pump variable or a test case with less uncertainty would be necessary to fully achieve the design specifications.

We can now analyze the simulations of combining both state uncertainty with input uncertainty along with channel drops. We choose the state uncertainty to be 0.001 and the input uncertainty to be 5%. The uncertainties are both chosen to cause the state and the pump to compensate together in the same direction. We would expect to see similar looking plots as the two uncertainties decoupled but with larger magnitudes of compensation.

If we examine figures 6.17 and 6.19 for the 2 channel and the 32 channel cases, respectively, we see our predicted results. Once again we notice a similar response to the state uncertainty case. The various channel drops distinguish themselves appropriately

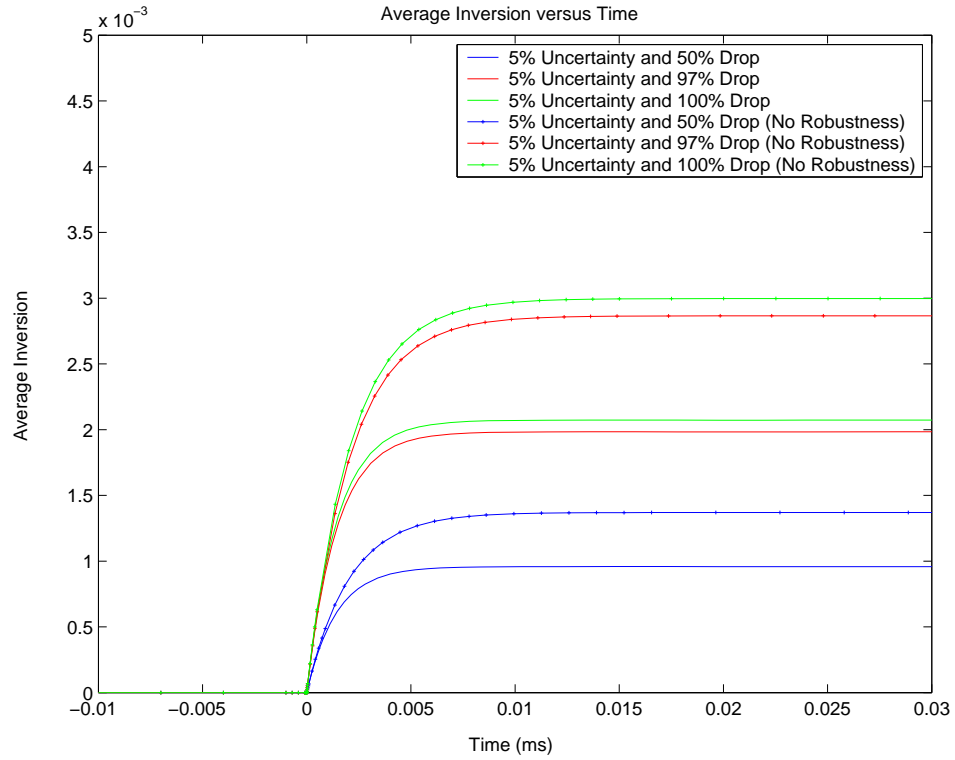


(a) Average Inversion versus Time for 2 Channels

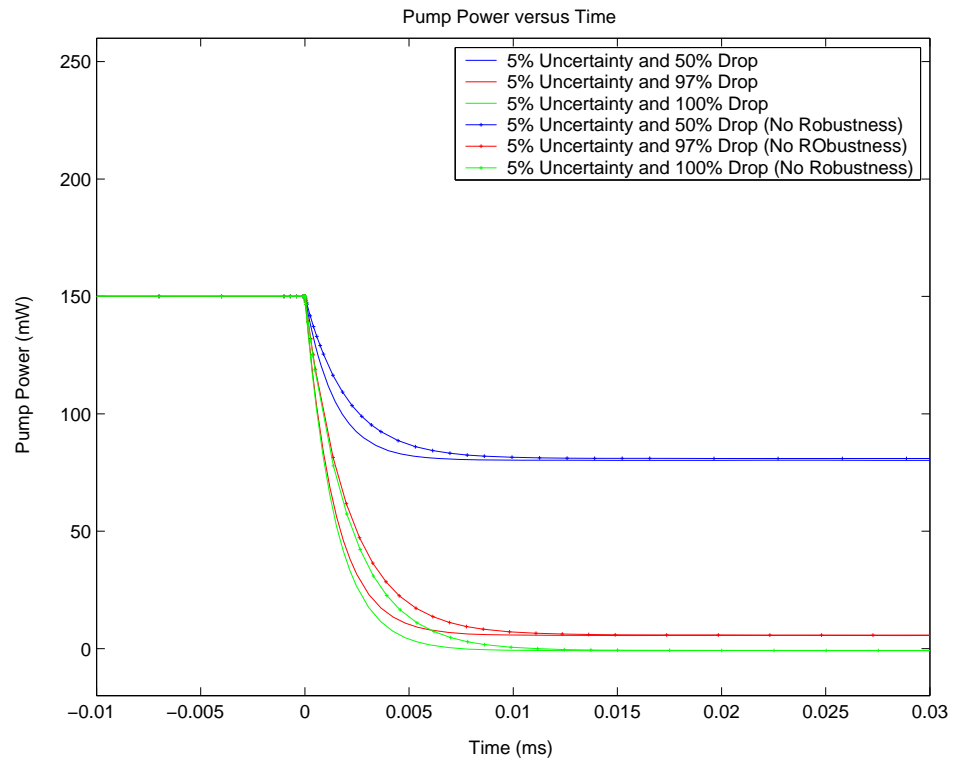


(b) p^{out} versus Time for 2 Channels

Figure 6.11: Input Multiplicative Case for 2 Channels with 5% Input Uncertainty and Channel Drops

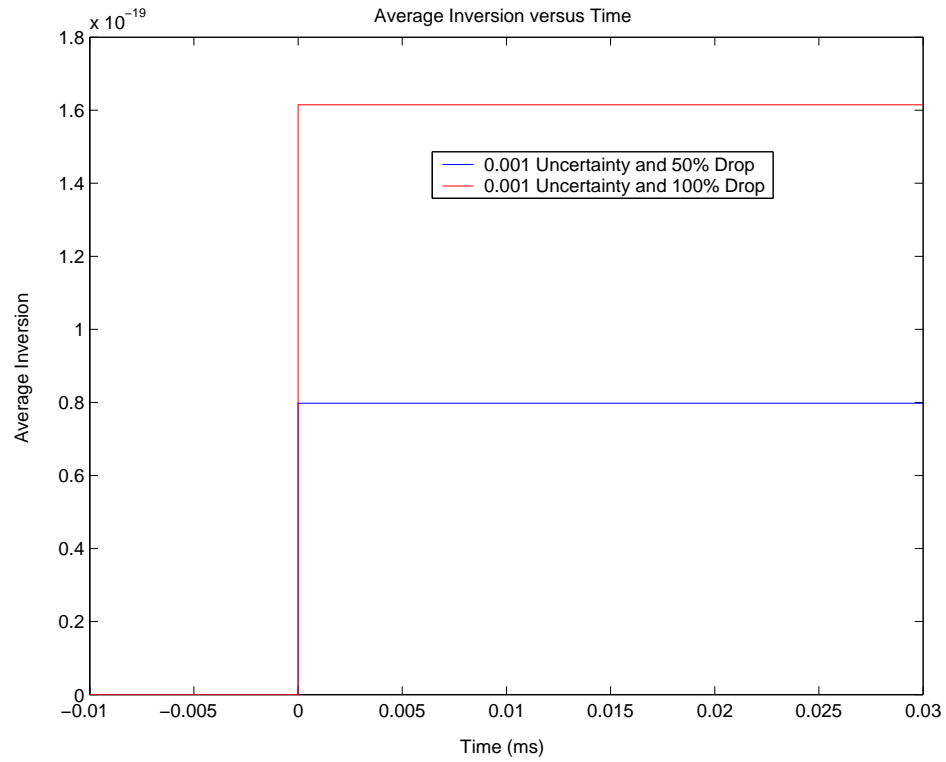


(a) Average Inversion versus Time for 32 Channels

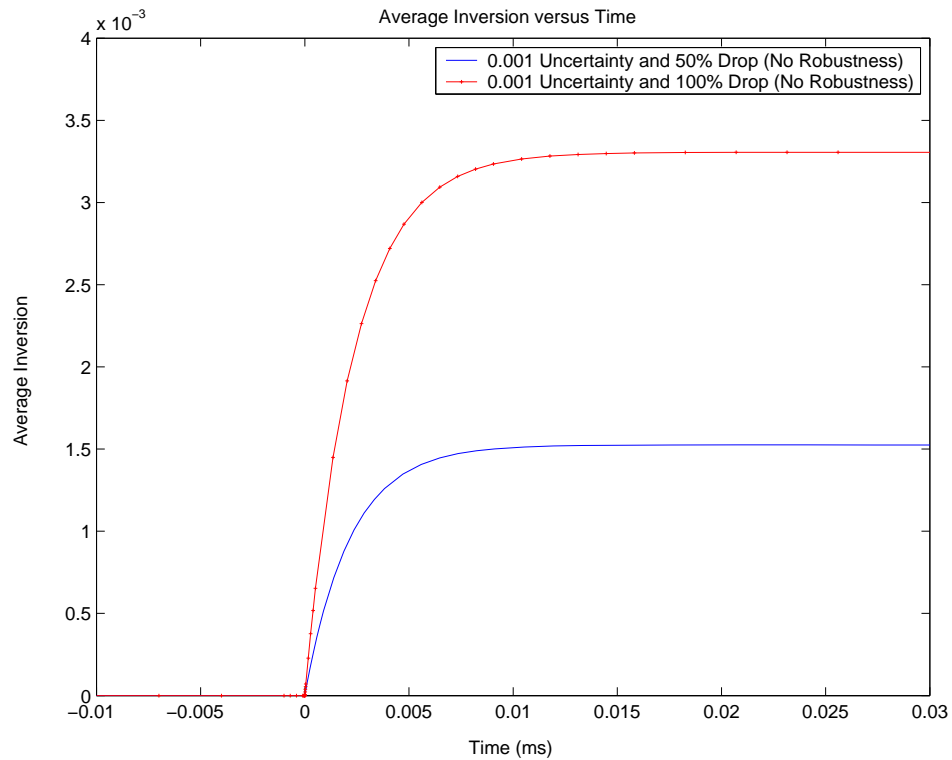


(b) p^{out} versus Time for 32 Channels

Figure 6.12: Input Multiplicative Case for 32 Channels with 5% Input Uncertainty and Channel Drops



(a) Average Inversion versus Time for 2 Channels



(b) Average Inversion versus Time for 2 Channels

Figure 6.13: State Uncertainty Case for 2 Channels with 0.001 State Uncertainty and Channel Drops

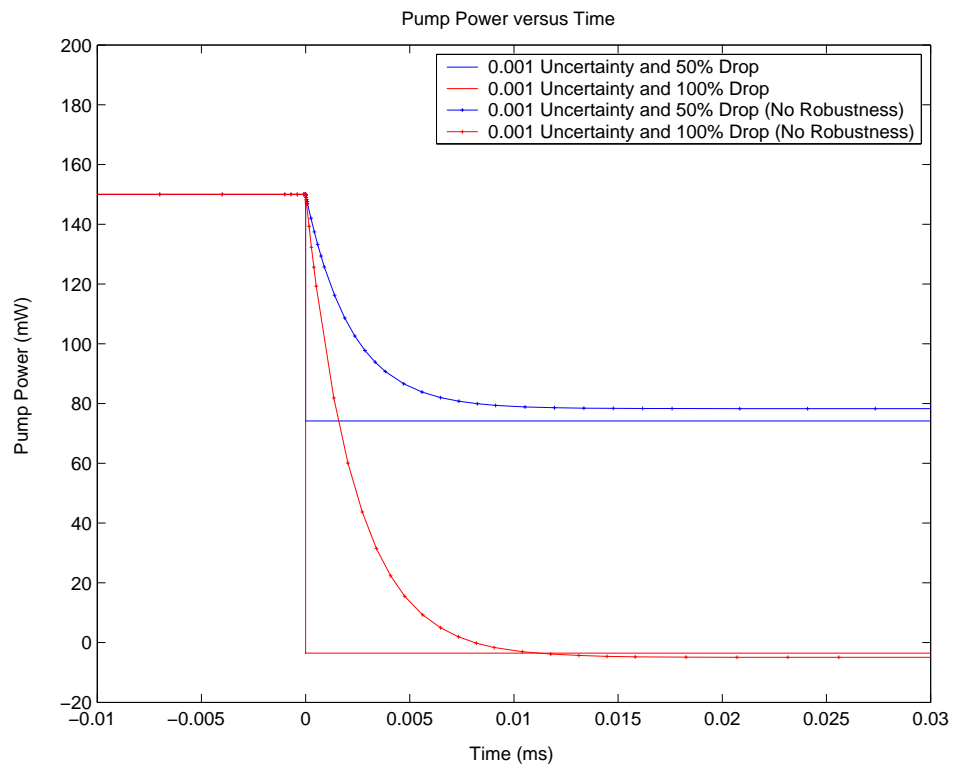
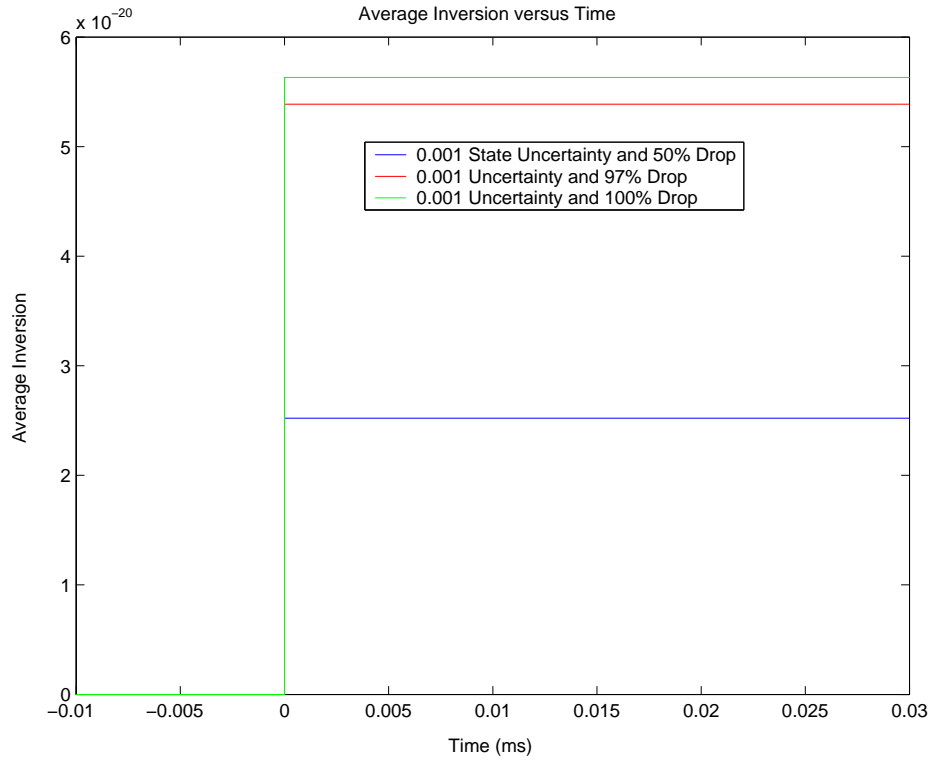
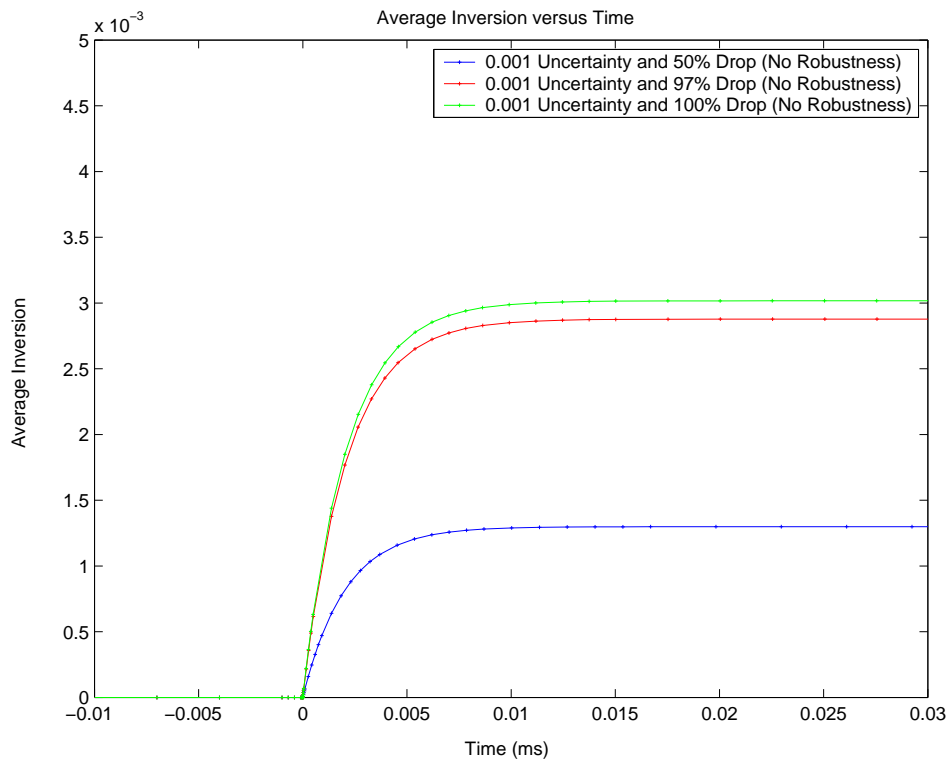


Figure 6.14: State Uncertainty Case for 2 Channels with 0.001 State Uncertainty and Channel Drops



(a) Average Inversion versus Time for 32 Channels



(b) Average Inversion versus Time for 32 Channels

Figure 6.15: State Uncertainty Case for 32 Channels with 0.001 State Uncertainty and Channel Drops

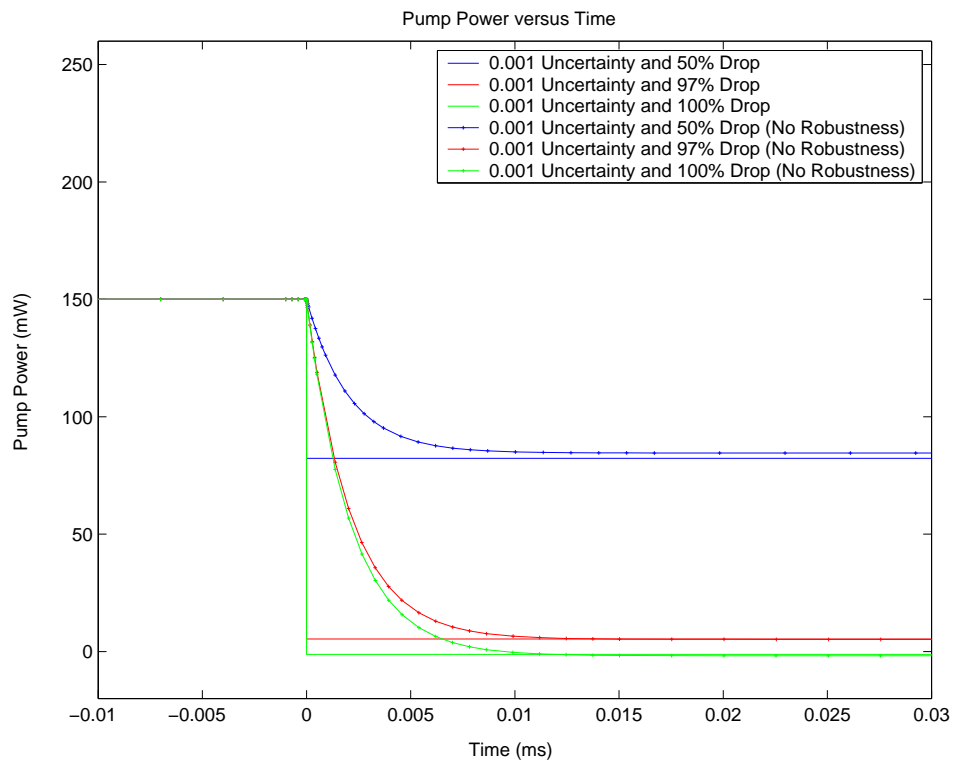
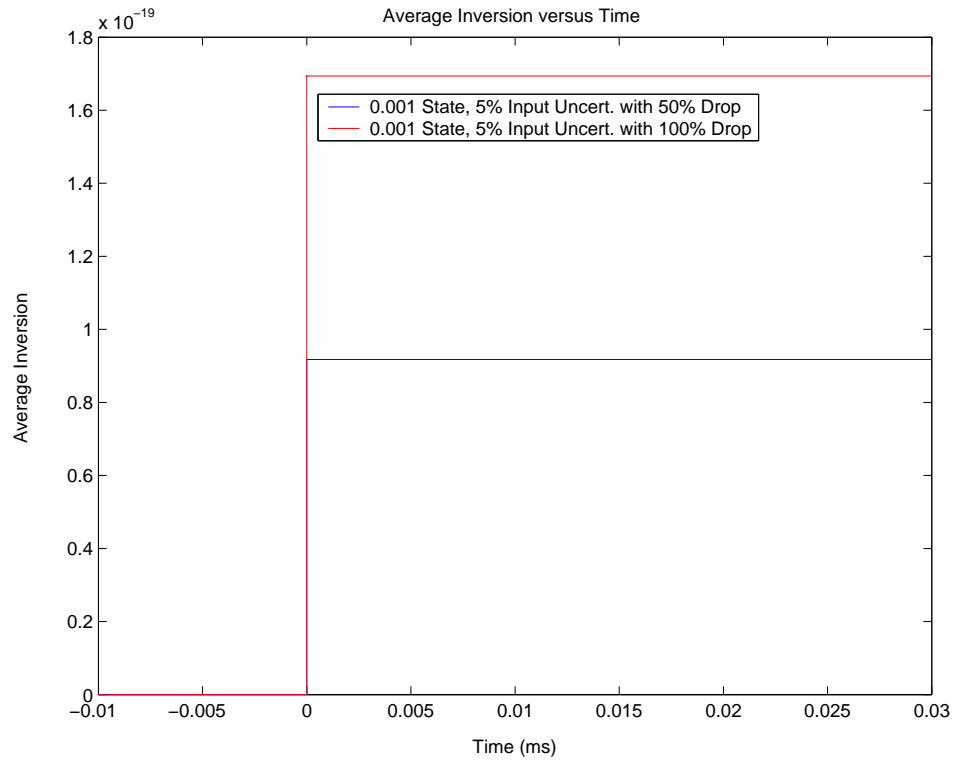
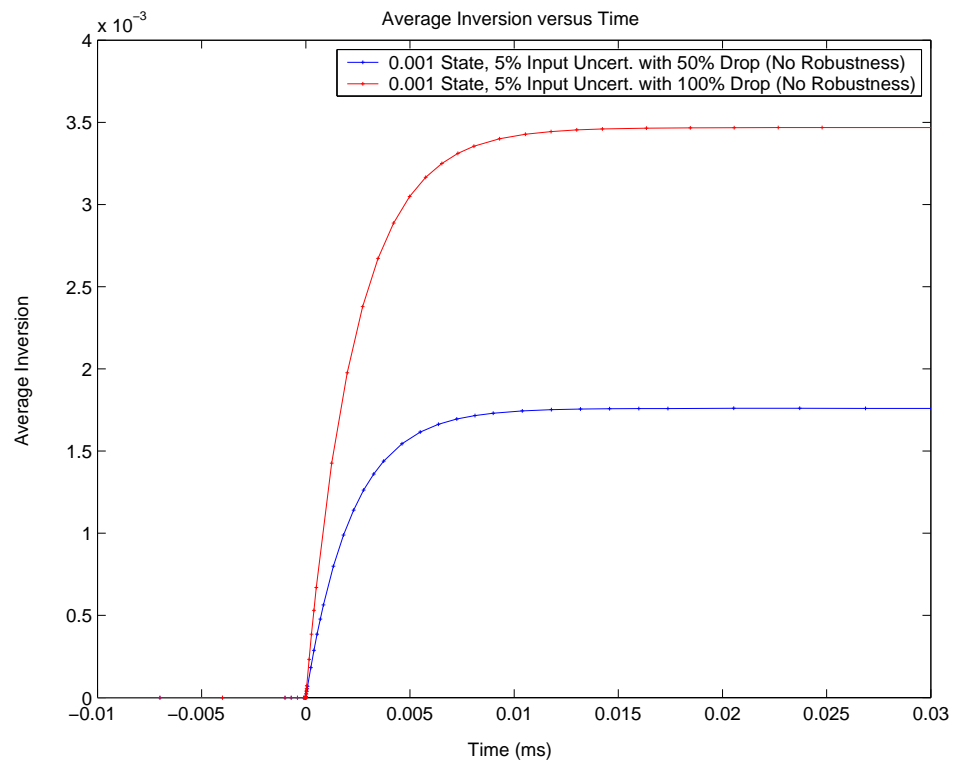


Figure 6.16: State Uncertainty Case for 32 Channels with 0.001 State Uncertainty and Channel Drops



(a) Average Inversion versus Time for 2 Channels



(b) Average Inversion versus Time for 2 Channels

Figure 6.17: State Uncertainty and Multiplicative Uncertainty Case for 2 Channels with 0.001 State Uncertainty and 5% Input Uncertainty with Channel Drops

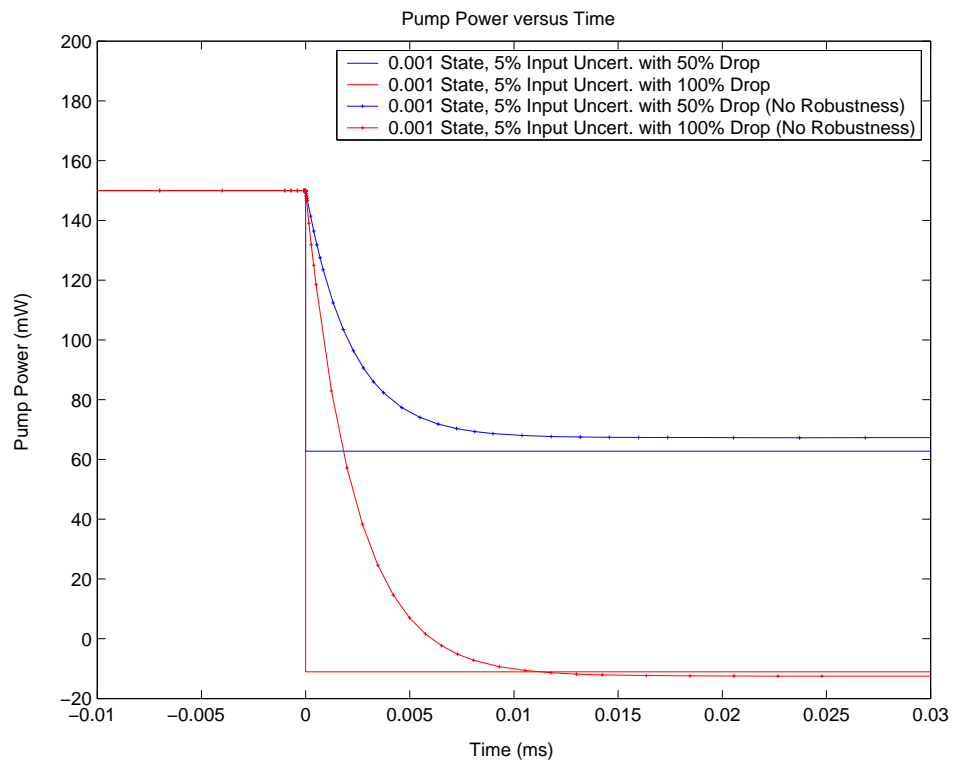
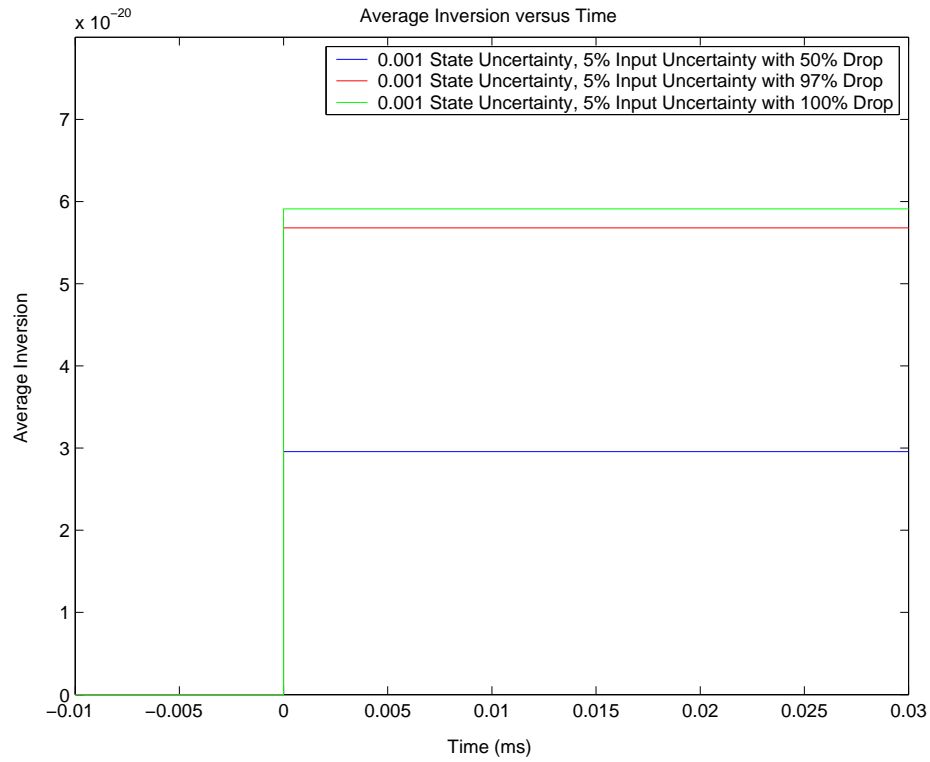
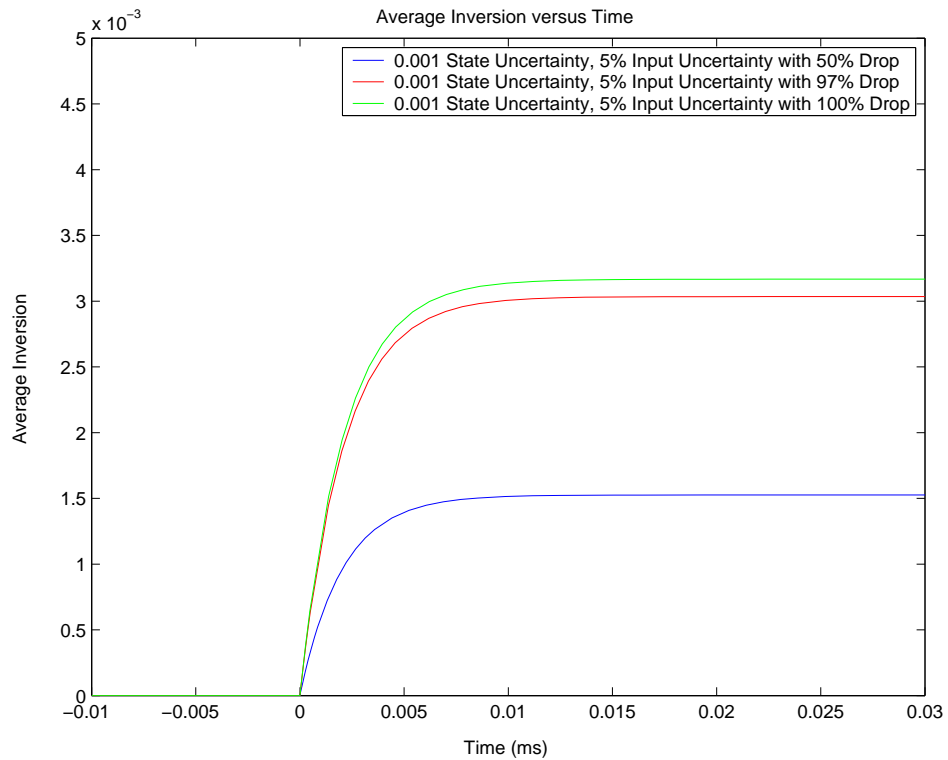


Figure 6.18: State Uncertainty and Multiplicative Uncertainty Case for 2 Channels with 0.001 State Uncertainty and 5% Input Uncertainty with Channel Drops



(a) Average Inversion versus Time for 32 Channels



(b) Average Inversion versus Time for 32 Channels

Figure 6.19: State Uncertainty and Multiplicative Uncertainty Case for 32 Channels with 0.001 State Uncertainty and 5% Input Uncertainty with Channel Drops

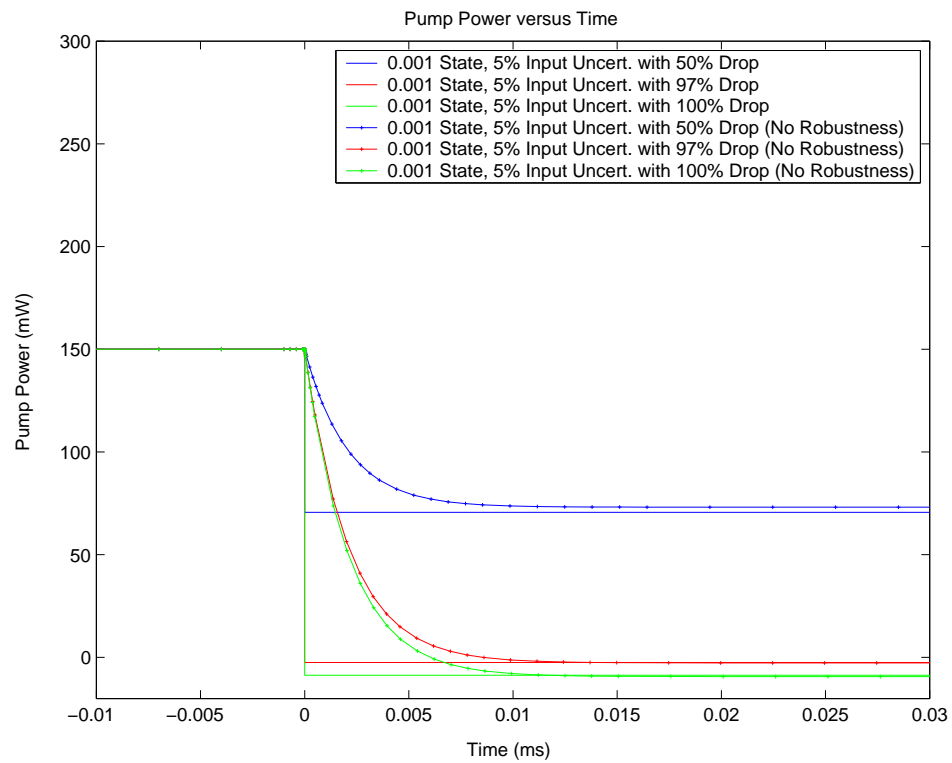


Figure 6.20: State Uncertainty and Multiplicative Uncertainty Case for 32 Channels with 0.001 State Uncertainty and 5% Input Uncertainty with Channel Drops

from each other. The state variables vary further from their origin than in the case of just state uncertainty by itself. The comparison to the state uncertainty case is justified in that the controller is the same one used there.

Upon examination of the pump power variation, we see a much larger drop below the 0mW boundary line as shown in figures 6.18 and 6.20. This is due to the fact that the pump is attempting to compensate for both uncertainties at once. The larger difference between the negative pump powers and the 0mW boundary means that this controller would be less successful at compensating for both uncertainties rather than one or the other as presented. The 32 channel case shows that both the 100% and the 97% drop cases would generate pump saturation at 0mW.

Overall, the response of the robust controller has significantly improved the performance of the system against uncertainties and channel drops. In addition, the cost of pump performance to achieve these improved results is almost negligible. Thus, the robust L_2 nonlinear controller does offer a genuine improvement over the L_2 nonlinear controller without robustness.

It should also be noted that the robust controller, as designed herein, does have limits to its performance. There were a number of extreme uncertainty cases and channel drops that would cause the pump to saturate at 0mW. If a better performance is necessary to handle certain extreme cases, a new controller design with more restriction on the pump may be tried. Otherwise, proper performance of the closed loop system would have to rely on smaller uncertainties to prevent pump saturation. Despite these few cases, the robust controller performed very well for the vast majority of its simulated tests.

Chapter 7

Conclusion

The summarized results of the thesis are presented in the first section. A short discussion of the limitations of the work are provided in the following section. The plans for future work are outlined in the remaining section.

7.1 Significant Results

We have successfully developed a more complete system representation for the EDFA that includes ASE. We have demonstrated the significant effect that ASE can have for the situation in which a large number of channels are dropped. We simulated the steady state effects of the terms in the state equation, where we took special note of the two new ASE terms where one was linear and the other nonlinear. We noted that for high average inversion levels the nonlinear ASE term can have a significant impact in the state equation. The dynamic simulations showed the effects of the average inversion, channel powers and ASE for channel drops.

We successfully took the more complete EDFA model with ASE and devised both a linear and nonlinear controller that solves the Full Information problem since the state is computable in real-time. As an example, we found a nonlinear controller that guarantees an L_2 gain of 0.0001 over the entire state space. We also noted that, if needed, the

transient performance requirements of the pump can be reduced by increasing the L_2 gain.

We took the L_2 nonlinear controller and compared its performance with a PID gain scheduling control scheme. The gain scheduling controller was an ideal baseline comparison since it used linearization approximations but the various controllers were systematically switched. This provided a quantifiable means to compare the linearized controller with the improved nonlinear control scheme. In addition, the gain scheduling scheme used the EDFA model without ASE to compare the added benefits of ASE in the L_2 nonlinear control scheme. The results showed a clear advantage to using the L_2 nonlinear control scheme since the pump power response was smoother and the response times were faster. Furthermore, we could directly impose restrictions on the state variable to control the output channel powers rather than relying on the indirect gain control.

Another layer of design was imposed by including robustness as part of the control design. The objective here was to improve the system performance with respect to uncertainties in the system parameters and the input and output signals. We began by adopting a control scheme from [15] [12] that used L_2 nonlinear control to reduce unstructured uncertainties in a model. We then extended the results into a new idea to include uncertainties in the state variable. These uncertainties could represent parametric imprecision. Output uncertainties such as imprecise output power measurement, state calculation imprecision, and state output delay would also improve. We represented the uncertainties as disturbances to the system model. The results yielded a better restriction on the state variables as compared with the non-robust L_2 controller using the same L_2 gain. Furthermore, the uncertainty test cases were combined with channel drops to provide a more realistic setting for the EDFA system. The results also corroborate that more restriction on the state variable is achieved. Furthermore, the cost to the pump performance was very small making the robust control scheme an excellent option for EDFA application.

We have proven that the robust L_2 nonlinear control scheme is superior to linearization techniques and ad hoc controller scheduling. Our EDFA model with amplified spontaneous emission is more inclusive and more accurate. We achieve a much better performance in transient time for the state variable to stabilize as well as a much better smoothness in pump power response. The nonlinear controller clearly outperforms the linearization technique as demonstrated in simulation. The robust control scheme further improves the system response to input and state uncertainties. Hence, the robust L_2 nonlinear control scheme is a significant improvement to EDFA output power control.

7.2 Limitations to Work

Although we found a nonlinear controller that satisfies the L_2 requirements for all of the state space, we must realize that this design was taken over Taylor approximated terms in the EDFA model. We chose to use three terms orders of polynomial terms to approximate all of the terms in the EDFA model. The accuracy of the approximate is high around the operating point, but as the state value moves further away, the approximation suffers. The approximation on the outer boundaries of the state space can be poor.

There is no explicit means to guarantee a viable L_2 nonlinear controller. The methodology outlined in the thesis still requires tuning to obtain a reasonable result. This relates to the fact that there is no explicit means to find a solution to the Hamilton Jacobi Equation (HJE). We must rely on a Taylor approximation to the solution to the HJE. Also, we use a computational approach to the HJE solution, where the final result is not known until after the computation. As such, a particular result may not be acceptable, and a new solution must be computed based on different parameters (ie. γ). This lack of knowledge of $V(x)$ from the HJE prevents an explicit solution to the L_2 nonlinear control problem.

It can be computationally expensive to produce simulations using L_2 nonlinear con-

trol. The highly nonlinear nature of the EDFA system with ASE makes the closed loop solution especially difficult to simulate. The robust control simulations in particular require the use of MATLAB's ode15s to obtain a solution in a reasonable time.

For any practical implementation of the simulation results, the L_2 control scheme is limited by the pump to provide enough power within a specified time period. Theoretically, there is no limit to the restriction of the EDFA channel output powers using L_2 nonlinear controller. However, a physical laser pump can only provide significant power within a 1 to $10\mu s$ time period. Hence, to improve the L_2 control performance beyond the simulated results presented herein, we would have to improve the actual laser pump hardware.

7.3 Future Work

Future work will look for an explicit set of design laws to guarantee a solution for the nonlinear L_2 control problem. A method that does not involve tuning and iteration would be ideal. Specifically, a method of explicit solution to the Hamilton Jacobi Equation which yields predictable features for $V(x)$ would greatly simplify the problem.

There is currently little to none commercially available software that solves the HJE. As such, an extensive MATLAB script has been written to use polynomial approximation for the work presented herein. One potential future application could be to develop the software into a more general and user friendly form such that any designer could use these tools. Also, the code could be optimized to attempt to reduce the computational time to derive the controller and run simulations.

An extremely important future development of the work within this thesis would be to implement the L_2 nonlinear control scheme onto a physical EDFA. So far, only simulations exist to verify the performance of the nonlinear controller. It would be very interesting to explore what practical difficulties could present themselves with the new

control design. Furthermore, a practical implementation would serve as an ultimate verification for the work presented herein.

Appendix A

Polynomial Solution To Hamilton-Jacobi Equation

The procedure for solving the Hamilton-Jacobi Equation using polynomial approximation was developed in [21]. A clear outline and example of the usage of the polynomial solution is presented in [12]. The formulation is reiterated below for clarity following the structure and notation of [12] based on the results in [21].

We define a homogeneous polynomial of degree m for $x = (x_1, x_2, \dots, x_n)$ as

$$P^{[m]}(x) = \sum_{i_1 + \dots + i_n = m} p_{i_1 \dots i_n} x_1^{i_1} x_2^{i_2} \dots x_n^{i_n} \quad (\text{A.1})$$

where $p_{i_1 \dots i_n}$ are coefficients. Let $x^{[m]}$ represent a matrix of elements such that,

$$x^{[m]} = \begin{bmatrix} x_1^m \\ x_1^{m-1} x_2 \\ \vdots \\ x_1^{i_1} x_2^{i_2} \dots x_k^{i_k} \dots x_n^{i_n} \\ \vdots \\ x_n^m \end{bmatrix} \quad \text{with} \quad \sum_{k=1}^n i_k = m$$

Using the above notation, we can represent a homogeneous polynomial of degree m as

$$P^{[m]}(x) = p^{(m)} x^{[m]} \quad (\text{A.2})$$

where $p^{(m)}$ is a row vector of polynomial coefficients.

We write out the Hamilton Jacobi Equation (HJE) as

$$H(V, x) = \frac{\partial V}{\partial x}(x)A(x) + \frac{1}{4} \frac{\partial V}{\partial x}(x)Q(x) \frac{\partial^T V}{\partial x} + R(x) \quad (\text{A.3})$$

where $A(x)$, $Q(x)$, and $R(x)$ are analytic, with $A(0) = 0$, $R(0) = 0$, $\frac{\partial R}{\partial x}(0) = 0$, $V(0) = 0$, and $\frac{\partial V}{\partial x}(0) = 0$.

Any function with a superscript $[m]$ will denote a homogeneous polynomial of degree m in x . We can thus represent the terms of the HJE in (A.3) as a power series about $x = 0$ as:

$$A(x) = \sum_{i=1}^{\infty} A^{[i]}(x) \quad Q(x) = \sum_{j=0}^{\infty} Q^{[j]}(x) \quad R(x) = \sum_{k=2}^{\infty} R^{[k]}(x) \quad (\text{A.4})$$

and we also represent $V(x)$ as the power series:

$$V(x) = \sum_{m=2}^{\infty} V^{[m]}(x) \quad (\text{A.5})$$

We further denote

$$A_L = \frac{\partial A}{\partial x}(0), \quad Q_L = Q(0), \quad R_L = \frac{1}{2} \frac{\partial^2 R}{\partial x^2}(0), \quad P_L = \frac{1}{2} \frac{\partial^2 V}{\partial x^2}(0) \quad (\text{A.6})$$

we can represent the first terms of (A.4) using (A.6) to obtain

$$A^{[1]}(x) = A_L x \quad Q^{[0]}(x) = Q_L \quad R^{[2]}(x) = x^T R_L x \quad V^{[2]}(x) = x^T P_L x \quad (\text{A.7})$$

and we can use (A.7) to rewrite (A.4) and (A.5) as

$$\begin{aligned} A(x) &= A_L x + A^h(x) \\ Q(x) &= Q_L x + Q^h(x) \\ R(x) &= x^T R_L x + R^h(x) \\ V(x) &= x^T P_L x + V^h(x) \end{aligned} \quad (\text{A.8})$$

where $A^h(x)$, $Q^h(x)$, $R^h(x)$, and $V^h(x)$ represent the higher-degree terms of the power series expansion.

Now, by substituting (A.8) into the HJE (A.3), we can obtain a Riccati equation

$$P_L A_L + A_L^T P_L + P_L Q_L P_L + R_L = 0 \quad (\text{A.9})$$

where Q_L is in general an indefinite matrix and the high degree equation

$$-\frac{\partial V^h}{\partial x}(x) A_{Lin} x = \frac{\partial V}{\partial x}(x) A^h(x) + \frac{1}{4} \frac{\partial V^h}{\partial x}(x) Q_L \frac{\partial^T V^h}{\partial x}(x) + \frac{1}{4} \frac{\partial V}{\partial x}(x) Q^h(x) \frac{\partial^T V}{\partial x}(x) + R^h(x) \quad (\text{A.10})$$

where $A_{Lin} = A_L + Q_L P_L$.

$V^{[m]}(x)$ can now be computed inductively for $m = 3, 4, \dots$. Let the the right hand side of (A.10) be denoted by $H^{[m]}(x)$

$$\frac{\partial V^{[m]}}{\partial x}(x) A_{Lin} x = -H^{[m]}(x) \quad (\text{A.11})$$

Denote P_L as the stabilizing solution of the Riccati equation (A.9) if A_{Lin} has its eigenvalues in the left half plane. We can rewrite (A.11) as a time derivative of $V^{[m]}(x)$ along the solution of the stable linear system $\dot{x} = A_{Lin} x$

$$\frac{d}{dt} V^{[m]}(x(t)) = -H^{[m]}(x) \quad (\text{A.12})$$

Integrating both sides from 0 to ∞ yields

$$V^{[m]}(x(\infty)) - V^{[m]}(x(0)) = - \int_0^\infty H^{[m]}(x(t)) dt \quad (\text{A.13})$$

where $x(t) = e^{A_{Lin} t} x(0)$. Taking into account that A_{Lin} is stable it follows that $x(\infty) = 0$.

For $x(0) = x$, (A.13) becomes

$$V^{[m]}(x) = \int_0^\infty H^{[m]}(e^{A_{Lin} t} x) dt \quad (\text{A.14})$$

Thus, $V^{[m]}(x)$ is determined by $H^{[m]}(x)$. Upon inspection of (A.10) and (A.11), it is apparent that $H^{[m]}(x)$ is characterized by $V^{[m-1]}(x), \dots, V^{[2]}$. Induction can therefore be used in the computation of $V^{[m]}(x)$ starting from $V^{[2]}(x) = x^T P_L x$.

If (A.4) and (A.5) are substituted into (A.10), $H^{[m]}(x)$ can be stated as

$$\begin{aligned}
H^{[m]}(x) &= \sum_{k=2}^{m-1} \frac{\partial V^{[k]}}{\partial x}(x) A^{[m+1-k]}(x) + \frac{1}{4} \sum_{k=2}^{m-1} \frac{\partial V^{[k]}}{\partial x}(x) Q^{[m-k]} \frac{\partial^T V^{[2]}}{\partial x}(x) \\
&\quad + \frac{1}{4} \sum_{k=3}^{m-1} \sum_{j=2}^{m-k+2} \frac{\partial V^{[k]}}{\partial x}(x) Q^{[m+2-k-j]}(x) \frac{\partial^T V^{[j]}}{\partial x}(x) + R^{[m]}(x) \quad (\text{A.15})
\end{aligned}$$

Equation (A.15) depicts an explicit form for calculating $H^{[m]}$.

Appendix B

EDFA System Parameters and Input Values

The following tables outline the parameters that characterize the EDFA. This includes the absorption and emission coefficients for the EDFA wavelength channels, the fiber length, and the chosen range of wavelengths that were used for the simulations in this thesis. In addition, the standard number of input channels, the signal channel powers and the pump power is listed as well.

The tables are outlined as follows. Table B.1 outlines the input powers and the number of channels used in EDFA simulations. Table B.2 lists important parametric data used to define any EDFA model. Table B.3 outlines the set of wavelengths and their absorption and emission coefficients that were used in simulations in this thesis.

Table B.1: EDFA Input Values

Channel Number, N	2,32
Channel Powers, $P_{in,k}$	42.6 μ W
Pump Power, P_{pump}	150 mW

Table B.2: EDFA parameters

Core Radius	1.8	μm
Er Radius	1.7	μm
Er ion Density, ρ	4.33E+24	$ions/m^3$
Metastable Lifetime, τ	10	ms
Channel Separation (for $\Delta\nu$)	0.75	nm
Fiber Length, L	13	m

Table B.3: EDFA Signal and Pump Bands

PUMP Band		
	absorption	emission
Wavelength (nm)	alpha (dB/m)	g* (dB/m)
980	3.229	0
Signal Band		
	absorption	emission
Wavelength (nm)	alpha (dB/m)	g* (dB/m)
1530.072	6.48847101	6.34602815
1530.822	6.46745262	6.42559327
1531.572	6.39438961	6.45346687
1532.322	6.25689043	6.41444007
1533.072	6.03760685	6.28728490
1533.822	5.75636541	6.08888521
1534.572	5.41688357	5.82005299
1535.322	5.05014027	5.51142318
1536.072	4.71437590	5.22590919
1536.822	4.42198205	4.97888926
1537.572	4.17915448	4.77939467
1538.322	4.00324142	4.65008448
1539.072	3.86698139	4.56225009
1539.822	3.76417861	4.51051485
1540.572	3.68863729	4.48912960
1541.322	3.62672670	4.48275331
1542.072	3.57225106	4.48434805
1542.822	3.52273204	4.49113609
1543.572	3.47197387	4.49536528
1544.322	3.41749823	4.49368075
1545.072	3.36302259	4.49080486
1545.822	3.30359031	4.47996451
1546.572	3.24167973	4.46420686
1547.322	3.17976914	4.44681532
1548.072	3.11538024	4.42422636
1548.822	3.05594797	4.40697230
1549.572	2.99279822	4.38259781
1550.322	2.92964848	4.35636191
1551.072	2.86525957	4.32633577
1551.822	2.80582730	4.30188284
1552.572	2.74515587	4.27367610
1553.322	2.68572360	4.24545752

Appendix C

List of MATLAB Simulation Files

The following tables summarize the main files used to generate the simulations in this thesis. Along with a list of files, a brief description of each file is presented. The files are organized according to open loop EDFA model with ASE simulations and closed loop L_2 control simulations. Both the L_2 nonlinear control simulation program and the robust simulation program are similar in terms of file names. Thus, only one set of files is presented for both. Due to the large number of files present in the closed loop simulators, only the main files are described.

The files in the 'MastersThesisASEmodel' directory are listed in Table C.1. This directory holds all files necessary to simulate the steady state and open loop dynamic response of the EDFA system with ASE.

The files located in the 'MastersThesisHJESolver \ FISolver' directory and 'MastersThesisRobustness \ robustsolver' are listed in table C.2. These files are responsible for calculating a taylor approximated L_2 nonlinear controller for the EDFA model with ASE. Furthermore, the files generate closed loop system response figures. These files comprise the most important simulation tool in this thesis. Ancillary files have been neglected due to volume.

Table C.1: Files in directory 'MastersThesisASEmodel'

File	Description
steadystateASEmodel.m	steady state EDFA model with ASE simulator
dynamicASEmodel.m	open loop dynamic EDFA model with ASE simulator
ASEmodelfzero.m	used to calculate operating point x value in 'dynamicASEmodel.m'
ASEmodel.m	dynamic EDFA model used with ode45 function in 'dynamicASEmodel.m'
ASEworkspace.mat	argument values to the steady state and dynamic simulation programs

Table C.2: Files in directory 'MastersThesisHJEsolver \ FIsolver' and 'MastersThesis-Robustness \ robustsolver'

File	Description
simul.m	main module from where all other functions are called.
ASEmodelLoader.m	loads EDFA parameters
ASEmodelfzero.m	used to calculate operating point x value in 'ASEmodelLoader.m'
testvu.m, gammacalc.m	calculates minimum γ value
offline.m	Creates taylor approximated plant, calls hji.m, calls parcontrFI.m tests FI theorem conditions visually
hji.m	hamilton-jacobi equation solver
parcontrfi.m	computes the FI controller
datanonl.m	computes taylor approximated system model and HJE terms
closed_any.m	closed form taylor approximated system used with ode solver
closed_anyfull.m	closed form full nonlinear system used with ode solver

Bibliography

- [1] L. Pavel, “Control design for transient power and spectral control in optical communication networks,” in *Proc. IEEE Conference on Control Applications*, vol. 1, June 2003, pp. 415 – 422.
- [2] R. Ramaswami and K. N. Sivarajan, *Optical Networks: A Practical Perspective*, 2nd ed. San Diego: Academic Press, 2002.
- [3] G. P. Agrawal, *Fiber-Optic Communication Systems*, Second Edition, New York: John Wiley and Sons, 1997.
- [4] A. K. Srivastava, Y. Sun, J. L. Zyskind, and J. W. Sulhoff, “EDFA transient response to channel loss in WDM transmission system,” *IEEE Photon. Technol. Lett.*, vol. 9, no. 3, pp. 386–388, Mar. 1997.
- [5] Y. Sun, A. K. Srivastava, J. L. Zyskind, J. W. Sulhoff, C. Wolf, and R. W. Tkach, “Fast power transients in WDM optical networks with cascaded EDFAs,” *Electronics Letters*, vol. 33, no. 4, pp. 313–314, Feb. 1997.
- [6] C. R. Giles and E. Desurvire, “Modeling erbium-doped fiber amplifiers,” *J. Light-wave Technol.*, vol. 9, no. 2, pp. 271–283, Feb. 1991.
- [7] Y. Sun, J. L. Zyskind, and A. K. Srivastava, “Average inversion level, modeling, and physics of erbium-doped fiber amplifiers,” *IEEE J. Select. Topics Quantum Electron.*, vol. 3, pp. 991–1007, Aug. 1997.

- [8] X. Feng, T. Jin, Y. Wang, Q. Wang, X. Liu, and J. Peng, "A simple control algorithm for wide-band channel-power clamped EDFA," *Optics Communications*, no. 213, pp. 285–292, 2002.
- [9] E. Desurvire and J. R. Simpson, "Amplification of spontaneous emission in erbium-doped single-mode fibres," *J. Lightwave Technol.*, vol. 7, no. 5, pp. 835–845, May 1989.
- [10] M. Ding and L. Pavel, "Gain Scheduling Control Design of an Erbium-Doped Fibre Amplifier by Pump Compensation", 2005 IEEE Conference of Control Applications, accepted for publication.
- [11] H. K.Khalil, *Nonlinear Systems*, New Jersey:Prentice Hall, 2002.
- [12] L. Pavel, "Nonlinear H_∞ (L_2) control with applications," Ph.D. dissertation, Queens University, Kingston, Ontario, June 1996.
- [13] A. J.van der Schaft, " L_2 -Gain Analysis of Nonlinear Systems and Nonlinear State Feedback H_∞ control", *IEEE Transactions on Automatic Control*, Vol.37, No.6, pp.770-784, June 1992.
- [14] A. J. van der Schaft, "On a state space approach to nonlinear H_∞ control," *Systems and Control Letters*, no. 16, pp. 1–8, 1991.
- [15] L. Pavel and F. W. Fairman, "Robust Stabilization of Nonlinear Plants - an L_2 Approach", *International Journal of Robust and Nonlinear Control*, Vol.6, pp.691-726, 1996.
- [16] W. M. Lu and J. C. Doyle, " H_∞ control of nonlinear systems via output feedback: A class of controllers," in *Proceedings of the 32nd Conference on Decision and Control*, Dec. 1993, pp. 166–171.

- [17] K. Glover and J. C. Doyle, “State-space formulae for all stabilizing controllers that satisfy an H_∞ -norm bound and relations to risk sensitivity,” *Systems and Control Letters*, vol. 11, no. 3, pp. 167–172, 1988.
- [18] J. C. Doyle, B. A. Francis, and A. R. Tannenbaum, *Feedback Control Theory*. New York: Maxwell Macmillan, 1993.
- [19] J. C. Doyle, K. Glover, P. P. Khargonekar, and B. A. Francis, “State-space solutions to standard H_2 and H_∞ control problems,” *IEEE Trans. Automat. Contr.*, vol. 34, no. 8, pp. 831–847, Aug. 1989.
- [20] W. H. Press, S. A. Teukolsky, W. T. Vetterling, and B. P. Flannery, *Numerical Recipes in C*, 2nd ed. New York: Cambridge University Press, 1992.
- [21] D. L. Lukes, “Optimal regulation of nonlinear dynamical systems,” *SIAM J Control*, vol. 7, no. 1, pp. 75–100, Feb. 1969.
- [22] E. Desurvire, *Erbium-Doped Fiber Amplifier*. New York: John Wiley and Sons, 1994.
- [23] K. Motoshima, N. Suzuki, K. Shimizu, K. Kasahara, T. Kitayama, and T. Yasui, “A channel-number insensitive erbium-doped fiber amplifier with automatic gain and power regulation function,” *J. Lightwave Technol.*, vol. 19, no. 11, pp. 1759–1767, Nov. 2001.
- [24] K. Motoshima, K. Shimizu, K. Takano, T. Mizuochi, T. Kitayama and K. Ito, “Automatic Gain Control of Erbium-Doped Fiber Amplifiers for WDM Transmission Systems,” *IEICE Trans. Commun.*, vol. E80-B, no. 9, pp. 1311–1319, Sept. 1997.
- [25] A. A. Rieznik and H. L. Fragnito, “Analytical solution for the dynamic behaviour of EDFAs with constant population inversion along the fiber,” *J. Lightwave Technol.*, submitted for publication.

- [26] C. I. Byrnes, A. Isidori, and J. C. Willems, “Passivity, Feedback Equivalence, and the Global Stabilization of Minimum Phase Nonlinear Systems” *IEEE Trans. Automat. Contr.*, vol. 36, no. 11, pp. 1228–1240, Nov. 1991.
- [27] N. Stefanovic and L. Pavel, “ L_2 Nonlinear Control of EDFA System with Amplified Spontaneous Emission”, 2005 IEEE Conference on Control Applications, accepted for publication.
- [28] N. Stefanovic, M. Ding and L. Pavel, “Control of an Erbium-Doped Fiber Amplifier: A Comparison Between L_2 Nonlinear Control and Gain Scheduling”, submitted for publication to IEEE Transactions on Control Technology.
- [29] W. J. Rugh, “Analytical framework for gain scheduling,” *IEEE Control Syst. Mag.*, vol. 11, pp. 79–84, Jan. 1991.
- [30] R. A. Nichols, R. T. Reichert, and W. J. Rugh, “Gain Scheduling for H-infinity Controllers: A Flight Control Example,” *IEEE Transactions on Control Systems Technology*, vol. 1, no. 2, pp. 69–79, June 1993.
- [31] S. Skogestad and I. Postlethwaite, *Multivariable Feedback Control: Analysis and Design*. Toronto: John Wiley and Sons, 1996.